CROP YIELD ESTIMATION FROM SIMULATED CARBON FLUX USING SCOPE: A CASE STUDY OF SAMRAKALWANA VILLAGE IN INDIA

RANIT DE
July, 2021

SUPERVISORS:

Dr. Ir. Christiaan van der Tol

Ir. Gabriel N. Parodi
Prof. (Dr.) Ir. Derrick Mario Denis (External advisor, SHUATS, Prayagraj, India)

CROP YIELD ESTIMATION FROM SIMULATED CARBON FLUX USING SCOPE: A CASE STUDY OF SAMRAKALWANA VILLAGE IN INDIA

RANIT DE
Enschede, The Netherlands, July, 2021

Thesis submitted to the Faculty of Geo-information Science and Earth Observation of the University of Twente in partial fulfilment of the requirements for the degree of Master of Science in Geo-information Science and Earth Observation.
Specialization: Water Resources and Environmental Management

SUPERVISORS:

Dr. Ir. Christiaan van der Tol

Ir. Gabriel N. Parodi
Prof. (Dr.) Ir. Derrick Mario Denis (External advisor, SHUATS, Prayagraj, India)

THESIS ASSESSMENT BOARD:

Dr. Ir. Chris Mannaerts (chair)

Dr. Katja Berger (External Examiner,

Ludwig-Maximilians-Universität, München, Germany)

ABSTRACT

The world has been facing a huge population boom for the last few decades. In this context, food security is a big challenge for many developing countries. Crop yield estimates play a crucial role in formulating food-related policies. They are generally produced using statistical data. But integrating actual remote sensing observations and deeper understanding of the dynamics of crops can help us to provide more accurate crop yield estimates. Moreover, we can have a sense of how crops respond to changing climatic conditions.

Several parameters (such as chlorophyll content, leaf area index [LAI], water content in leaf etc.) defining crop dynamics are essential inputs for modelling ecosystem carbon and water fluxes. It is possible to retrieve values of these parameters from remote sensing observations.

This study focuses on two wheat-growing seasons (2018-19 and 2019-20) at Samrakalwana village, located in the northern part of India. The main objective of this study is to simulate ecosystem fluxes using Soil Canopy Observation of Photosynthesis and Energy fluxes (SCOPE) with vegetation parameters retrieved from Sentinel-3 (S3) and Sentinel-2 (S2) data. Then, the simulated carbon flux was used to provide crop yield estimate.

Two radiative transfer models (i.e., Optical Radiative Transfer Routine [RTMo] of SCOPE and Soil-Plant-Atmosphere Radiative Transfer [SPART]) were inverted to retrieve mainly crop parameters from S3 Ocean and Land Color Imager (OLCI) and S2 Multispectral Instrument (MSI) observations. The RTMo in SCOPE only represents a soil-vegetation system, whereas the SPART includes atmosphere also and it is possible to retrieve parameters defining atmospheric conditions (Aerosol Optical Thickness [AOT], columnar water and ozone content). The data from S3 OLCI was used as it has observations from 21 different bands with a higher temporal resolution of 1.1 days. In contrast, the advantage of S2 MSI is its higher spatial resolutions (4, 6 and 3 bands with 10m, 20m and 60m resolution respectively).

The retrieved parameters and meteorological data from ECMWF ERA5 dataset were then used to model ecosystem fluxes (Gross Primary Production [GPP] and Evapotranspiration [ET]) using SCOPE. The SCOPE simulated GPP and ET were compared against MODIS and ECOSTRESS bases GPP and ET products. Then simulated GPP fluxes were used to provide crop yield estimate. Supplementary information, such as Water Use Efficiency (WUE), Light Use Efficiency (LUE) and Evaporative fraction (EF), were also calculated.

The retrieved parameters, in general, are affected by spikes due to noisy input data. In some cases, the expected pattern of crop dynamics can be observed and retrieved LAI agrees with field-measured LAI. The SCOPE simulated GPP flux was in a range of 0 to 12 $\mu mol\ m^2 s^{-1}$. The simulated ET was in a range of 0 to 11 mm/day. It was found that the values of simulated fluxes are mostly higher than the MODIS based estimate. Crop yield estimates from simulated carbon fluxes were also bit higher than the actual field measurements.

Keywords: *Sentinel-3 OLCI, Sentinel-2 MSI, RTMo, SPART, SCOPE, Gross Primary Production, Evapotranspiration, Crop yield*

ACKNOWLEDGEMENTS

The path to coming to Netherlands for my master's studies and gradually completing an MSc thesis was not very smooth. But I was fortunate enough to receive substantial help, support and guidance from my supervisors, teachers, friends, and families, which helped me to reach where I am today. It is a great pleasure to thank each of them.

I would like to express my sincere gratitude to my supervisors, without their guidance completing this thesis would not have been possible. I am incredibly thankful to my first supervisor, Dr. Ir. Christiaan van der Tol for his constant guidance and support at each stage of my thesis. He motivated me to explore different technical ideas related to my thesis and always generously helped me by answering all of my questions and doubts, and he made me very enthusiastic about my thesis topic. I very much appreciate his efforts in checking my writing with great details and polishing it. I am very much thankful to my second supervisor, Ir. Gabriel N. Parodi for his confidence in me and helping me direct my thesis in the right direction. I must acknowledge his efforts to check every minute details of my thesis draft and provide me with numerous suggestions to improve it.

I would like to thank Prof. (Dr.) Ir. Derrick Mario Denis from my previous university (SHUATS, Prayagraj, India) for extending his support and collaboration for this thesis. I duly acknowledge his effort in providing field data and substantial information about the study area. Moreover, I really appreciate his help in guiding me before I came to ITC. I am also thankful to Mr. Abhishek Ranjan, who has organized and sent me many of this field data and provided me with information regarding data collection.

I am thankful to Mr. Egor Prikaziuk, who helped me to learn and execute several essential tools/ applications necessary for my thesis. I am grateful to Dr. Peiqi Yang for helping me in integrating Sentinel-2 with SPART and answering my doubts related to it.

I also really appreciate the effort of ITC for a smooth transition and for all the administrative support. I want to sincerely acknowledge "ITC Excellence Scholarship Programme" for its generous financial help, without which it would not be possible for me to come to Netherlands.

I want to express my heartfelt gratitude to my parents and family members for their enormous mental and emotional support during my studies and for calling and checking on me almost every day. Thanks for being the strongest pillars of my life.

Life and studying at ITC became more enjoyable with the company of my friends and peers of the WREM course. I am also very thankful to them for asking me many questions at different instances, which helped me dive deeper into various study topics.

A very special thanks goes to all my current housemates (Praneeth, Vijay, Dhananjay, Mahesh and Abbas). I really enjoyed your company during the stay at Enschede as we spent most of the time together in a partially lock-down state. Moreover, I am very thankful for their endless support and motivation.

TABLE OF CONTENTS

LIST OF FIGURES

LIST OF TABLES

Chapter 1

Introduction

1.1 GENERAL BACKGROUND

The world population was 7.7 billion in 2019, and it has been predicted to rise by 10% and to 8.5 billion in 2030 and by 26% to 9.7 billion by 2050. Geographically this population boom will be concentrated in South Asia and Africa. It is projected that India will overtake China as the world's most populous country by 2027 (United Nations, Department of Economic and Social Affairs, Population Division, 2019). This rapid population growth will impose great pressure on agriculture to produce the food required to sustain society. It will further increase the competition among the limited resources of water, land and energy (Godfray et al., 2010).

India is an agriculturally intensive country as 54.6% of India's total human power is involved in this sector. The agriculture and allied sector contributed 16% of India's Gross Value Added (GVA) during 2018 – 19. India also produced 284.83 million tonnes of food grain in the growing season of 2017 – 2018 (Department of Agriculture, Cooperation and Farmers Welfare, Government of India, 2019). Despite the involvement of a large workforce and production of such a massive amount of food, the problem of malnutrition still exists in India. Farmers, as well as the customers also suffer from the problem of fluctuating price of food grains. Farmers are forced to sale their produced grain with a considerable loss which leads to a high number of farmer's suicide cases (Merriott, 2016). The common people also have to buy food at higher prices which make food grains inaccessible to a huge population living below poverty level.

Government and policymakers highly rely on crop yield estimates to formulate policies aiding food security in order to avoid above described situations. Crop yield forecasts are also crucial for developing efficient land and water management practices and determining various business policies (White et al., 2020). The Directorate of Economics and Statistics of the Department of Agriculture provides four advance estimates of major crop yields in September, February (in the following year), April – May and July – August respectively. They rely on different methodologies like econometric modelling, previous years statistics and trends, meteorological factors to validate production and yield data reported by different state governments (Department of Agriculture, Cooperation and Farmers Welfare, Government of India, 2019).

There are also various types of crop growth models, which incorporates crop growth parameters to simulate crop biophysical parameters, grain yield, energy fluxes etc. (Mandal & Rao, 2020). Statistical models exploit historical crop yield data to generate a future trend of crop yield for a large area. Mechanistic models simulate different plant functions and soil mechanisms to reach to a specific output. The functional model tries to simplify complex natural processes and provide empirical relations (Basso et al., n.d.). Nowadays, these functional models are also integrating remote sensing data with meteorological observations to predict crop yield. Few examples of these types of functional model include Forecasting Agricultural output using Space, Agro-meteorological and Land based observation (FASAL) (Parihar & Oza, 2006), Monitoring Agriculture with Remote Sensing (MARS) Crop Yield Forecasting System (MCYFS) of the European Commission Joint Research Centre (JRC) (Genovese et al., 2004), Integrated Canadian Crop Yield Forecaster (ICYF) of Agriculture and Agri-Food Canada (Chipanshi et al., 2012) and CropWatch (Wu et al., 2014).

Besides, crop growth models, there are radiative transfer models coupled with photochemistry or light use efficiency model which can provide information about ecosystem functioning using remote sensing data. The ecosystem functioning is evaluated by plant Evapotranspiration (ET) and photosynthesis or Gross Primary Production (GPP) which are provided as the output of these models (Bayat et al., 2019).

Europe's Copernicus programme provides a large amount of satellite observed data for various applications including monitoring of land, atmosphere, ocean etc. Sentinel-3 (S3) and Sentinel-2 (S2) are two of the optical satellites of Copernicus programmes which provides a wide range of observations. The advantage of S3 is its high temporal resolution and more number of bands. Whereas, S2 has higher spatial resolution. A research framework is adopted to use these satellite based observations along with radiative transfer models to retrieve key crop biophysical parameters and later simulating primary production of crop and other ecosystem fluxes. This framework is shown in Figure 1.1.

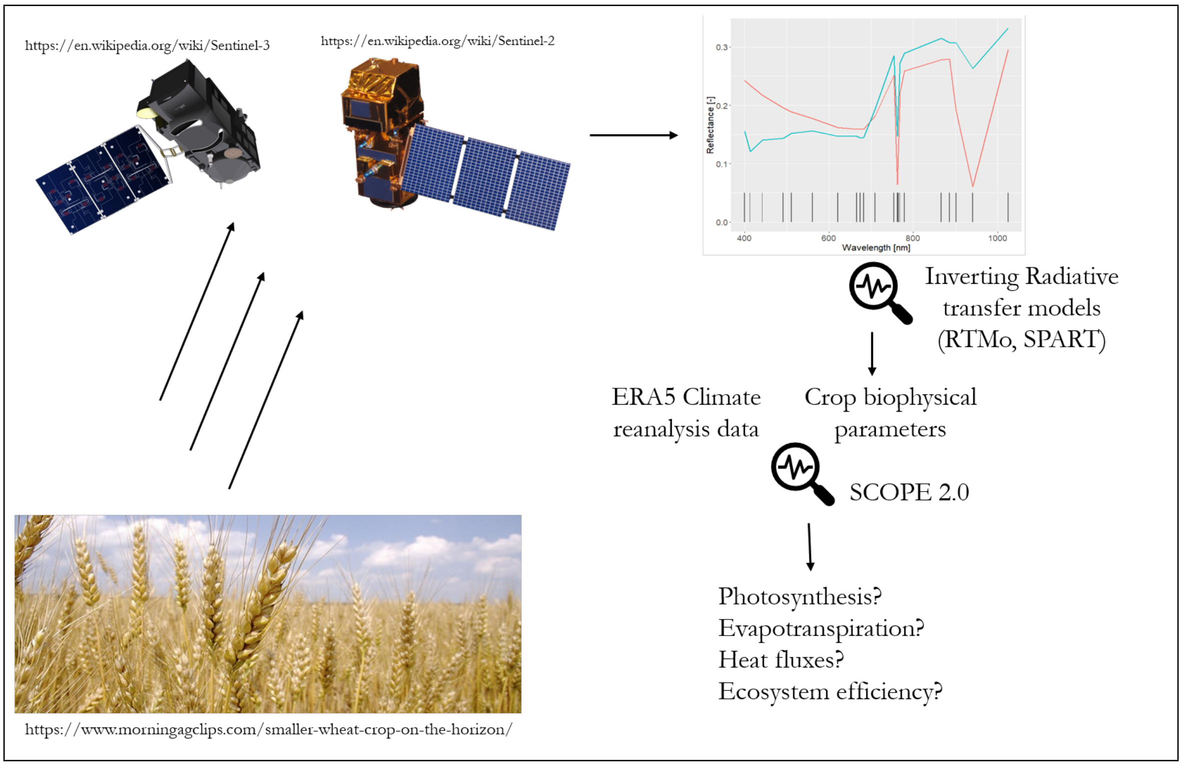

Figure 1.1: *A brief representation of the research*

1.2 MODELS FOR CROP BIOPHYSICAL PARAMETERS RETRIEVAL

The key indicators of vegetation growth and thus crop productivity include leaf chlorophyll concentration (Cab), Leaf Area Index (LAI) and equivalent leaf water thickness (Cw). Together, these indicators can provide insight into the spatial dynamics of vegetation. They can be retrieved from satellite observations, for example S3 or S2. Various modelling approaches or model inversion techniques can be adopted for this purpose. Some of the possibilities are using a physically-based model (e.g., inverting radiative transfer models by numerical optimization or look-up tables) or data driven approaches (e.g. training neural networks) or hybrid modelling approaches combining the advantages of both (Berger et al., 2020; Combal et al., 2003; Darvishzadeh et al., 2008; De Grave et al., 2020).

Inversion of two different integrated radiative transfer models have been performed during this study. The first one is the Optical Radiative Transfer Routine (RTMo) of the **S**oil **C**anopy **O**bservation of **P**hotosynthesis and **E**nergy fluxes (SCOPE) model. This model utilizes the Brightness-Shape-Moisture (BSM) and Fluspect for soil and leaf reflectance respectively and then they are integrated to canopy level by using SAIL model (Prikaziuk & van der Tol, 2019). The second one is Soil-Plant-Atmosphere Radiative Transfer (SPART) which is constructed using BSM to account for soil, PROSPECT + SAIL (PROSAIL) to account for canopy and Simplified Method for Atmospheric Correction (SMAC) to account for atmosphere (Yang, van der Tol, Yin et al., 2020). More details about these models are given in Sections 2.1 and 2.2.

There is a key difference between the RTMo of SCOPE and SPART related to the model domain. SCOPE is only a soil-vegetation model. So, Top of Canopy (TOC) reflectance is necessary for retrieval using SCOPE. Thus, atmospheric correction of Top of Atmosphere (TOA) reflectance has to be performed first. On the other hand, SPART is a coupled surface-atmosphere model. So, TOA reflectance/ radiance can be directly used for retrieval using this model. It is also possible to retrieve parameters related to atmosphere, such as Aerosol Optical Thickness (AOT), ozone content, water vapour content etc.

1.3 SOIL CANOPY OBSERVATION OF PHOTOSYNTHESIS AND ENERGY FLUXES (SCOPE) MODEL

SCOPE model has been applied and validated in different study area with different ecosystems for simulating water, carbon fluxes and developing different aspects of the model. SCOPE model was developed between 2006 – 2009 under the framework of the ECO-RTM project, which was supported by the Netherlands Organization for Scientific Research (NWO-SRON-EO-071) (Abd El Baki, 2013). The details on the theoretical construction of the model and how the model works along with required input parameters were first published in 2009 by van der Tol et al., 2009.

A recently published version of the SCOPE model, known as SCOPE 2.0 includes an improved representation of heterogeneous canopy, capturing effect of xanthophyll cycle on leaf and canopy reflectance and increasing computational efficiency (Yang, Prikaziuk et al., 2020).

The SCOPE is a one dimensional vertical model. Thus, spatially it considers vertical fluxes only and ignores any horizontal interaction of fluxes. SCOPE performs simulations for a given set of instantaneous vegetation and weather conditions. Thus, in temporal domain, it does not has a memory effect and each individual simulation is independent from each other. The model considers a wide range of wavelength (0.4 to 50 µm) including visible, near and shortwave infrared, thermal domain. Besides, it can also simulate fluorescence emission in the domain of 640 to 850 nm.

SCOPE has been used in various studies. Pardo et al., 2018 applied SCOPE for simulating carbon and energy fluxes for rapeseed in Spain. Bayat et al., 2018 exploited optical and thermal infrared observations of Landsat along with SCOPE to apply for a drought case in U.S.A. Wolanin et al., 2019 combined machine learning with SCOPE using Landsat and S2 data for simulating GPP in test sites at U.S.A. and Germany. Sinha et al., 2020 applied SCOPE for a tropical deciduous forest in India. SCOPE has also been widely used for researches related to Sun-Induced Fluorescence (SIF). For example, Migliavacca et al., 2017 used SCOPE to assess the relationship between SIF and GPP with a variation in canopy structure induced by different nutrient conditions. SCOPE has also been also used to successfully retrieve SIF in order to monitor plant stress recovery after a herbicide treatment by Celesti et al., 2018.

1.4 JUSTIFICATION

Agricultural ecosystems or croplands are unique ecosystems. The behaviour of these ecosystems not only depends on natural factors (e.g. weather conditions, such as temperature, humidity, precipitation etc.) but also on the management practices by human (e.g. irrigation, application of fertilizer, pesticides). Thus, crop growth and crop yield also depend on these factors.

The changing climatic conditions are threatening the production of crops or agricultural ecosystem (Flach et al., 2021). The monitoring of crops at different stages can contribute to understanding crop response better. It is not always possible to monitor ecosystem fluxes, such as carbon and water fluxes, with in-situ measurements. In this case, satellite-based observations and monitoring have proven to be useful. The potential of new generation satellite-based products along with integrated radiative transfer models have been explored to quantify ecosystem fluxes of a cropping ecosystem that lacks in-situ instrumentation.

1.5 PROBLEM STATEMENT

Many retrieval algorithms and approaches exist to retrieve vegetation parameters from satellite remote sensing. These algorithms have been individually applied to retrieve vegetation biophysical parameters for different biome classes. For example, Yang, van der Tol, Yin et al., 2020 and Yang et al., 2021 have applied SPART model for biome classes, such as mixed forest, cropland, Savannah etc. Prikaziuk and van der Tol, 2019 have performed a global sensitivity analysis of combined BSM and RTMo routines of the SCOPE model with S3 observations. But there is a need of comparative study between SPART and SCOPE to assess suitability of a certain model or to find out advantages of a certain model in combination with specific satellite observations.

The agricultural field size in the study area in India is usually very small as most of the farmers in India are small and marginal farmers. In fact, the average size of farm holding in India was 1.08 ha in 2015-16 (Department of Agriculture, Cooperation and Farmers Welfare, Government of India, 2020). It is not easy to quantify ecosystem fluxes in these small farms with remote sensing data. Moreover, these farms also lacks ground measurements or instrumentation, such as eddy-covariance based flux measurements. It is important to explore the potential of new generation high resolution satellites, such as S2 to quantify the fluxes and ecosystem efficiency parameters.

1.6 OBJECTIVES

1.6.1 General Objective

The research aims to simulate carbon flux (photosynthesis or GPP) and water flux (ET) by SCOPE model using remote sensing data for an agricultural ecosystem to provide crop yield estimation and ecosystem efficiency parameters.

1.6.2 Specific Objectives

The specific objectives formulated for this research are as follows.

1. To retrieve key crop biophysical parameters that determine for agricultural productivity.
    - To implement an existing retrieval algorithm for the inversion of RTMo in SCOPE with TOC S3 and S2 observations.
    - To implement an existing retrieval algorithm for the inversion of SPART model with TOA S3 and S2 observations.
2. To evaluate the retrieved crop biophysical parameters from TOC and TOA observations (specifically, LAI).
    - against in-situ measurements.
    - against other global remote sensing based LAI products.
3. To select a suitable time-series of crop parameters for the simulation of ecosystem fluxes using SCOPE.
4. To assess the ability of SCOPE to simulate radiative and non-radiative ecosystem fluxes.
5. To compare simulated GPP and ET with similar remote sensing based products.
6. To provide crop yield estimation and ecosystem efficiency parameters.

1.7 RESEARCH QUESTIONS

The research questions formulated based on the above specific objectives are as follows.

1. Are there any specific advantages of using a coupled atmosphere-surface model (SPART) over using an only soil-vegetation model (RTMo in SCOPE) for the retrieval of crop parameters?
2. Which satellite observations (S3 or S2) are more suitable for retrieval of the crop biophysical parameters for the chosen study area?

3. Is it possible to meaningfully perform a one-to-one comparison between LAI retrieved from S3 and S2 observations, and ground measured LAI?
4. To what extent, do SCOPE simulated GPP and ET estimates agree with similar satellite-based products?
5. How well the crop yield estimation from SCOPE simulated photosynthesis agree with the actual field measurement of crop yield?

1.8 SIGNIFICANCE OF THE STUDY

A previous study was conducted by Denis, 2013 in the same study area to quantify ET using Surface Energy Balance System (SEBS) and SCOPE with Moderate Resolution Imaging Spectroradiometer (MODIS) imagery. The algorithms and satellites have evolved since then. In this study, a new generation of satellites (S3 and S2) have been explored to retrieve crop biophysical parameters. A newer version of SCOPE model (v2.0) has been used in this research to quantify both water and carbon flux of the study area.

This study also aims to apply both SPART and SCOPE along with S3 and S2 data in a comparative analysis between them. The current publicly available version of SPART is only compatible with LANDSAT-4,5,6,7 & 8, S3 A & B, and MODIS Terra/Aqua observations. S2 specifications have also been integrated with SPART model during this study in order to meet the objectives of this research.

This research also aims at going a step further with modelled GPP and explore if it can be used to get a rough estimate of crop yield.

1.9 RESEARCH OUTLINE

The details of the research is presented in 7 chapters in this thesis and they are structured in the following way.

- The first chapter presents the general background of the research and brief description of retrieval algorithms and SCOPE model. It also outlines justification, problem statement, objectives, research questions, significance of the study.
- The second chapter provides a more detailed description and the theoretical background of the models (RTMo of SCOPE and SPART) used for retrieval as well as that of SCOPE.
- The third chapter gives a general description of the study area, study period, cropping details. It also describes the major data used in this research.
- The fourth chapter describes all the methodological steps in detail.
- The fifth chapter describes the results obtained at different steps of research methodology.
- The sixth chapter provides a discussion on the achieved result.
- The seventh chapter gives main research conclusions and recommendations.

Chapter 2

Theoretical Basis of the Models Used

The three major models used in this research are RTMo, SPART and SCOPE. RTMo is also a sub-model of the SCOPE. Each of these model is described in the following sections.

In this study, the RTMo of SCOPE and SPART were used for the retrieval of certain soil, vegetation and atmospheric parameters from satellite observations in an inverse scheme. But in this chapter, the forward scheme of these models is described in terms of model structure, main input and output parameters in general. The inversion of the models or the retrieval methods are described in detail in Section 4.4.

2.1 OPTICAL RADIATIVE TRANSFER ROUTINES IN SCOPE

The RTMo is part of the original SCOPE model (van der Tol et al., 2009), and it is described in detail in Prikaziuk and van der Tol, 2019.

2.1.1 Model Structure

The RTMo is made of various sub-models representing leaf, canopy and soil in order to represent a vegetation layer bounded by a soil layer. The Fluspect model (Vilfan et al., 2016) is used to represent the leaf layer which calculates reflectance, fluorescence and transmittance of it using leaf optical parameters (Table 2.1). The BSM model (Jiang & Fang, 2019; Verhoef et al., 2018) is used to represent soil layer and it calculates soil reflectance using four soil parameters (Table 2.1). A numerical SAIL model (Verhoef, 1984) integrates the output of BSM model and Fluspect at canopy level using canopy parameters and parameters describing illumination-observation geometry (Table 2.1). RTMo provides four TOC reflectance factors for direct (s) and diffuse sunlight (d), to reflected radiance in observation (o) and hemispherical direction (d) as output which are known as bidirectional (r_{so}), directional-hemispherical (r_{sd}), hemispherical-directional (r_{do}) and bihemispherical (r_{dd}). TOC reflectance (ρTOC) depending on angle of observation or sun-observer geometry is then calculated by four of the outputs and direct TOC irradiance (E_{dir}) and diffuse TOC irradiance (E_{dif}) using Equation 2.1. The interactions between these sub-models and their input and output are described in Figure 2.1.

$$\rho TOC = \frac{E_{dir} \cdot r_{so} + E_{dif} \cdot r_{do}}{E_{dir} + E_{dif}} \tag{2.1}$$

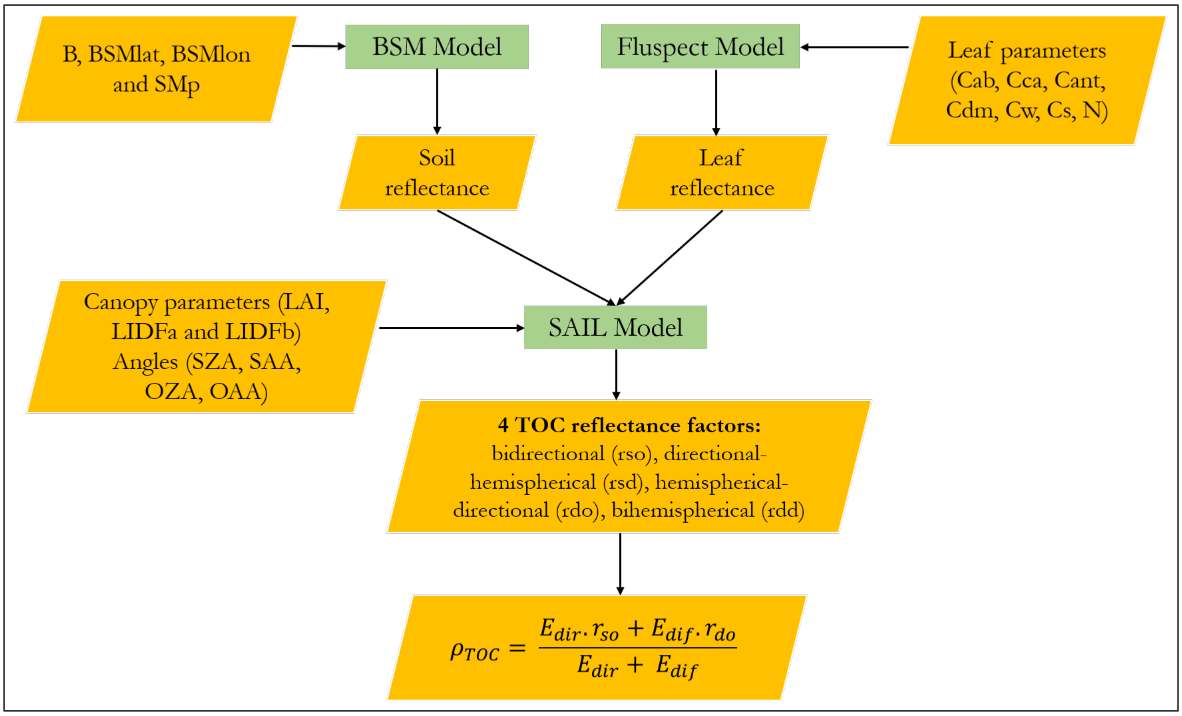

Figure 2.1: *Structure of the forward radiative transfer of incident radiation in the SCOPE model (BSM, Fluspect and RTMo).*

2.1.2 Inputs of the SCOPE Radiative Transfer of Incident Radiation

The inputs of this algorithm are classified into four types, i.e., soil, leaf, canopy and illumination-observation geometry parameters. These parameters are summarized in Table 2.1.

2.1.3 Outputs of the SCOPE Radiative Transfer of Incident Radiation

The combined BSM, Fluspect and RTMo can simulate TOC reflectance for a specific sensor and for a given set of input parameters (Table 2.1). If the actual observed TOC reflectance from a sensor is given as input, the soil, leaf and canopy parameters can be retrieved by inverting the model.

2.2 SOIL-PLANT-ATMOSPHERE RADIATIVE TRANSFER (SPART)

This section provides a brief description of SPART, based on the original paper by Yang, van der Tol, Yin et al., 2020.

2.2.1 Model Structure

SPART consists of three sub-models to represent radiative transfer in soil-vegetation-atmosphere continuum. The soil, canopy and atmosphere are represented by BSM (Verhoef et al., 2018), PRO-

Table 2.1 Input parameters required for RTMo model

Parameters	Units	Description
Soil parameters		
B	-	Soil brightness
BSMlat	Degree	BSM model parameter lat
BSMlon	Degree	BSM model parameter lon
SMC	%	Volumetric soil moisture content
Leaf parameters		
Cab	μg cm^{-2}	Leaf chlorophyll content
Cca	μg cm^{-2}	Leaf carotenoid content
Cant	μg cm^{-2}	Leaf anthocyanin content
Cdm	g cm^{-2}	Leaf mass per area (dry matter)
Cw	cm	Equivalent leaf water thickness
Cs	-	Senescent material (brown pigments)
N	-	Mesophyll structure parameter
Canopy parameters		
LAI	m^2 m^{-2}	Canopy leaf area index
LIDFa	-	Leaf inclination distribution function parameters
LIDFb	-	Leaf inclination distribution function parameters
Parameters describing illumination-observation geometry		
SZA	Degree	Solar zenith angle
OZA	Degree	Observation zenith angle
SAA	Degree	Solar azimuth angle
OAA	Degree	Observation azimuth angle

SAIL (Jacquemoud & Baret, 1990; Verhoef, 1984) and SMAC (Rahman & Dedieu, 1994) respectively. Interactions of these sub-models in SPART produce both TOA and TOC reflectance/ radiance for a certain sensor at any viewing direction. Each of these sub-models are briefly described in following sections. The structure of the SPART model is shown in Figure 2.2.

There are few key differences in model structure between the SCOPE and SPART. These differences are as follows.

1. The SMAC is integrated with SPART to represent the atmosphere. SCOPE lacks this atmospheric component.
2. SCOPE has an energy balance module and capable of simulating photosynthesis and heat fluxes. Whereas, SPART can only simulate TOC or TOA radiance/reflectance for a given set of soil, vegetation and atmospheric conditions.
3. SCOPE is capable of simulating fluorescence using Fluspect. On the other hand, SPART uses PROSPECT to only simulate reflectance and radiance.

BSM Soil Reflectance Model

The BSM was applied in two different ways for dry soil and wet soil in SPART. Three basis spectra or Global Spectral Vectors (GSV) (Jiang & Fang, 2019) were used in this model to simulate reflectance from a dry soil surface. In case of dry soil, three main parameters, i.e., soil brightness (B),

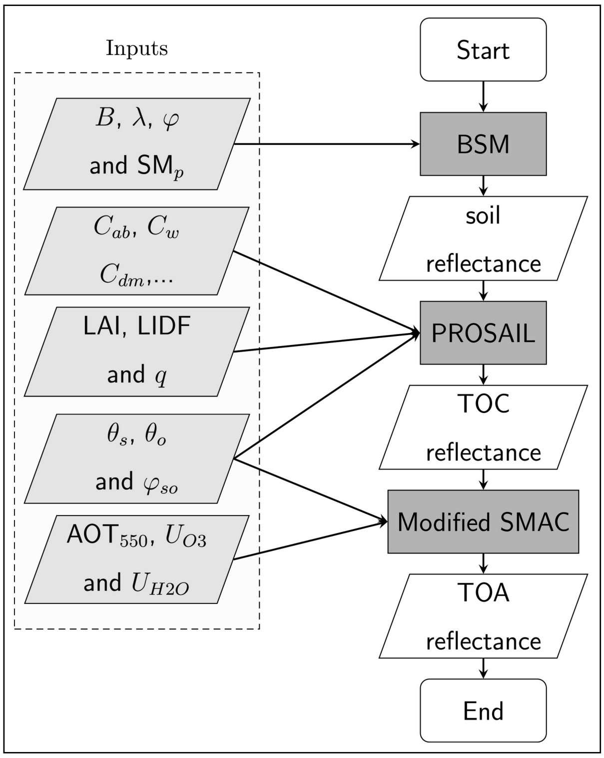

Figure 2.2: *Structure of the forward SPART model (from Yang, van der Tol, Yin et al., 2020)*

soil spectral latitude (ϕ), soil spectral longitude (λ) are needed for the simulation. B determines the 'intensity' of soil reflectance. The other two parameters account for the other soil properties (roughness, organic matter content and mineralogical composition etc.) and responsible for the 'shape' of the simulated reflectance.

In case of wet soil, SPART uses a water film coating approach (Ångström, 1925). In this approach, wet soil is represented by a dry soil layer covered by a thin layer of water. So, the effective reflectance comes from the combined contributions (it includes **i.**Fresnel reflection from the top of water film, **ii.**reflection from the dry soil layer and **iii.**multiple reflection between bottom of water and top of dry soil layer) of dry soil and the thin water layer.

PROSAIL Canopy Radiative Transfer Model

PROSAIL is a combination of two radiative transfer models, i.e., PROSPECT and SAIL. The most recent version of PROSPECT (known as, PROSPECT-D) (Féret et al., 2017) has been used in SPART. More specifically, the Fluspect was used with the fluorescence simulation eliminated. It outputs the reflectance and transmittance of a leaf. The SAIL up-scales this leaf reflectance to canopy level using canopy parameters (Table 2.2) and angles defining viewing-illumination geometry. A version of SAIL model, (SAILH) (Verhoef, 1998) which considers hotspot effect has been used for this purpose. SPART uses a lighter version of RTMo for SAILH, in which the computation of net radiation is eliminated.

It should be emphasized, that SCOPE and SPART yield identical TOC reflectance for identical input.

SMAC Atmosphere Radiative Transfer Model

A substantially modified version of the SMAC (Rahman & Dedieu, 1994) has been used in the SPART to represent the atmosphere. It was revised in order to simulate TOA reflectance from non-lambertian surfaces to represent the anisotropic vegetation. SMAC is an empirical simplification of 5S, the predecessor of the widely used Second Simulation of the Satellite Signal in the Solar Spectrum (6S) model (Vermote et al., 1997). The input parameters required for SMAC are given in Table 2.2.

2.2.2 Inputs of SPART

The inputs of the SPART can be divided into five broad categories, i.e., soil, leaf, canopy, atmosphere, sun-viewing geometry parameters. These parameters are required as input to each of the sub-models representing different layers in SPART. All these parameters are listed in Table 2.2.

Table 2.2 Input parameters required by SPART

Parameters	Units	Description
Soil parameters		
B	-	Soil brightness
ϕ	Degree	Soil spectral latitude
λ	Degree	Soil spectral longitude
SM_p	-	Soil moisture volume percentage
Leaf parameters		
Cab	$\mu g\ cm^{-2}$	Chlorophyll a and b content
Cdm	$g\ cm^{-2}$	Dry mass per unit leaf area
Cw	cm	Equivalent leaf water thickness
Cs	-	Senescent material (brown pigments)
Cca	$\mu g\ cm^{-2}$	Leaf carotenoid content
Cant	$\mu g\ cm^{-2}$	Leaf anthocyanin content
N	-	Leaf internal structure parameter
Canopy parameters		
LAI	$m^2\ m^{-2}$	Leaf area index
LIDFa	-	Leaf inclination determination parameter a
LIDFb	-	Leaf inclination determination parameter b
q	-	Hot-spot parameter (leaf width/canopy height)
Atmosphere parameters		
AOT_{550}	-	Aerosol optical thickness at 550 nm
U_{O3}	cm-atm	Ozone content
U_{H2O}	$g\ cm^{-2}$	Water vapour content
P_a	hPa	Air pressure
Viewing-illumination geometry		
θ_s	Degree	Solar zenith angle
θ_o	Degree	Observation zenith angle
Φ_{so}	Degree	Difference between solar and zenith azimuth angles

2.2.3 Outputs of SPART

The forward SPART can simulate both TOA and TOC radiance or reflectance a spectral resolution and interval of 1 nm. After convolution to a specific sensor (for example, Multispectral Instrument (MSI) on S2), the forward model can be inverted with observations from these sensors to retrieve a large number of different soil, leaf, canopy and atmosphere parameters based on the number and position of available bands.

2.3 SOIL CANOPY OBSERVATION OF PHOTOSYNTHESIS AND ENERGY FLUXES (SCOPE)

This section is based on Yang, Prikaziuk et al., 2020, where SCOPE 2.0 model has been described in detail.

2.3.1 Model Structure

The SCOPE 2.0 model uses various sub-models to simulate different radiative and non-radiative fluxes. The various outputs produced by each sub-model can be used as an input to other sub-models or can be given as final output. The sub-models can be broadly divided into radiative transfer modules and energy balance module. Besides, there is a leaf biochemical model and all these modules interact with each other. A brief description of these sub-models is provided in the following sections.

Radiative Transfer Modules (RTMs)

SCOPE integrates seven Radiative Transfer Modules (RTMs) in order to model radiance from a vegetation-soil stand. BSM (Verhoef et al., 2018) is used to represent soil layer, Fluspect (Vilfan et al., 2016) is used for leaf layer and five other RTMs represents the integrated vegetation-soil layer. These five RTMs are responsible for different functions. They are **i)** RTMo (for sun and sky incident radiation), **ii) and iii)** RTMt_sb and RTMt_planck (for radiation from soil and vegetation in thermal domain), **iv)** RTMf (for chlorophyll fluorescence), **v)** RTMz (to capture change in leaf reflectance or transmittance due to change in pigments in the xanthophyll cycle). A table with brief descriptions of these RTMs are taken from Yang, Prikaziuk et al., 2020 and given as Table 2.3.

Energy Balance Module

The energy balance module is responsible for minimizing the energy balance closure error (e_{ebal}). This error is calculated using Equation 2.2. This minimization is done by changing the temperature of all leaf and soil layers in iteration. In this equation, R_n, H, λE and G are net radiation, sensible heat flux, latent heat flux and ground heat flux respectively. The unit of all these parameter is Wm^{-2}.

$$e_{ebal} = R_n - H - \lambda E - G \tag{2.2}$$

Table 2.3 Description of different RTMs of SCOPE (from Yang, Prikaziuk et al., 2020)

Sl. No.	RTMs	Main functions	Main input	Main output
i.	BSM	simulating soil reflectance	soil moisture, brightness and two spectral shape related parameters	anisotropic soil reflectance
ii.	Fluspect	leaf RTM	leaf biophysical properties	leaf reflectance, transmittance and fluorescence emission matrices
iii.	RTMo	RTM for incident radiation	canopy structure, leaf reflectance, transmittance and soil reflectance	canopy reflectance, radiation absorbed by each leaf
iv.	RTMf	RTM for fluorescence fluxes	canopy structure, leaf reflectance, transmittance, soil reflectance and fluorescence emission matrices	fluorescence of each leaf and of the whole canopy
v. and vi.	RTMt_sb/ RTMt_planck	RTM for thermal fluxes	leaf temperature, incoming thermal radiation, emissivity of soil and leaves	thermal emission of each leaf and of the whole canopy
vii.	RTMz	RTM for fluxes induced by the xanthophyll cycle	leaf absorbed radiation, canopy structure, leaf reflectance, transmittance, soil reflectance	dynamic modulations of canopy reflectance

The net radiation in SCOPE is calculated by RTMo and RTMt sub-modules. A scheme for the aerodynamic resistance, which depends on wind speed, surface roughness and atmospheric stability, is used for the calculation of sensible and latent heat fluxes (van der Tol et al., 2009). The ground heat flux is calculated either as a default fraction of soil surface net radiation, or with the force-restore method as a function of previous soil temperatures and soil thermal properties.

Leaf Biochemical Model

The leaf biochemical module is required to partition energy into heat dissipation, photochemistry and fluorescence in photosystems (Maxwell & Johnson, 2000). This part is based on two photosynthesis model by Collatz et al., 1991 and Collatz et al., 1992 for C3 and C4 plants respectively. The differentiation between C3 and C4 plants is necessary because they use two different pathways, i.e., Calvin cycle and Hatch-Slack pathway respectively for the dark reactions of photosynthesis. The photosynthetic light use efficiency is simulated by this model using carbon dioxide concentrations, leaf temperature, leaf irradiance intencity maximum carboxylation rate (V_{cmo}) etc. Empirical relationships established by van der Tol et al., 2014 are used to differentiate between the leaf fluorescence and heat dissipated from the absorbed radiation.

Interactions between the Sub-models

A run with the SCOPE model starts with the BSM and the Fluspect model. These two sub-models take soil and leaf parameters and simulate soil reflectance and leaf transmittance and reflectance respectively. The output of BSM and Fluspect are passed to RTMo for simulation of net radiation in the optical domain. The RTMt module requires temperature of soil and leaves to perform the simulation in thermal domain. This information is initially not available. RTMt iterates with the calculation of fluxes in the energy balance module until e_{ebal} is minimized by adjusting the soil and leaf temperatures. RTMf uses leaf fluorescence emission excitation matrices and output of Fluspect model to simulate the fluorescence emission of leaves. Finally, RTMz captures the effect of xanthophyll cycle on leaf transmittance and reflectance. All these processes are summarized in Figure 2.3.

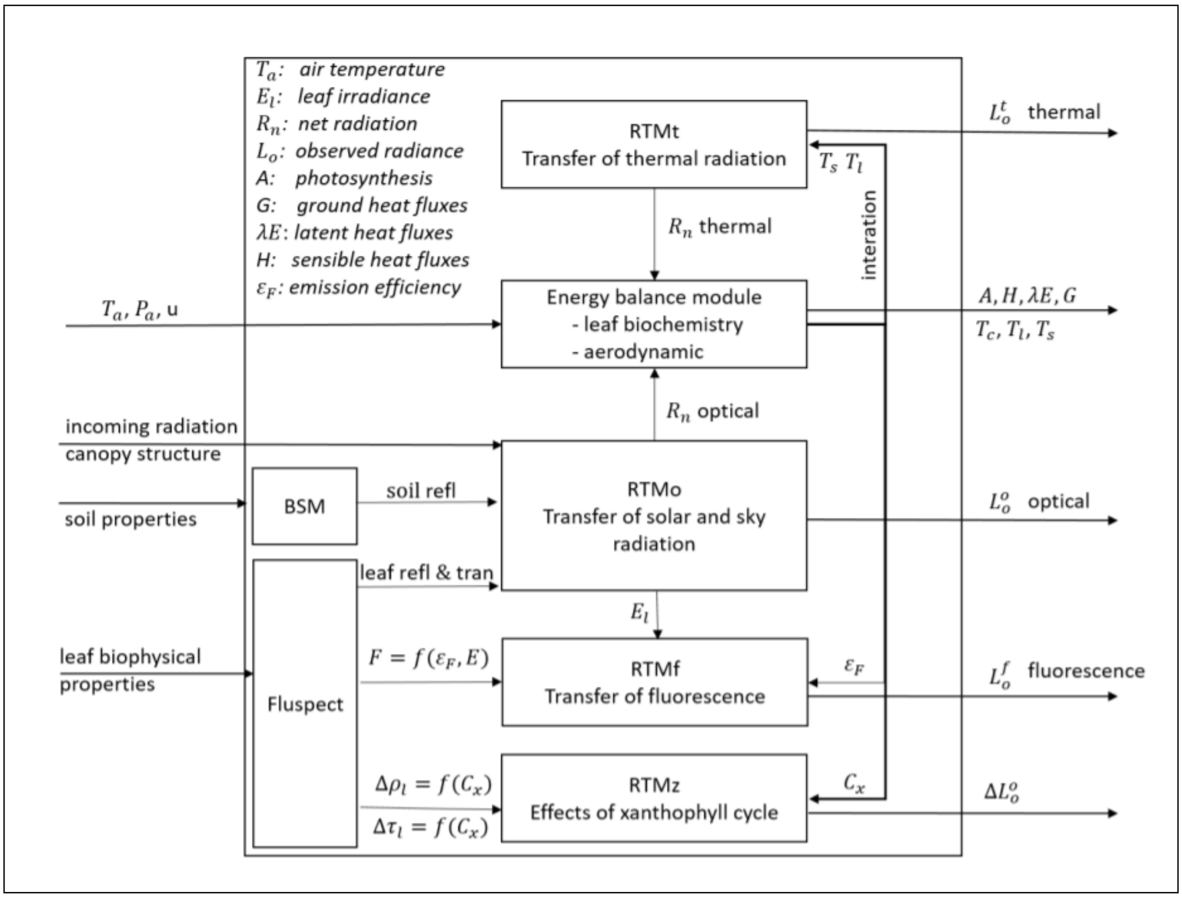

Figure 2.3: *Structure of the SCOPE model (from Yang, Prikaziuk et al., 2020)*

2.3.2 Inputs of SCOPE

The SCOPE input parameters can be divided into soil, leaf, canopy, sun-observer geometry parameters and weather variables. These parameters are listed in Table 2.4.

Table 2.4 Main input parameters required by SCOPE

Parameters	Units	Sub-model	Description
Cab	$\mu g\ cm^{-2}$	Fluspect	leaf chlorophyll concentration
Cca	$\mu g\ cm^{-2}$	Fluspect	leaf carotenoid concentration
Cw	cm	Fluspect	equivalent water thickness in leaves
Cs	-	Fluspect	leaf senescence parameters
Cdm	$g\ cm^{-2}$	Fluspect	leaf dry matter content
Cant	$\mu g\ cm^{-2}$	Fluspect	Anthocyanin content
N	-	Fluspect	leaf structure parameter
LAI	$m^2\ m^{-2}$	canopy RTMs	projected leaf area per unit ground area
hc	m	canopy RTMs	vegetation height
LIDFa	-	canopy RTMs	parameter for the mean leaf zenith angle
LIDFb	-	canopy RTMs	bimodality of leaf angle distribution
tts	Degree	canopy RTMs	solar zenith angle
tto	Degree	canopy RTMs	viewing zenith angle
psi	Degree	canopy RTMs	absolute azimuth difference
Rin	$W\ m^{-2}$	canopy RTMs	shortwave irradiance
Rli	$W\ m^{-2}$	canopy RTMs	longwave irradiance
p	hPa	energy balance	air pressure
T	°C	energy balance	air temperature
u	$m\ s^{-1}$	energy balance	wind speed
ea	hPa	energy balance	vapour pressure
z	m	energy balance	measurement height
SMC	-	BSM, energy balance	surface volumetric soil moisture content
BSMBrightness	-	BSM	soil brightness
BSMlat	Degree	BSM	soil 'latitude' parameter (not geographical)
BSMlon	Degree	BSM	soil 'longitude' parameter (not geographical)
Ca	ppm	biochemical model	atmospheric CO_2 concentration
Vcmo	$\mu mol\ m^{-2}$	biochemical model	carboxylation capacity at 25 degC
m	-	biochemical model	Ball-Berry stomatal parameter

2.3.3 Outputs of SCOPE

The main outputs of SCOPE includes spectral simulation of radiance in optical and thermal domain, incoming and outgoing shortwave and longwave radiation, sensible, latent and ground heat fluxes and absorption of radiation by canopy. The outputs are listed in Table 2.5.

Table 2.5 Outputs of the SCOPE (from Yang, Prikaziuk et al., 2020)

Output	Description	Units
spectral simulation		
Eout_spectum	hemispherical leaving irradiance	$[Wm^{-2}\mu\, m^{-1}]$
Lo_spectrum	radiance in the viewing direction	$[Wm^{-2}\mu\, m^{-1}sr^{-1}]$
fluorescence	fluorescence radiance in the viewing direction	$[Wm^{-2}\mu\, m^{-1}sr^{-1}]$
fluorescence_hemis	hemispheric leaving fluorescence irradiance	$[Wm^{-2}\mu\, m^{-1}]$
reflectance	TOC reflectance in the viewing direction	[]
vegetation		
aPAR	PAR absorbed by the vegetation	$[\mu molm^{-2}s^{-1}]$
aPARbyCab	PAR absorbed by chlorophyll	$[\mu molm^{-2}s^{-1}]$
aPARbyCab_en	PAR energy absorbed by chlorophyll	$[Wm^{-2}]$
Photosynthesis	canopy photosynthesis rate	$[\mu molm^{-2}s^{-1}]$
LST	black-body radiometric land surface temperature	$[K]$
fluxes		
Rnctot	Net radiation of canopy	$[Wm^{-2}]$
lEctot	Latent heat flux of canopy	$[Wm^{-2}]$
Hctot	Sensible heat flux of canopy	$[Wm^{-2}]$
Actot	Net photosynthesis of canopy	$[Wm^{-2}]$
Tcave	Average canopy temperature	$[^{\circ}C]$
Rnstot	Net radiation of soil	$[Wm^{-2}]$
lEstot	Latent heat flux of soil	$[Wm^{-2}]$
Hstot	Sensible heat flux of soil	$[Wm^{-2}]$
Gtot	Soil heat flux	$[Wm^{-2}]$
Tsave	Average soil temperature	$[^{\circ}C]$
Rntot	Total net radiation	$[Wm^{-2}]$
lEtot	Total latent heat flux	$[Wm^{-2}]$
Htot	Total sensible heat flux	$[Wm^{-2}]$
radiation		
ShortIn	Incoming shortwave radiation	$[Wm^{-2}]$
LongIn	Incoming longwave radiation	$[Wm^{-2}]$
HemisOutShort	hemispherical outgoing shortwave radiation	$[Wm^{-2}]$
HemisOutLong	hemispherical outgoing longwave radiation	$[Wm^{-2}]$
Lo	radiance in observation direction	$[Wm^{-2}sr^{-1}]$
Lot	thermal radiance in observation direction	$[Wm^{-2}sr^{-1}]$
Lote	emitted radiance in observation direction	$[Wm^{-2}sr^{-1}]$

Chapter 3

Study Area and Data Description

3.1 STUDY AREA

3.1.1 General Description

The study area, Samrakalwana (also known as, Semra Kalbana) village is located in Bara Tehsil of Allahabad district of Uttar Pradesh state in the northern part of India. The study area is situated between 25° 17' North latitude and 81° 49' East longitude, and the elevation is approx. 137 m a.s.l. This village is part of very fertile Indo-Gangetic plane and the main occupation of the villagers is farming cereal crops. The study area is also closely located to the confluence of two important Indian rivers, i.e., Ganga and Yamuna river. The study area is shown in Figure 3.1.

3.1.2 Climatic Conditions

The climate of the study area is classified as humid subtropical climate (Cwa) during the analysis of 1980 – 2016 in Köppen-Geiger climate classification map (Beck et al., 2018). The maximum and minimum temperature recorded until now in the study area are 48°C and -2°C respectively. The annual average temperature is 26.1°C and monthly average temperatures are between 18 – 29°C. Allahabad experiences a hot dry summer (temperature often exceeds 40°C) between April and June), a warm humid monsoon between July and September and a cold dry winter between December to February. The average annual rainfall in Allahabad district between 2014 – 2018 was 727 mm.

3.1.3 Demographics

The Samrakalwana village has a total population of 4,509 of which 2,369 are males and 2,140 are females. There are total 892 families residing in the village. Whereas, the Allahabad district has 5,959,798 residents and a population density of 1087 per km^2. The district has experienced a population growth of 26.61% between 2001 and 2011 census (Directorate of Census Operations, Uttar Pradesh, 2011).

3.1.4 Agricultural Practices

The soils at the study area is mainly clay loam to sandy loam. There are three main agricultural seasons in India. They are termed as Rabi (October – March), Zaid (April – June) and Kharif (June – September). The major crop of the Rabi season are wheat and other crops cultivated are tomato, potato, and mustard. Pigeon pea and paddy are cultivated dominantly during Zaid and Kharif season, respectively.

Chemical fertilizers are also used during the cultivation of crops. The application dose of these fertilizers have been summarized in Table 3.1.

Table 3.1 General dosage of application of fertilizers/manures in the study area

Sl. No.	Description	Dose (Kg/hectares)
	Manures and Fertilizer application for Wheat	
1.	Basal dressing N:P:K (at the time of sowing)	112:58:55
2.	1st top dressing of N (After 1st Irrigation)	56
3.	2nd top dressing of N	28
4.	3rd top dressing of N	28
	Manures and Fertilizer application for Rice	
1.	Basal dressing N:P:K (at the time of sowing)	152:76:60
2.	1st top dressing of N (After 1st Irrigation)	76
3.	2nd top dressing of N	38
4.	3rd top dressing of N	38

3.1.5 Considerations for This Study

The study has been conducted for the wheat growing season between November 2018 to April 2019 and November 2019 to April 2020. Wheat (*Triticum aestivum*) was chosen for this study as it is the major cereal crop in India. Two points (shown as red squares in Figure 3.1) were selected for 2018 - 2019 season and three points (shown as green triangles in Figure 3.1) were selected for 2019 - 2020 season for carrying out all the analysis. These points were chosen based on the availability of ground measurements at these locations. The coordinates of these points and the wheat variety cultivated is given in Table 3.2.

Table 3.2 Coordinates of point of interest and the cultivated variety of wheat at these points

ID	Latitude	Longitude	Wheat variety
2018_a	25.3056	81.8220	AAIW4
2018_b	25.3034	81.8139	AAIW 10 and AAIW 13
2019_a	25.2943	81.8137	AAIW 16
2019_b	25.3033	81.8159	K1317
2019_c	25.2969	81.8228	SHIATSW 9

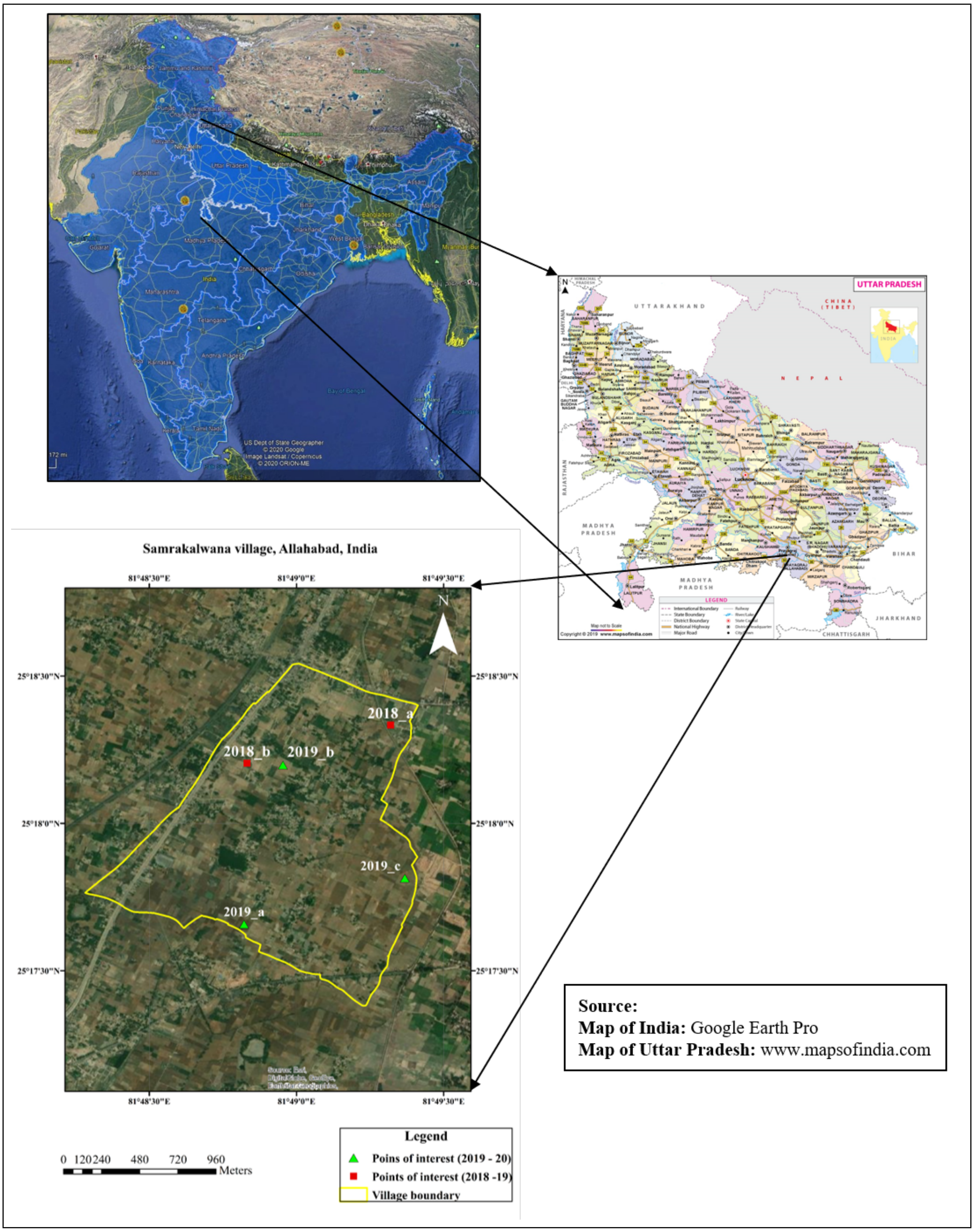

Figure 3.1: *The whole area of India (top left), map of Uttar Pradesh state (right) and a map of the study area (bottom left)*

3.2 DATA DESCRIPTION

The major data used in this research are described in the following sections. A comprehensive list with all the data, codes or programmes used in this study along with their sources are listed in Appendix B.

3.2.1 Sentinel-3 OLCI Data

S3 is a constellation of two satellites with four instruments on-board namely, Synthetic Aperture Radar Altimeter (SRAL), Microwave Radiometer (MWR), Ocean and Land Color Imager (OLCI) and dual-view Sea and Land Surface Temperature Radiometer (SLSTR). These instruments are responsible for monitoring of topography (SRAL, MWR), ocean (OLCI) and temperature (SLSTR). Besides, the upcoming Fluorescence Explorer (FLEX) mission of European Space Agency (ESA) has also been tasked to fly in tandem with S3 in order to provide complementary information on global photosynthesis and SIF. Although the agricultural fields in the study area are relatively small, the retrieval of vegetation parameters from OLCI observations was approached as this can be used in future studies in synergy with data from FLEX. Furthermore, the temporal resolution of S3 is nearly daily which is helpful for monitoring different crop growth stages.

In this study, observations only from OLCI were used to retrieve crop biophysical parameters. This instrument has 21 bands and central wavelength of these bands varies from 400 to 1020 nm. The Spectral Response Function (SRF) of S3 OLCI bands has been plotted in Figure 3.2. A full spatial resolution of 300 m and a reduced spatial resolution of 1200 m is provided by this instrument. It has a swath width of 1270 km and a revisit time of 1.1 days at the equator.

S3 OLCI Level 1 (L1) full resolution images (OL_1_EFR_) from November 2019 to April 2020 were downloaded from Copernicus Open Access Hub (Sentinel, 2018) using a bulk-downloader, called aria2. Similar images for November 2018 to April 2019 are placed in Long Term Archive (LTA) by Copernicus Open Access Hub. There is a cap of downloading one product per half an hour through Graphical User Interface (GUI) and 20 products per 12 hours through Application programming interface Hub (API Hub) of Copernicus Open Access Hub (Copernicus Open Access Hub, 2021). As an alternative Open Data Protocol (OData) Application programming interface (API) of ONDA Data and Information Access Services (DIAS) has been used to download products from LTA which has a higher cap of 20 products per hour. Moreover, the retrieval of products from LTA through ONDA DIAS portal (takes approx. 20 minutes) is also much faster compared to Copernicus Open Access Hub (which has no defined time limit).

A semi-automated pipeline was formulated using Python and batch script for retrieval of LTA products from ONDA DIAS portal. First, a OData API query was built to find all the unique ids for the products of interest. These ids were provided in JSON format. This JSON files were flattened by Pandas (v1.0.5) (The pandas development team, 2020) in Python (v3.7.7). Then multiple batch scripts were generated (for 20 products at a time) by a Python script, for putting requests for retrieval from LTA and downloading these products. Automatic execution of these batch scripts were scheduled using 'Windows Task Scheduler' considering the time frames described in the above paragraph.

The bulk of S3 images were downloaded in the above described way for the growing seasons in order to retrieve certain crop parameters from the satellite observations using radiative transfer models.

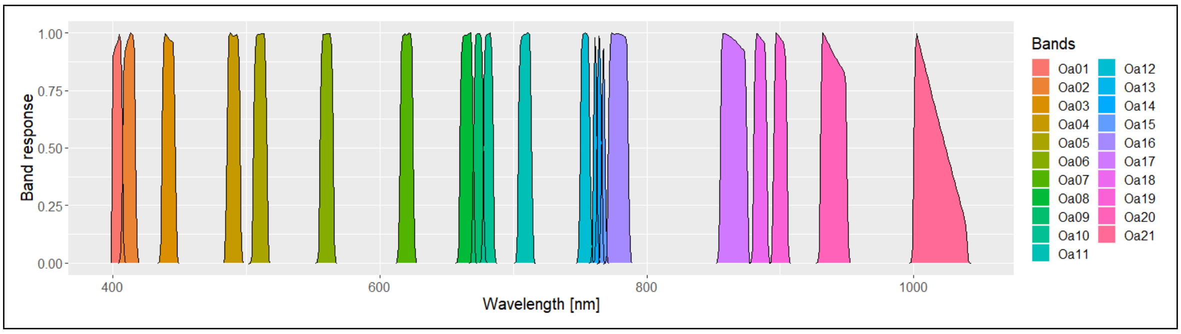

Figure 3.2: *Spectral response functions of Sentinel-3 OLCI bands*

3.2.2 Sentinel-2 MSI Data

S2 is also a constellation of a pair of twin satellites. Both satellites are equipped with a MSI. This instrument was designed to provide remote sensing data suitable for applications in thematic areas, such as spatial planning, monitoring of agriculture and environment, water monitoring, natural resources monitoring etc. The first satellite of S2 constellation was launched on 23rd June 2015 and the second was launched on 7th March 2017. These satellites together now provide a revisit time of 5 days.

The data observed by MSI was used to retrieve crop parameters. The instrument has total 13 bands with central wavelength ranging from 443 nm to 2190 nm. 4 of these bands have a spatial resolution of 10 metres, 6 bands have a spatial resolution of 20 metres and 3 bands have a spatial resolution of 60 metres. The swath width of this instrument is 290 km. The SRF of MSI is shown in Figure 3.3.

Time series of “COPERNICUS/S2” (for S2 TOA reflectance) and “COPERNICUS/S2_SR” (for S2 TOC reflectance) products were downloaded for the coordinates of interest (Table 3.2) from Google Earth Engine (GEE). Pixels affected by clouds were filtered out from the time-series using ‘Bitmask’ filter for S2 products available in GEE.

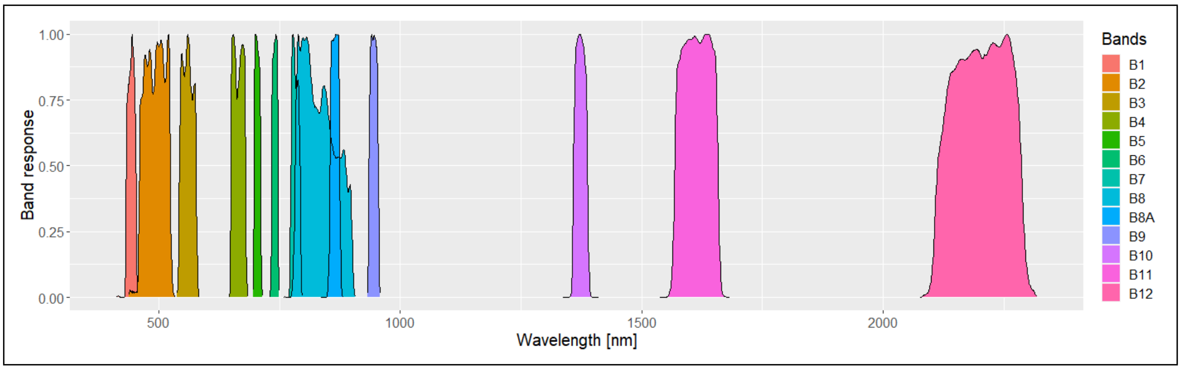

Figure 3.3: *Spectral response functions of Sentinel-2 MSI bands*

3.2.3 ECMWF CAMS Near-Real-Time Data

European Centre for Medium-Range Weather Forecasts (ECMWF) provides global re-analysis data sets with parameters defining atmospheric conditions (such as concentration of different gases, aerosols and water vapour). Some of these atmospheric parameters were necessary for this study. For example, values of AOT at 550 nm was necessary for atmospheric correction with 6S. Other parameters, such as total columnar water vapour (H_2O) and GEMS total columnar ozone (O_3) data along with AOT data from CAMS re-analysis was necessary as initial guess for retrieval of atmospheric parameters using SPART. These data were downloaded for 3:00 hrs. and 6:00 hrs. at a daily time scale for the study periods from ECMWF CAMS Near-real-time in NetCDF format. The data were downloaded at a spatial resolution of $0.125° \times 0.125°$.

3.2.4 MODIS Based Global Remote Sensing Products

Different MODIS based global remote sensing products were used in this study for plausibility check of retrieved or modelled parameters. These products are described below.

MODIS LAI Product

The MODIS LAI product which has been used in this study is MODIS/Terra+Aqua Leaf Area Index/FPAR 4-Day L4 Global 500 m SIN (MCD15A3H v006) (Myneni et al., 2015). The MCD15A3H v006 data were downloaded from Land Processes Distributed Active Archive Center (LPDAAC) **Appl**ication for **E**xtracting and **E**xploring **A**nalysis **R**eady **S**amples (A$\rho\rho$EEARS) portal which converts MODIS SIN grid to proper coordinate system (World Geodetic System 1984 (WGS84)) and extract pixel values for the given coordinates of interest and provide analysis ready time series data in .csv file. This specific service was used to save time for the processing of MODIS products and also to save local storage space. This product is generated using a Look-Up-Table (LUT) (which is generated using 3D radiative transfer equation (Knyazikhin et al., 1998)) approach by exploiting the surface reflectance from MODIS red (648 nm) and near-infrared (858 nm) bands. In case of dense forests or high vegetation (when the LUT approach fails), empirical relationships between Normalized Difference Vegetation Index (NDVI) and LAI for different biome classes are used as backup method.

MODIS ET Products

Four MODIS ET products has been used in this study. These products are listed in Table 3.3. The values of these data products for the coordinates of interest were extracted also using A$\rho\rho$EEARS portal. The algorithm for generating these products are based on Penman-Monteith (PM) equation and it utilizes 8 day vegetation property dynamics measured by MODIS and daily weather reanalysis data (Mu et al., 2013).

Table 3.3 MODIS ET products used in this study

Sl. No.	Product name	Reference
1.	MODIS/Terra Net Evapotranspiration 8-Day L4 Global 500 m SIN Grid (MOD16A2) v006	(Running et al., 2017a)
2.	MODIS/Terra Net Evapotranspiration Gap-Filled 8-Day L4 Global 500 m SIN Grid (MOD16A2GF) v006	(Running et al., 2019a)
3.	MODIS/Aqua Net Evapotranspiration 8-Day L4 Global 500 m SIN Grid (MYD16A2) v006	(Running et al., 2017b)
4.	MODIS/Aqua Net Evapotranspiration Gap-Filled 8-Day L4 Global 500 m SIN Grid (MYD16A2GF) v006	(Running et al., 2019b)

MODIS GPP Products

Four different MODIS products were also used in this study for GPP. These products are listed in Table 3.4. These products were also extracted in A$\rho\rho$EEARS portal. These GPP products were created by establishing a relationship between it and Absorbed Photosynthetically Active Radiation (aPAR) by using output of Biome-BGC simulations. The algorithm also estimates vegetation Maintenance Respiration (MR) and Growth Respiration (GR) from ecophysiological parameter lists from Biome-BGC in order to compute Net Primary Production (NPP) (Running et al., 1999).

Table 3.4 MODIS GPP products used in this study

Sl. No.	Product name	Reference
1.	MODIS/Terra Gross Primary Productivity 8-Day L4 Global 500 m SIN Grid (MOD17A2H) v006	(Running et al., 2015a)
2.	MODIS/Terra Gross Primary Productivity Gap-Filled 8-Day L4 Global 500 m SIN Grid (MOD17A2HGF) v006	(Running & Zhao, 2019)
3.	MODIS/Aqua Gross Primary Productivity 8-Day L4 Global 500 m SIN Grid (MYD17A2H) v006	(Running et al., 2015b)
4.	MODIS/Aqua Gross Primary Productivity Gap-Filled 8-Day L4 Global 500 m SIN Grid (MYD17A2HGF) v006	(Running & Zhao, 2019)

3.2.5 ECOSTRESS Based Global Remote Sensing Products

ECOsystem Spaceborne Thermal Radiometer Experiment on Space Station (ECOSTRESS) mission is implemented by installing the Prototype HyspIRI Thermal Infrared Radiometer (PHyTIR) instrument on the Japanese Experiment Module External Facility (JEM-EF) of International Space Station (ISS). It was launched to ISS on 29th June 2018 and become autonomously operational on 20th August 2018. This instrument has 5 thermal bands present with wavelengths in 8 - 12.5 μm range. But after 15th May 2019, only three of these bands (with central wavelength of 8.78 μm [Band 2], 10.49 μm [Band 4] and 12.09 μm [Band 5]) are being used to optimize acquisition approach and counter failure of the Mass Storage Units (MSU).

ET is derived from the observations using two algorithms. The first algorithm is Disaggregation of Atmosphere–Land Exchange Inverse (DisALEXI) (Anderson et al., 1997) which is used to derive ET at a finer spatial resolution (30 m) only for targeted agricultural sites within continental United States (CONUS). The second algorithm, called Priestley-Taylor Jet Propulsion Laboratory (PT-JPL) (J. B. Fisher et al., 2008) uses surface temperature and emissivity measurements from ECOSTRESS and ancillary MODIS and Landsat products to compute ET at a global scale with 70 m spatial resolution. In the event of absence of ancillary data from MODIS or Landsat, data from Visible Infrared Imaging Radiometer Suite (VIIRS) and Global Modeling and Assimilation Office (GMAO) Modern Era Retrospective-Analysis for Research and Applications (MERRA) are used as backup. The PT-JPL algorithm also provides different components of ET, such as soil evaporation, canopy transpiration and ET of intercepted water (J. B. Fisher & ECOSTRESS Algorithm Development Team, 2015).

The time-series of ECOSTRESS Evapotranspiration PT-JPL Daily L3 Global 70 m (ECO3ETPTJPL) (v001) (Hook & Fisher, 2019a) product was downloaded for the coordinates of interest for the two crop growing seasons using the A$\rho\rho$EEARS portal.

A global Water Use Efficiency (WUE) product (ECOSTRESS Water Use Efficiency Daily L4 Global 70 m (ECO4WUE) v001) (Hook & Fisher, 2019b) is also computed from ECO3ETPTJPL product and MODIS GPP (J. B. Fisher & ECOSTRESS Algorithm Development Team, 2018). This product was downloaded to compare against modelled ecosystem efficiency parameters.

3.2.6 Meteorological Data from ECMWF ERA5

Time series of weather parameters have an important role in controlling simulation of photosynthesis in SCOPE. ECMWF provides a variety of weather parameters as gridded data (9 km spatial resolution) in 'GRIB' and 'NetCDF' format. ECMWF Reanalysis 5th Generation (ERA5)-land hourly data which is an improved (can be used in all types of applications for land) and light version (as no calculation is performed for the oceans) of the original ERA5 data was used in this study (Muñoz Sabater, 2019). The variables downloaded were surface solar radiation downwards (ssrd), surface thermal radiation downwards (strd), 2m temperature (t2m), 2m dewpoint temperature (d2m), surface pressure (sp), 10m u-component of wind (u10) and 10m v-component of wind (v10). The data were downloaded at an hourly time scale for both the crop growing seasons in 'NetCDF' format.

3.2.7 In-situ Data Collection

The in-situ data were not primarily collected as part of this study. Secondary in-situ measurements (which were already acquired), were collected from the local University (SHUATS, Prayagraj, India). Ground measurements of LAI and crop yield were used in this study for evaluation of modelled results.

The in-situ LAI measurements were taken using a Leaf Area Meter 211 (Systronics, India). There were 10 measurements of LAI taken in each wheat growing season (2018 - 19 and 2019 - 20) between January to March. The measurements were not taken at any fixed interval. The LAI measurements were taken on same days of 2019 and 2020. These dates are given in Table 3.5.

Crops from a small number of representative areas at the given coordinates (Table 3.2) were harvested. Crop grains were separated and weighed in a weighing balance to estimate crop yield. The crop yield from this small area was used to exponentially calculate crop yield per hectare.

The coordinates for the measurements for LAI and crop yield were not measured using a professional Global Positioning System (GPS). The coordinates were measured using recreational GPS of mobile phone which led to some wrong ground locations. These were later corrected using digitized map of agricultural plots of the study area. This method may add some amount of uncertainty to the measurements and it is not easy to quantify the inaccuracy. This may lead to incorrect comparison between ground measurement and modelled data from remote sensing observations.

Table 3.5 Dates of in-situ LAI measurements in 2019 and 2020

Serial number	LAI measurement dates (in 2019 and 2020)
1	10-January
2	17-January
3	20-January
4	30-January
5	02-February
6	18-February
7	20-February
8	02-March
9	06-March
10	12-March

This page is intentionally left blank.

Chapter 4

Methodology

4.1 METHODOLOGY FLOWCHART

A detailed methodology was formulated to accomplish the objectives of this research. This methodology is summarized in a flowchart in Figure 4.1. The different steps of the methodologies are described in detail in the later sections.

4.2 DATA PRE-PROCESSING

4.2.1 Extraction of Pixel Values from Sentinel-3 OLCI Images

The values from different OLCI bands, tie-point grids and masks from each S3 OL_1_EFR_ products were extracted for the coordinates of interest using "Extract Pixel Values" function of SeNtinel Application Platform (SNAP) 8.0. The pixel values were extracted using geo-coordinates. Then the observations flagged as bright, invalid, dubious pixels and saturated bands were removed. These flags were used as proxy to identify clouded pixels or pixels with erroneous values.

S3 OL_1_EFR_ products also come with columnar H_2O and O_3 in the atmosphere at the time of overpass. These variables are provided in kg/m^2. These values were changed to suitable units needed for atmospheric correction using Equation 4.1 and 4.2.

$$H_2O\ [g/cm^2] = 0.1 \times H_2O\ [kg/m^2] \tag{4.1}$$

$$O_3\ [cm-atm] = \frac{100}{(2.144 \times O_3\ [kg/m^2])} \tag{4.2}$$

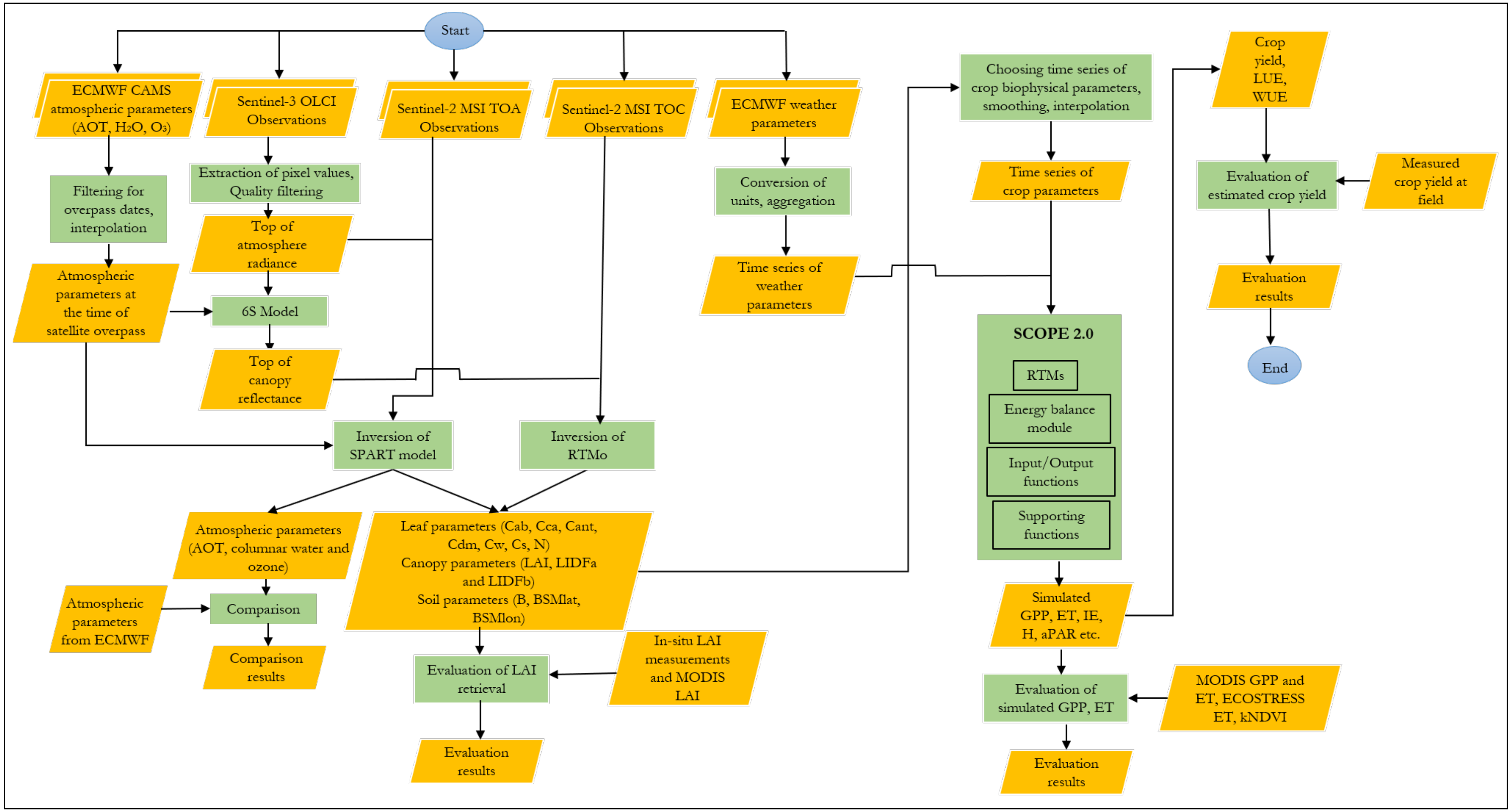

Figure 4.1: *Flowchart of the methodology. The inputs and outputs of various stages are defined as orange parallelograms and processes are defined as green rectangles*

4.2.2 Interpolation of CAMS Atmospheric Data

This study requires values of atmospheric parameters such as, AOT, H_2O and O_3 during the time of S3 and S2 overpass, over the study area.

In case of S3, these atmospheric parameters were necessary for atmospheric correction of S3 OLCI data. Among these, values of atmospheric H_2O and O_3 concentrations at the time of overpass were already extracted from S3 OLCI products as described in 4.2.1. Only the interpolation of ECMWF AOT value from was necessary.

Whereas, in case of S2 MSI data in GEE, it does not come with these atmospheric parameters. But these data were necessary for inversion of SPART. So, all the three parameters (AOT, H_2O and O_3) from were ECMWF interpolated for the time of S2 overpass.

The values of atmospheric parameters were extracted from the 'NetCDF' files using 'ncread' function of MATLAB R2019a for the pixels of interest. Then the values only for the dates of satellite overpass (S3 or S2) were kept. The both satellites over-passed on the study area between 3:00 hrs. and 6:00 hrs. So, a time weighted interpolation of extracted atmospheric parameters at these time-steps were performed to estimate the values at the time of satellite overpass. Numpy (v1.18.5) 1D interpolation (numpy.interp) function (Harris et al., 2020) in Python 3.7.7 was used for this purpose.

4.2.3 Atmospheric Correction of Sentinel-3 OLCI TOA Radiance

The 6S model can be used to simulate the effect of the atmosphere on the path of electromagnetic wave from the illumination source to the target and back to the sensor (Vermote et al., 1997). A Python interface to 6S (Py6S) (which is a Python wrapper on the original MODTRAN code of 6S model) has been used to simulate the optical coefficients (atmospheric transmittance factors) (Wilson, 2013). These coefficients (X_a, X_b, X_c) were simulated for a given atmospheric condition (for a certain amount of columnar aerosol, ozone and water vapour in the atmosphere), sun and sensor geometry (defined by Solar Zenith Angle (SZA), Solar Azimuth Angle (SAA), Observation Zenith Angle (OZA), Observation Azimuth Angle (OAA)) and day of the year. Later, TOC reflectance (R_{TOC}) was calculated using these coefficients from TOA radiance (L_{TOA}) (as shown in Equations 4.3 and 4.4).

In some cases, the atmospherically corrected R_{TOC} values were found to be negative for a certain band. In this case, it is assumed that the atmospheric correction cannot be performed with confidence and the whole spectrum was removed and not used for retrieval of crop biophysical parameters.

$$y = (X_a \times L_{TOA}) - X_b \tag{4.3}$$

$$R_{TOC} = \frac{y}{1 + (X_c \times y)} \tag{4.4}$$

4.2.4 Unit Conversion and Aggregation of ECMWF ERA5 Meteorological Data

Several meteorological parameters were downloaded at hourly time scale from ERA5 climate reanalysis data as described in Section 3.2.6. These parameters need to be converted into the units of SCOPE and renamed as required by SCOPE. These meteorological parameters were also aggregated to a daily time scale as the time step for SCOPE simulation was chosen as daily.

ssrd and strd were converted to integrated incoming shortwave radiation (Rin) and integrated incoming longwave radiation (Rli) using Equation 4.5 and 4.6 respectively. t2m was converted from degree centigrade to Kelvin using Equation 4.7 and renamed as air temperature (Ta). sp was used to calculate air pressure (p) using Equation 4.8. Wind speed (u) was calculated from u10 and v10 by Equation 4.9. d2m was first converted from Kelvin to degree centigrade (Equation 4.10). Then 2m dewpoint temperature in degree centigrade (T) was used to calculate atmospheric vapour pressure (ea) using Equation 4.11.

$$Rin\ [Wm^{-2}] = \frac{ssrd\ [Jm^{-2}]}{60 \times 60 \times 24} \tag{4.5}$$

$$Rli\ [Wm^{-2}] = \frac{strd\ [Jm^{-2}]}{60 \times 60 \times 24} \tag{4.6}$$

$$Ta\ [°C] = t2m\ [K] - 273.15 \tag{4.7}$$

$$p\ [hPa] = sp\ [Pa] \times 0.01 \tag{4.8}$$

$$u\ [ms^{-1}] = \sqrt{u10^2\ [ms^{-1}] + v10^2\ [ms^{-1}]} \tag{4.9}$$

$$T\ [°C] = d2m\ [K] - 273.15 \tag{4.10}$$

$$ea\ [hpa] = 6.107 \times 10^{\frac{7.5 \times T}{237.3+T}} \tag{4.11}$$

4.3 INTEGRATION OF S2 MSI WITH SPART AND SENSITIVITY ANALYSIS

4.3.1 Integration of S2 MSI

SPART has earlier been used for S3 (Yang, van der Tol, Yin et al., 2020; Yang et al., 2021), but not for S2. In order to make it applicable to S2, it was necessary to integrate sensor characteristics with SPART. This enabled the retrieval of vegetation parameters from S2 MSI observations.

A total of 49 sensor specific coefficients for each band are required for functioning of SMAC model (which is a sub-model of SPART, as described in Section 2.2) (Rahman & Dedieu, 1994). These SMAC coefficients were calculated using a best fit technique and provided for a large number of sensors in a public repository hosted by Centre d'Etudes Spatiales de la Biosphère (CESBIO), Centre national d'études spatiales (CNES). The SMAC coefficients were downloaded from this repository for this study. It is worth noting that only SMAC coefficients for S2A are available in the mentioned repository. As S2A and S2B are twin-satellites and their spectral characteristics are similar, these coefficients were used interchangeably for SPART simulation of both the cases.

Besides these coefficients, another piece of necessary information was SRFs of S2 MSI which is shown in Figure 3.3. The other required general sensor characteristics are summarized in Table 4.1 and 4.2. All information has been collected from S2 document library, which is managed by ESA.

Table 4.1 Overview of Sentinel-2 MSI sensor

Attribute	Values
Mission	Sentinel-2
Name	MSI
Swath width	290 km
Revisit period	5 days

Table 4.2 Characteristics of MSI sensor

Band	Central wavelength (nm)	Spectral width (nm)	Spatial resolution (m)
B1	443	20	60
B2	490	65	10
B3	560	35	10
B4	665	30	10
B5	705	15	20
B6	740	15	20
B7	783	20	20
B8	842	115	10
B8A	865	20	20
B9	945	20	60
B10	1375	30	60
B11	1610	90	20
B12	2190	180	20

4.3.2 Sensitivity Analysis of SPART Model with Sentinel-2 MSI

Yang, van der Tol, Yin et al., 2020 performed a sensitivity analysis of SPART with spectral characteristics of S3 OLCI sensor. In this study, a similar sensitivity analysis of SPART has been performed for S2 MSI sensor using the same code as published by the authors. The effect of only Cab, LAI and AOT on simulated TOC or TOA reflectance has been investigated in this study.

4.4 RETRIEVAL OF CROP BIOPHYSICAL, SOIL AND ATMOSPHERIC PARAMETERS

4.4.1 Inversion of RTMo module of SCOPE

The radiative transfer of incident radiation in SCOPE, thus RTMo coupled with Fluspect and BSM, was used to retrieve crop biophysical parameters and some soil parameters using TOC reflectance observed by S3 and S2 satellites.

In case of S3 OLCI, time-series of TOC reflectance from 19 bands (excluding band 13 and 14), time-series of SZA and central wavelengths of used bands were provided as input for the inversion of RTMo. Band 13 and 14 were removed as a dip can be observed in those bands which may not be ideal for spectral fitting using RTMo. Moreover, these bands are O_2 absorption and atmospheric correction bands. So, these bands are highly sensitive to errors in the atmospheric correction of TOA to TOC.

Atmospherically corrected TOC reflectance from 12 bands (excluding band 10) of S2 MSI, their central wavelengths and time series of SZA were also used for retrieval of crop and soil parameters by inverting RTMo. Band 10 was not used as TOC reflectance of this band is not provided by GEE. The most likely reason behind the non-availability of TOC reflectance from band 10 is that the atmospheric correction of this band is prone to error as it is responsible for detection of cirrus clouds. Moreover, this band may not be very useful for retrieval of vegetation parameters.

The retrieval was carried out by inverting forward RTMo of SCOPE (as described in Section 2.1) using numerical optimization. The numerical optimization in RTMo was implemented by using a built-in function in MATLAB Optimization Toolbox, known as 'lsqnonlin' (Prikaziuk & van der Tol, 2019). A trust-region-reflective algorithm was used in this case to update parameters in iteration and find a local minimum for the defined cost function (Coleman & Yuying, 1994, 1996). An optimality tolerance of 1×10^{-6} and 30 as number of maximum iteration were set as stopping criteria for 'lsqnonlin'. An initial guess was provided for each parameter and parameters were updated within their upper and lower bounds (summarized in Table 4.3). This procedure is described in detail by van der Tol et al., 2016; Verhoef et al., 2018; Yang et al., 2019.

Two different cost functions were defined in RTMo (van der Tol et al., 2016), one is without using any prior information (Equation 4.12) and another using prior information (Equation 4.13). Root Mean Square Error (RMSE) between the measured spectra and final modelled spectra was also calculated and given as output by RTMo.

$$f_0(i) = [R_{TOC_{mod}}(i) - R_{TOC_{meas}}(i)] \tag{4.12}$$

Where $f_0(i)$ is the cost function which is to be minimized. $R_{TOC_{mod}}$ and $R_{TOC_{meas}}$ are modelled and measured TOC reflectance respectively. $R_{TOC_{meas}}$ is same as the atmospherically corrected TOC reflectance measured by S3 OLCI (defined as R_{TOC} in Section 4.2.3) as well as observed TOC reflectance by S2 MSI (which were extracted from GEE). i is the measurement index in the time-series.

$$\begin{aligned} f(i) &= f_0(i) + f_p(i) \\ f_0(i) &= [R_{TOC_{mod}}(i) - R_{TOC_{meas}}(i)] \\ f_p(i) &= w \times \left(\frac{X(i) - X_0}{\sigma_p}\right) \end{aligned} \tag{4.13}$$

In this case the cost function ($f(i)$) has two components. The first component ($f_0(i)$) is same as Equation 4.12. The second component ($f_p(i)$) considers a prior information in the cost function. In this component w is the weight given the prior information (here 0.03), X is the posterior value,

X_0 is the initial guess/ prior values (as given in Table 4.3) and σ_p is the uncertainty associated with each parameter (as given in Table 4.3).

Table 4.3 Initial guess, upper and lower bounds, uncertainty of parameters retrieved using RTMo

Parameters	Initial guess (X_0)	Lower bound	Upper bound	Uncertainty (σ_p)	Units
Soil parameters					
B	0.5	0	0.9	0.3	-
BSMlat	25	20	40	12	Degree
BSMlon	45	40	60	9	Degree
SMC	30	5	55	12	%
Leaf parameters					
Cab	40	0	100	30	μg cm^{-2}
Cca	5	0	25	4	μg cm^{-2}
Cant	1	0	5	1	μg cm^{-2}
Cdm	0.012	0	0.02	0.006	g cm^{-2}
Cw	0.009	0	0.2	0.02	cm
Cs	0.6	0	1.2	0.4	-
N	1.4	1	3.5	0.75	-
Canopy parameters					
LAI	3	0	7	1	m^2 m^{-2}
LIDFa	-0.35	-1	1	0.6	-
LIDFb	-0.15	-1	1	0.6	-

A description of different parameters which can be retrieved using RTMo are provided in Table 2.1. A different combinations of these parameters were retrieved at a time with or without using prior information in cost function to assess the performance of RTMo. These combinations are summarized in Table 4.4.

Table 4.4 Combinations used for retrieval using RTMo

Combination number	Usage of prior in cost function	Retrieved parameters
1	No prior used in cost function	Leaf and canopy parameters (Cab, Cca, Cant, Cdm, Cw, Cs, N, LAI, LIDFa and LIDFb)
2	No prior used in cost function	Soil parameters (B, BSMlat, BSMlon), leaf and canopy parameters (Cab, Cca, Cant, Cdm, Cw, Cs, N, LAI, LIDFa and LIDFb)
3	Prior used in cost function	Leaf and canopy parameters (Cab, Cca, Cant, Cdm, Cw, Cs, N, LAI, LIDFa and LIDFb)
4	Prior used in cost function	Soil parameters (B, BSMlat, BSMlon), leaf and canopy parameters (Cab, Cca, Cant, Cdm, Cw, Cs, N, LAI, LIDFa and LIDFb)

4.4.2 Inversion of SPART

A numerical optimization method was applied to invert SPART and retrieve crop parameters, soil parameters and parameters describing atmospheric composition from S3 OLCI TOA radiance and S2 MSI TOA reflectance measurements. The MATLAB function 'lsqnonlin' was used for this purpose. Details on this function are described in Section 4.4.1. The stopping criteria for 'lsqnonlin' are as described in Section 4.4.1. The initial guess, upper and lower bounds used in case of retrieval from SPART are summarized in Table 4.5.

Two different cost functions were defined for minimization. The first cost function (given as Equation 4.14) was only defined using measured and modelled TOA radiance or reflectance, whereas, the second function (Equation 4.15) utilizes additional prior information.

$$f_0(i) = [L_{TOA_{meas}}(i) - L_{TOA_{mod}}(i)]^T \times [L_{TOA_{meas}}(i) - L_{TOA_{mod}}(i)] \tag{4.14}$$

Where $f_0(i)$ is the cost function which is to be minimized. $L_{TOA_{mod}}$ and $L_{TOA_{meas}}$ are modelled and measured TOA radiance respectively. In case of S2, measured and modelled TOA reflectance has been used. i is the measurement index in the time-series.

$$\begin{aligned} f(i) &= f_0(i) + f_p(i) \\ f_0(i) &= [L_{TOA_{meas}}(i) - L_{TOA_{mod}}(i)]^T \times [L_{TOA_{meas}}(i) - L_{TOA_{mod}}(i)] \\ f_p(i) &= w \times \left(\frac{X(i) - X_0}{\sigma_p}\right)^T \times \left(\frac{X(i) - X_0}{\sigma_p}\right) \end{aligned} \tag{4.15}$$

In this case the cost function ($f(i)$) has two components. The first component ($f_0(i)$) is same as Equation 4.14. The second component ($f_p(i)$) considers prior information in the cost function. In this component w is the weight given the prior information (here 0.006, background on this value is given in the next paragraph). X is the posterior value retrieved, X_0 is the initial guess/ prior values (as given in Table 4.5) and σ_p is the standard deviation of parameters, which is calculated for parameters with uniform distribution over a given interval by $1/\sqrt{12}$ ($\approx$ 0.3) of difference between upper and lower bound of each parameter (Lumen learning, n.d.).

The value of w provides a weight to the part of the cost function with prior information. If a higher weight is provided to the prior part, then the retrieved parameter will remain closer to the initial guess. Whereas, if a lower value is provided, then the retrieval will go closer to the retrieval without any prior information in the cost function. A sensitivity analysis was performed by using different values of weight from 0.005 to 0.05 in order to remove spikes from the retrieved values. However, many spikes remain in the retrieved parameters even after using this cost function (Equation 4.15).

In case of observations from S3 OLCI, all the soil, leaf and canopy parameters (as listed in Table 4.5) and AOT values were retrieved as S3 OLCI has many bands (21 nos.). Other parameters, such as H_2O, O_3, SZA, OZA and difference between SAA and OAA, Day of Year (DOY) were provided as constant from actual S3 observations. All the 21 bands were used for retrieval.

It is required to have an equal or higher number of observations from different bands of a sensor than the numbers of parameters which can be retrieved. In case of S2 MSI, a limited number of parameters can be retrieved at a time, as it has 13 bands. First, an image with bare soil was identified and spectral fitting was performed using SPART to find out a fixed set of values for two of the BSM soil parameters, i.e., ϕ and λ. Then constant values were assumed for some of the other parameters, i.e., 15 for soil moisture volume percentage (SMp), 0.05 for the hot-spot parameter (q) and 10 for the leaf carotenoid content (Cca). Actual values from S2 observations were provided for parameters related to viewing-illumination geometry. In case of atmospheric parameters (H_2O, O_3 and AOT), interpolated values during satellite overpass from ECMWF data were provided as initial guess and then optimized by the model. All other soil, leaf and canopy parameters (as listed in Table 4.5) were retrieved.

Table 4.5 Initial guess, upper and lower bounds of parameters retrieved using SPART

Parameters	Unit	Lower bound	Upper bound	Initial guess (X_0)
Soil parameters				
B	-	0	0.9	0.5
ϕ	Degree	-30	30	0
λ	Degree	80	120	100
SM_p	-	5	55	15
Leaf parameters				
Cab	$\mu g\ cm^{-2}$	0	80	40
Cdm	$g\ cm^{-2}$	0	0.02	0.01
Cw	cm	0	0.1	0.02
Cs	-	0	1	0
Cca	$\mu g\ cm^{-2}$	0	30	10
Cant	$\mu g\ cm^{-2}$	0	30	10
N	-	1	4	1.5
Canopy parameters				
LAI	$m^2\ m^{-2}$	0	8	3
LIDFa	-	-1	1	-0.35
LIDFb	-	-1	1	-0.15
q	-	0	0.2	0.05
Atmosphere parameter				
AOT_{550}	-	0	2	0.3246 or ECMWF data
U_{O3}	cm-atm	0	0.8	0.35 or ECMWF data
U_{H2O}	$g\ cm^{-2}$	0	8.5	1.41 or ECMWF data

4.5 FILTERING OF RETRIEVALS WITH HIGHER RMSE BETWEEN MEASURED AND MODELLED SPECTRA

This step was aimed to remove values of retrievals from the time-series obtained in above steps (during inversion of SCOPE, thus RTMo and SPART), where the fit between modelled spectra (by retrieval algorithms) and measured spectra were insufficient after minimization of the cost function. A threshold RMSE value between measured and modelled spectra was chosen for each sensor and model combination by plotting histograms of RMSE values. In case of inversion of SPART model with S3 data, two different values for this threshold were chosen for inversion using cost function with prior and no prior respectively. The retrievals were rejected where the RMSE during spectral fitting were higher than this chosen threshold, and was assumed that the parameters could not be retrieved with confidence in these cases.

4.6 EVALUATION OF RETRIEVED PARAMETERS

4.6.1 Parameters Retrieved from Sentinel-3 OLCI Data

Prikaziuk et al., 2021 explored the extraction of time-series of TOA radiance of S3 OLCI observations by different means, and warned users for potential problems. They also highlighted the problem that the effective footprint of S3 observations can vary based on the extraction method and source of data. The authors also warned that S3 has 365 different orbits and almost every point can be observed from different angles with high temporal resolution. But this leads to jumping pixel centres around the point of interest and a larger effective footprint.

In this study, original images were downloaded from Copernicus Open Access Data Hub Service (DHUS) or ONDA DIAS and time-series was extracted using geo-coordinates by SNAP tool (as described in Sections 3.2.1 and 4.2.1), as recommended by Prikaziuk et al., 2021. Figure 4.2 shows the actual pixel centres extracted from S3A and S3B dataset for the point 2019_a for 2019 - 2020 crop growing season. A buffer of 212 m (background on choosing this distance is given in next paragraph) was drawn around these pixel centres and merged to get the blue polygon (in Figure 4.2), which shows the effective footprint. Another buffer of 212 m (transparent pink circle in Figure 4.2) was drawn around the actual point of interest. This shows that all the pixel centres lie inside this buffer (transparent pink circle). But their actual footprint (blue polygon) covers a larger area and the pixel centres are located on may different agricultural fields rather than on the actual point of interest. There may be different vegetation on different fields and land-cover inside the effective footprint may not be homogeneous. This makes retrieved LAI with field measured LAI (which was measured at the actual point of interest) unrelated with each other. For this reason, in this study this type comparison has not been approached. The comparison between retrieved time-series of LAI from S3 dataset and MODIS LAI has been carried out just for a plausibility check, acknowledging that both of remote sensing based datasets have their limitations.

The buffer distance of 212 m in the above description was considered based on the S3 OLCI pixel resolution (300 m). Theoretically, the nearest pixel to the point should lie at a half distance ($\frac{300\ m}{2}$ = 150 m) to pixel centre. But considering possible pixel rotation, the distance was calculated from the corner of a pixel, which is, $150\ m \times \sqrt{2} \approx 212\ m$. This threshold was also suggested by Prikaziuk et al., 2021.

Besides crop biophysical parameters, atmospheric parameters were also retrieved with SPART model using S3 data. These retrieved parameters were compared against that of ECMWF estimation.

4.6.2 Parameters Retrieved from Sentinel-2 MSI Data

S2 MSI has comparatively higher spatial resolution (Table 4.2) than S3 OLCI sensor. This higher spatial resolution enabled a one-to-one comparison between in-situ LAI (described in Section 3.2.7) and LAI retrieved using S2 observations. In some cases, there are no S2 overpass exactly on the date of in-situ measurements. In these cases, in-situ measurements were compared with retrievals from 1 - 3 days before or after S2 overpass, assuming that plant parameters like LAI are conservative over this time frame (with the exception of harvest).

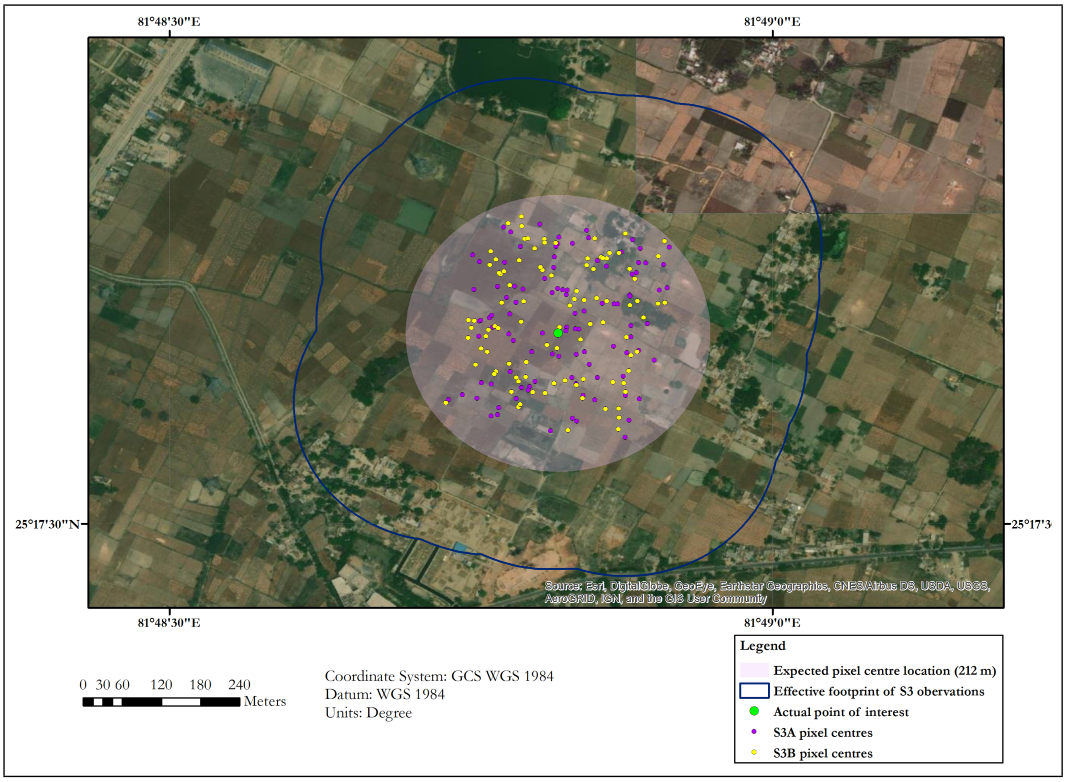

Figure 4.2: *Effective ground footprint (blue polygon) of Sentinel-3 OLCI dataset, expected ground footprint (transparent pink polygon) and S3A (magenta dots) and S3B (yellow dots) pixel centres.*

The correlation coefficient (r), coefficient of determination (R^2) and RMSE were calculated using Equations 4.16, 4.17 and 4.18 respectively:

$$r = \frac{\sum_{i=1}^{n}(x_i - \bar{x})(y_i - \bar{y})}{\sqrt{\sum_{i=1}^{n}(x_i - \bar{x})^2}\sqrt{\sum_{i=1}^{n}(y_i - \bar{y})^2}} \tag{4.16}$$

$$R^2 = r^2 \tag{4.17}$$

$$RMSE = \sqrt{(\frac{1}{n})\sum_{i=1}^{n}(x_i - y_i)^2} \tag{4.18}$$

Where x_i and y_i are i^{th} point in dataset x and y respectively. $\bar{x}$ and $\bar{y}$ are mean of dataset x and y respectively. n is number of points in the dataset. Here x and y are measured and retrieved LAI respectively.

A comparative check between MODIS LAI product (described in Section 3.2.4) and retrieved LAI was also performed. A comparative check between atmospheric parameters retrieved by SPART with that of provided by ECMWF has also been performed in this study.

4.7 PREPARING TIME-SERIES OF RETRIEVED PARAMETERS AS INPUT TO THE SCOPE

4.7.1 Choosing Best Performing Time-series

Different parameters were retrieved using different models, sensors and settings of the retrieval algorithms. A total of 12 time-series were retrieved per point of interest, resulting in 60 different time-series for the 5 points (Table 3.2) considered in this study. It was important to choose a few of the best performing time-series from it for further simulation of carbon and water fluxes with SCOPE.

There were four cases involved, i.e., **i)** parameters retrieved with SPART and S2 data, **ii)** parameters retrieved with RTMo (thus SCOPE) and S2 data, **iii)** parameters retrieved with SPART and S3 data, **iv)** parameters retrieved with RTMo and S3 data.

For the first two cases, a one-to-one comparison between retrieved LAI and ground measured LAI was performed and statistical parameters were calculated as described in Section 4.6.2. The time series with retrieved LAI values that shows lowest RMSE with ground measured LAI was chosen for further steps. In the third case, no one-to-one comparison with in-situ measurements was performed. Instead, the time series with the most realistic seasonal cycle was selected from the SPART retrievals for further analysis, which appeared to be the retrieval without considering any prior information in the cost function. In the fourth case, all time-series exhibited spikes, no one-to-one comparison was performed, and none of the retrievals was selected for further analysis.

4.7.2 LOESS Curve Fitting

It was found that the chosen time-series of retrieved parameters were not very smooth and contains some unrealistic spikes. A curve fitting method has been adopted to smooth the time-series: the Locally Estimated Scatterplot Smoothing (LOESS) algorithm (Cleveland et al., 1992) as implemented in R (R Core Team, 2020). In this method, multiple regressions are fitted in a local neighborhood. The size of the local neighbourhood plays an important role as for fitting at a certain point, points within its local neighbourhood are considered which are weighted by its distance from the point in consideration. The size of the neighbourhood is defined by an argument called 'span' in the LOESS function (which is part of 'stats' package) in R (R Core Team, 2020). In this study, a fixed value of 0.4 (which means 40% smoothing span will be used for curve-fitting) was set to this 'span' argument as there was many time-series with many parameters were involved.

The retrieved parameters were interpolated to a daily interval from the fitted LOESS curve using 'predict' (part of 'Companion to Applied Regression (car)' package) function (Fox & Weisberg, 2019) in R (R Core Team, 2020). Sometimes, some of the predicted values of certain parameters goes to a physically implausible range (i.e., lower than the lower bound or higher than the upper bound). In these cases, the values were replaced by values of lower and upper bound of parameters respectively. An example of this case is, sometimes the values of LAI were almost closer to zero for few consecutive retrievals. When the values of LAI were interpolated for the missing dates from these retrievals, it was found some of the interpolated values are in negative range (but closer to zero). In this case, those negative values were replaced by zero, as negative value of LAI is physically not possible.

4.8 ECOSYSTEM FLUX SIMULATION WITH SCOPE MODEL

The main input parameters for the SCOPE are listed in Table 2.4. The input parameters can be broadly classified into two types, i.e., **i)** parameters describing soil and canopy and **ii)** parameters describing meteorological conditions. The time series of retrieved canopy and soil parameters (in some cases) as well as time series of meteorological variables from ERA5 data (from Section 4.2.4) were used as input for the SCOPE simulation. For some other parameters, either default values from Yang, Prikaziuk et al., 2020 or constant values were used. The values of the input parameters used for SCOPE are summarized in Table 4.6.

Two of the important parameters for SCOPE simulation are V_{cmo} and Ball-Berry stomatal parameter (m). Unlike LAI and other crop biophysical parameters, these parameters can not retrieved using remote sensing data. These parameters can only be measured with some in-vivo experimentation in the study area, which was not possible during the course of this study. As an alternative, a constant value of 85 $\mu mol\ m^2 s^{-1}$ and 12 were used for V_{cmo} and m. SCOPE can not simulate respiration of the vegetation. But it can use a respiration rate as proportion of V_{cmo} (Rdparam). The use of this Rdparam was leading to negative GPP values in some cases as it was considering a higher respiration than carbon assimilation. So, zero was used as the value of Rdparam. In case of solar zenith angle in SCOPE (tts), a constant value of 30 were used as sensitivity of the simulated fluxes is low to tts.

Table 4.6: Values of input parameters used in SCOPE simulation

Variable	Values used	Unit	Description
FLUSPECT			
Cab	Retrieved time-series	$\mu g\ cm^{-2}$	leaf chlorophyll concentration
Cca	10 or retrieved time-series	$\mu g\ cm^{-2}$	leaf carotenoid concentration
Cdm	Retrieved time-series	$g\ cm^{-2}$	leaf dry matter content
Cw	Retrieved time-series	cm	equivalent water thickness in leaves
Cs	Retrieved time-series	-	leaf senescence parameters
Cant	Retrieved time-series	$\mu g\ cm^{-2}$	Anthocyanin content
N	Retrieved time-series	-	leaf structure parameter
rho_thermal	0.01	-	broadband thermal reflectance
tau_thermal	0.01	-	broadband thermal transmittance
Leaf_Biochemical			
Vcmo	85	$\mu mol\ m^2 s^{-1}$	carboxylation capacity at 25 degC
m	12	-	Ball-Berry stomatal parameter
BallBerry0	0.01	-	Minimum stomatal resistance
Type	0	-	Photochemical pathway: 0=C3, 1=C4
kV	0.6396	-	extinction coefficient for Vcmax in the vertical (maximum at the top). 0 for uniform Vcmax
Rdparam	0	-	Respiration = Rdparam*Vcmcax
Tparam	0.2, 0.3, 281, 308, 328	-	These are five parameters specifying the temperature response

Continued on next page

Table 4.6 – *Continued from previous page*

Variable	Values used	Unit	Description
Soil			
spectrum	1	-	Spectrum number
rss	2000	sm^{-1}	soil resistance for evaporation from the pore space
rs_thermal	0.06		broadband soil reflectance in the thermal range (1-emissivity)
cs	1180	$JKg^{-1}\,K^{-1}$	specific heat capacity of the soil
rhos	1800	$Kg\,m^{-3}$	specific mass of the soil
lambdas	1.55	$J\,m^{-1}\,K^{-1}$	heat conductivity of the soil
SMC	15	-	volumetric soil moisture content in the root zone
BSM Brightness	0.5 or retrieved time-series	-	BSM model parameter for soil brightness
BSMlat	-11.21 or retrieved time-series	deg	BSM model parameter 'lat'
BSMlon	91.34 or retrieved time-series	deg	BSM model parameter 'long'
Canopy			
LAI	Retrieved time-series	$m^2\,m^{-2}$	leaf area index
hc	2	m	vegetation height
LIDFa	Retrieved time-series	-	leaf inclination
LIDFb	Retrieved time-series	-	variation in leaf inclination
leafwidth	0.1	m	leaf width
Meteo			
z	2	m	measurement height of meteorological data
Rin	ERA5 time-series	Wm^{-2}	shortwave irradiance
Ta	ERA5 time-series	$^{\circ}C$	air temperature
Rli	ERA5 time-series	Wm^{-2}	longwave irradiance
p	ERA5 time-series	hPa	air pressure
ea	ERA5 time-series	hPa	vapour pressure
u	ERA5 time-series	ms^{-1}	wind speed
Ca	410	ppm	atmospheric CO_2 concentration
Oa	209	per mille	atmospheric O_2 concentration
Aerodynamic			
zo	0.25	m	roughness length for momentum of the canopy
d	1.34	m	displacement height
Cd	0.3	-	leaf drag coefficient
rb	10	$s\,m^{-1}$	leaf boundary resistance
CR	0.35	-	Drag coefficient for isolated tree
CD1	20.6	-	fitting parameter
Psicor	0.2	-	Roughness layer correction
CSSOIL	0.01	-	Drag coefficient for soil
rbs	10	$s\,m^{-1}$	soil boundary layer resistance

Continued on next page

Table 4.6 – *Continued from previous page*

Variable	Values used	Unit	Description
rwc	0	$s\,m^{-1}$	within canopy layer resistance
timeseries			
startDOY	20060618	date (yyyymmdd)	date of start of simulations
endDOY	20300101	date (yyyymmdd)	date of end of simulations
LAT	actual latitude of point of interest	decimal deg	Latitude
LON	actual longitude of point of interest	decimal deg	Longitude
timezn	0	hours	east of Greenwich
Angles			
tts	30	deg	solar zenith angle
tto	0	deg	observation zenith angle
psi	0	deg	azimuthal difference between solar and observation angle

4.9 EVALUATION OF SCOPE SIMULATED ECOSYSTEM FLUXES

4.9.1 Comparison with Other Global Remote Sensing Products

Direct ground measurements of ecosystem fluxes (such as, carbon flux, sensible, latent and ground heat fluxes) were not available for the study area. For this reason the simulated ecosystem fluxes were compared against other global remote sensing based products only. SCOPE simulated GPP was compared to MODIS GPP products given in Table 3.4 and simulated ET was compared to MODIS ET (Table 3.3) and ECOSTRESS ET products. The gap-filled MODIS GPP products (MOD17A2HGF and MYD17A2HGF) were used for November 2018 to April 2019 and November to December 2019. The gap-filled products are discontinued after this period. The standard MODIS GPP products (MOD17A2H and MYD17A2H) were used for January to April 2020.

The gap-filled MODIS ET (MOD16A2GF and MYD16A2GF) products were used for the period November 2018 to April 2019 and November 2019 to December 2019. Although the gap-filled product should be available until the present date (according to the product description), in reality, it ends at December 2019. So, from January 2020 to April 2020 the MOD16A2 and MYD16A2 were used for this study.

An argument for choosing data derived from ECOSTRESS instrument is to investigate if there is any significant difference in ET estimates derived from an instrument with thermal bands and an instrument (as OLCI observations are used in SCOPE modelling) with mainly optical (VIS-SWIR) bands, but no thermal bands. However, very limited observations of ECOSTRESS were available (only 9) between January 2019 to March 2019 for the crop growing season 2018-19. It is due to the fact that ECOSTRESS was facing consistent anomaly with its MSU in the early stage of its operation. For 2019-20 season, there are 14 observations between November 2019 to April 2020. It is due to the data anomaly created in band 4 of the instrument in February 2020 and also the instrument was in ISS SAFEHOLD for some time.

4.9.2 Comparison against a Unified Vegetation Index

Vegetation indices such as NDVI are commonly used for satellite based monitoring of vegetation. NDVI exploits information from red (vegetation absorbs radiation in visible domain for photosynthesis) and Near-infrared (NIR) (vegetation reflects more NIR radiation as it is unsuitable for photosynthesis) bands. A limitation of NDVI is the saturation with higher green biomass. A more robust nonlinear NDVI, which is known as kernel NDVI (kNDVI) has been suggested by Camps-Valls et al., 2021. This index has proven to better correspond with measured GPP at flux tower sites and remotely sensed SIF by the authors.

In this study, kNDVI has been calculated using Equation 4.19, as suggested by the authors. In case of S3 OLCI, TOC reflectances from band 8 and 17 were used as red and NIR band respectively to calculate kNDVI. For S2 MSI, TOC reflectance from band 4 and 8 were used as red and NIR bands respectively for the same.

The kNDVI was calculated to check if it corresponds to SCOPE simulated GPP and MODIS GPP products as a means of qualitative evaluation.

$$\begin{gathered} NDVI = \frac{NIR - Red}{NIR + Red} \\ kNDVI = tanh(NDVI^2) \end{gathered} \tag{4.19}$$

4.10 ECOSYSTEM EFFICIENCY PARAMETERS AND CROP YIELD ESTIMATION

4.10.1 Ecosystem Efficiency Parameters

The output of the SCOPE can be used to calculate some of the ecosystem efficiency parameters. For example, Light Use Efficiency (LUE) can be calculated using GPP and aPAR (Equation 4.20), WUE can be calculated using GPP and ET (Equation 4.21) and Evaporative fraction (EF) can be calculated using Latent heat flux (lE) and sensible heat flux (H) (Equation 4.22). These equations were taken from Prikaziuk et al., 2020. This ecosystem efficiency parameters or ecosystem functional properties were calculated as complementary information.

$$LUE = \frac{GPP}{aPAR} \tag{4.20}$$

$$WUE = \frac{GPP}{ET} \tag{4.21}$$

$$EF = \frac{lE}{lE + H} \tag{4.22}$$

4.10.2 Crop Yield Estimation

GPP or photosynthesis was simulated by the SCOPE model at a daily time step. The SCOPE model provides GPP in $\mu mol\ m^{-2}\ s^{-1}$. The simulated GPP was converted into mass flux density and aggregated from the date of sowing to the date of harvesting. Ideally, the GR and MR should have been subtracted from the GPP and then crop yield should be calculated. Because SCOPE cannot simulate plant respiration, a Harvest Index (HI) of 0.4 (Maheswarappa et al., 2011) was directly multiplied with GPP to have an estimation of crop yield as shown in Equations 4.23:

$$\begin{aligned}
GPP\ [gC\ m^{-2}\ s^{-1}] &= GPP\ [\mu mol\ m^{-2}\ s^{-1}] \times 12 \times 10^{-6} \\
GPP\ [gC\ ha^{-1}\ day^{-1}] &= GPP\ [gC\ m^{-2}\ s^{-1}] \times 24 \times 3600 \times 10000 \\
GPP\ [gC\ ha^{-1}\ season^{-1}] &= \sum_{sowing\ date}^{harvesting\ date} GPP\ [gC\ ha^{-1}\ day^{-1}] \\
GPP\ [t\ ha^{-1}\ season^{-1}] &= GPP\ [gC\ ha^{-1}\ season^{-1}] \times 10^{-6} \\
yield\ [t\ ha^{-1}\ season^{-1}] &= GPP\ [t\ ha^{-1}\ season^{-1}] \times 0.4
\end{aligned} \tag{4.23}$$

The sowing and harvesting date for wheat for each points of interest are given in Table 4.7.

Table 4.7 Sowing and harvesting date of wheat at the points of interest

Location ID	Sowing date	Harvesting date
2018_a	01-December-2018	19-April-2019
2018_b	07-December-2018	19-April-2019
2019_a	18-November-2019	12-April-2020
2019_b	28-November-2019	12-April-2020
2019_c	04-December-2019	21-April-2020

This page is intentionally left blank.

Chapter 5

Results

The results obtained from different stages of the methodologies are described in the following sections.

5.1 DATA PRE-PROCESSING

5.1.1 Atmospheric Correction of Sentinel-3 OLCI TOA Radiance

Two different spectra observed on 21st December 2018 (04:21:29 hrs.) and 22nd December 2018 (04:56:21 hrs.) by S3A and S3B respectively were chosen to illustrate the results of atmospheric correction for two points of interest (i.e., 2018_a and 2018_b) of crop growing season 2018-19. For the other crop growing season (2019-20), there were S3A and S3B observations on a same day (21st December 2019) at 04:58:28 hrs. and 04:19:30 hrs. respectively and these two were chosen to illustrate the atmospheric correction results at three points of interest (i.e., 2019_a, 2019_b and 2019_c). Figure 5.1 shows some differences in the observation of S3A and S3B. Moreover, the difference between TOA and TOC reflectance can be noticed, as well as dips in reflectance near band 13 and 14 (which may not be very ideal for retrieval).

Time-series of TOC reflectance for both the crop growth season were plotted to show the variation of S3 observed reflectance at different crop stages. For this purpose, a spectrum was plotted from an observation around the middle of each month (from November to April) in the two crop growing seasons. Figure 5.2 shows the reflectance time-series for the season 2018-19. The same for the wheat growing season for 2019-20 is shown in Figure 5.3. It can be observed from both the Figure 5.2 and Figure 5.3 that the reflectance in the visible range was lower when the crop was greener (DOY 349[2018], 44[2019], 47[2020], 76[2020]) due to the absorption of light by chlorophyll.

5.1.2 Unit Conversion and Aggregation of ECMWF ERA5 Meteorological Data

The variation of different weather parameters for the two crop seasons of 2018-19 and 2019-20 are plotted in Figure 5.4 and 5.5 respectively. This data served as an input for SCOPE. The weather parameters were identical for all selected points due to the coarse spatial resolution of ERA5 weather data (9km).

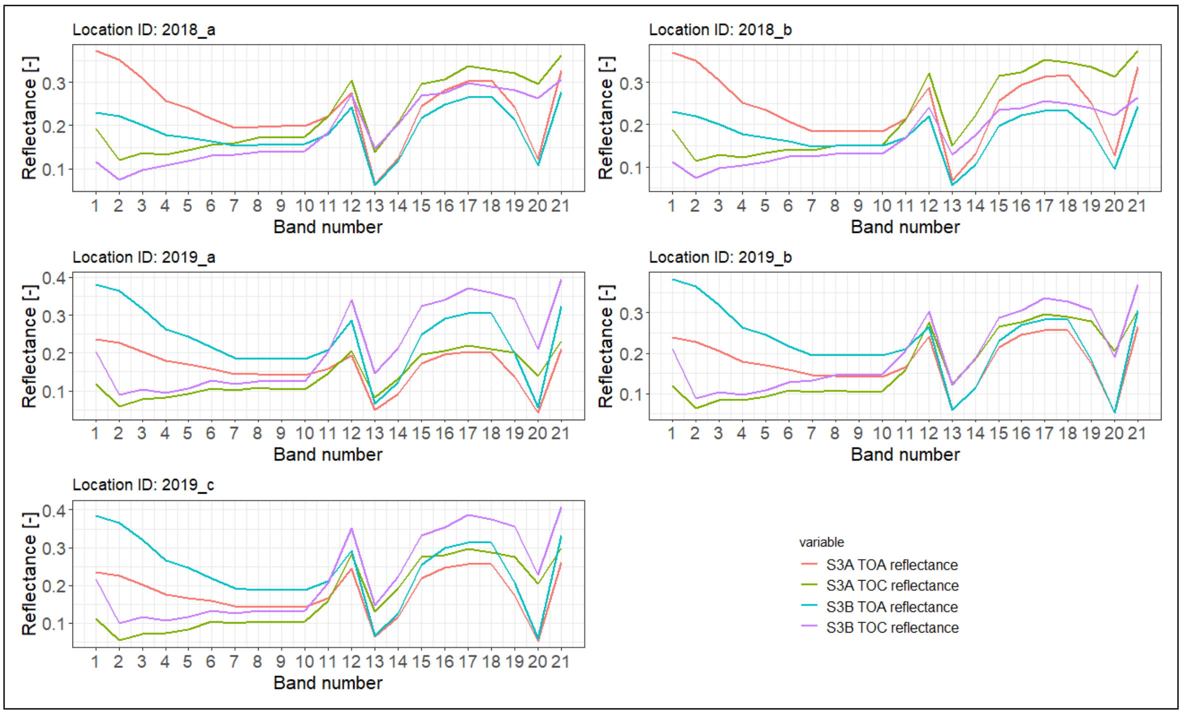

Figure 5.1: *Atmospheric correction of S3A and S3B OLCI bands for coordinates of interest*

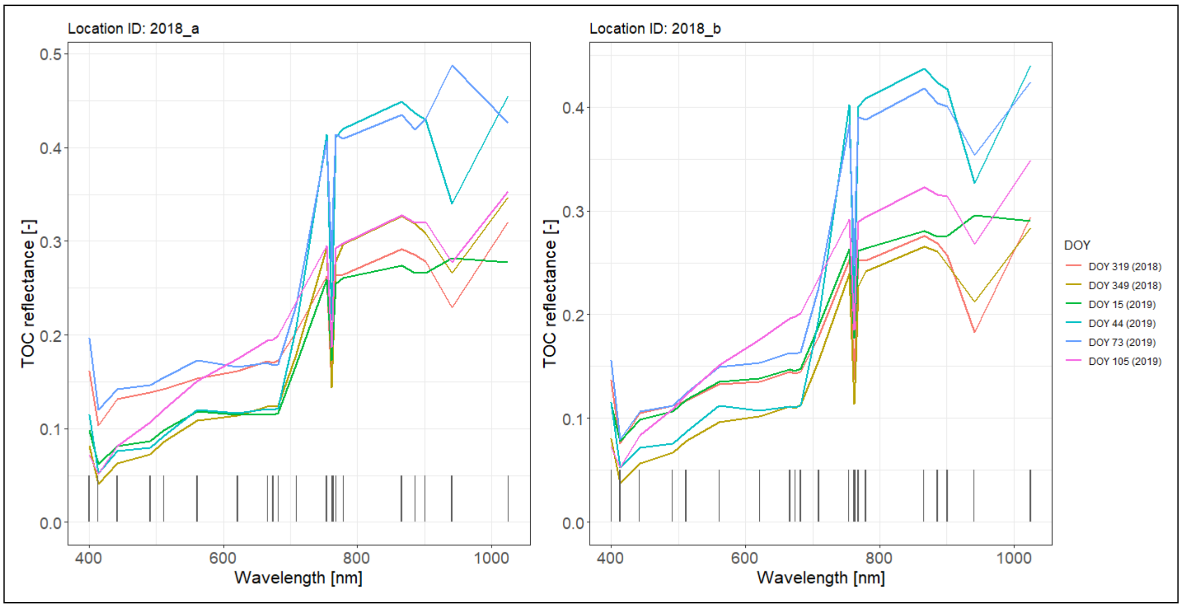

Figure 5.2: *Time-series of TOC reflectance for the coordinates of interest for 2018-19 season. The black solid lines denote the central wavelengths of each band of S3*

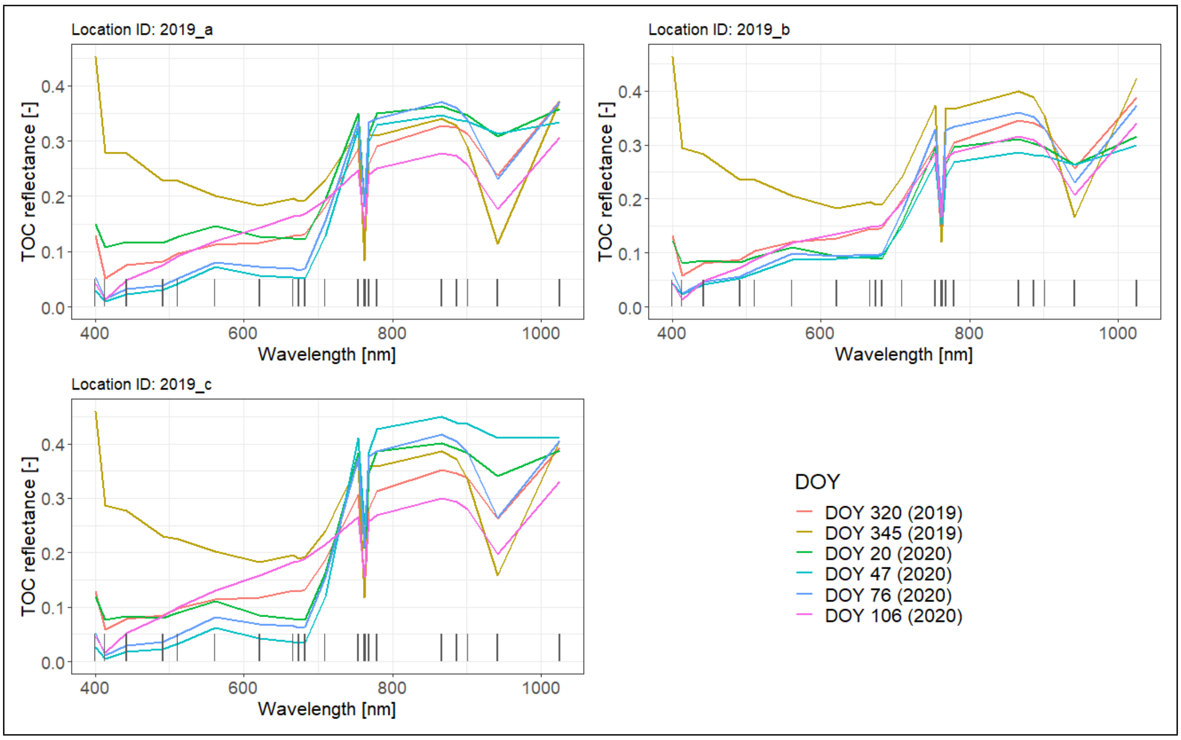

Figure 5.3: *Time-series of TOC reflectance for the coordinates of interest for 2019-20 season. The black solid lines denote the central wavelengths of each band of S3*

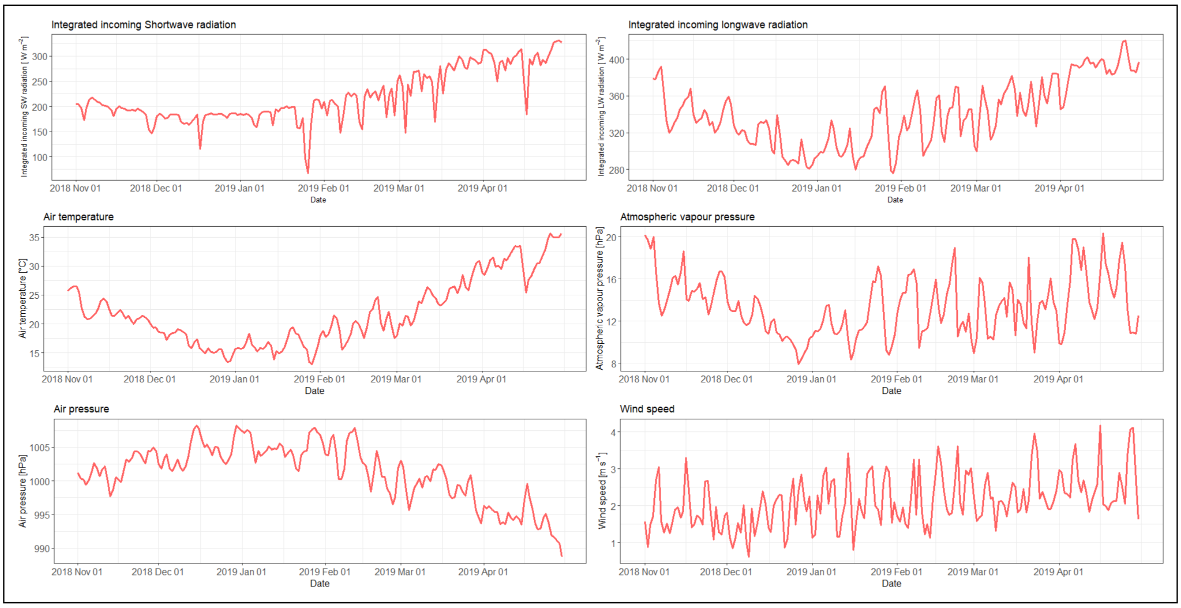

Figure 5.4: *Variation of different weather parameters for 2018-19*

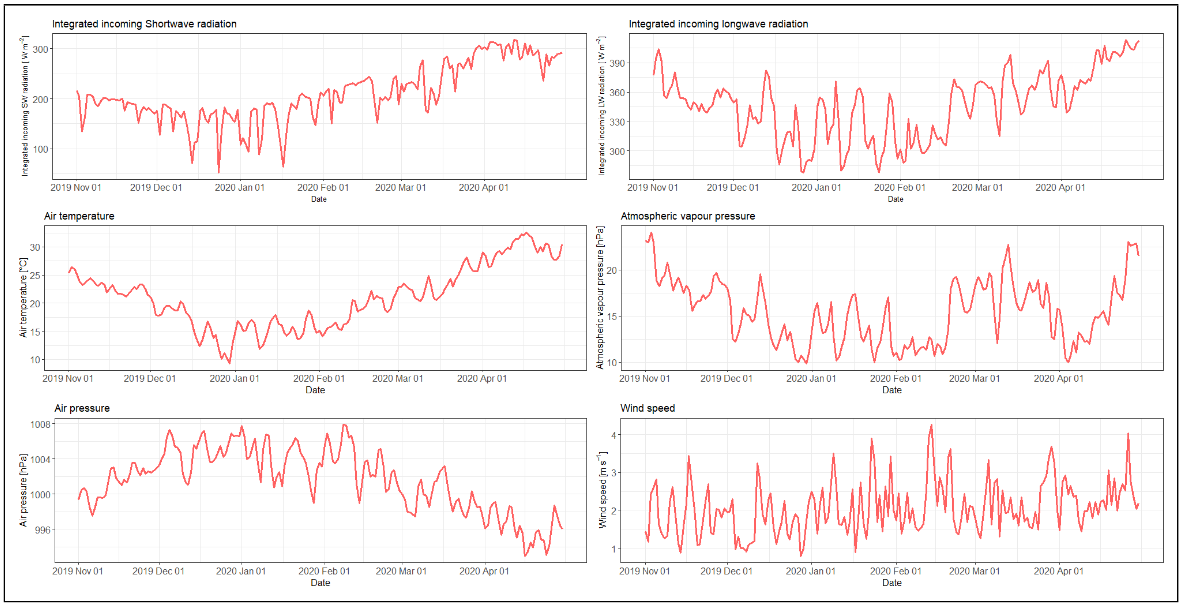

Figure 5.5: *Variation of different weather parameters for 2019-20*

5.2 SENSITIVITY OF SPART MODEL TO CAB, LAI AND AOT, WITH S2 OBSERVATIONS

The response of SPART with varying Cab values has been shown in Figure 5.6. It can be observed that there is little effect of Cab in the spectral region between 400 nm to 500 nm as well as between 800 nm to 2200 nm. But, as expected, a decreasing trend in TOC and TOA reflectance with increasing Cab values can be observed between 500 nm to 800 nm as chlorophyll absorbs light in this spectral region for photosynthesis.

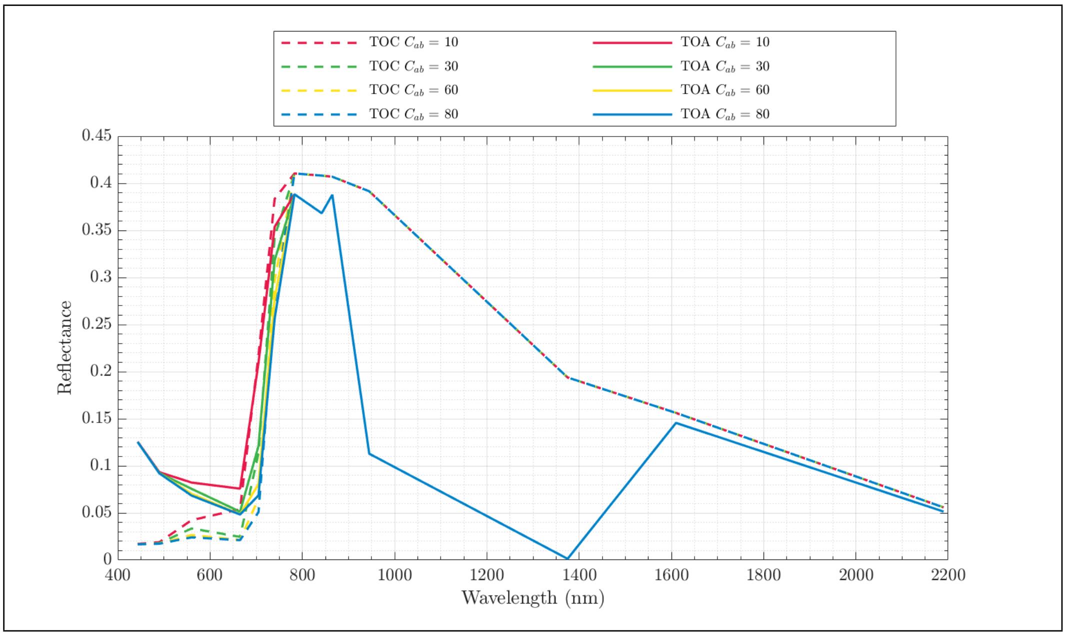

Figure 5.6: *Response of SPART model with varying chlorophyll content*

Figure 5.7 shows the effect of LAI on SPART simulation. No change in TOA reflectance can be observed between 1100 nm to 1400 nm, whereas, in visible and NIR region (400 nm to 1100 nm), a strong effect of LAI can be observed as TOC reflectance is gradually decreasing with increasing LAI values.

The effect of varying AOT on the simulation of SPART model has also been plotted in Figure 5.8. It can be observed the AOT values largely effect TOA reflectance as expected (as AOT is one of the representative parameters for the atmospheric conditions). However, there is no effect of AOT on TOC reflectance can be observed.

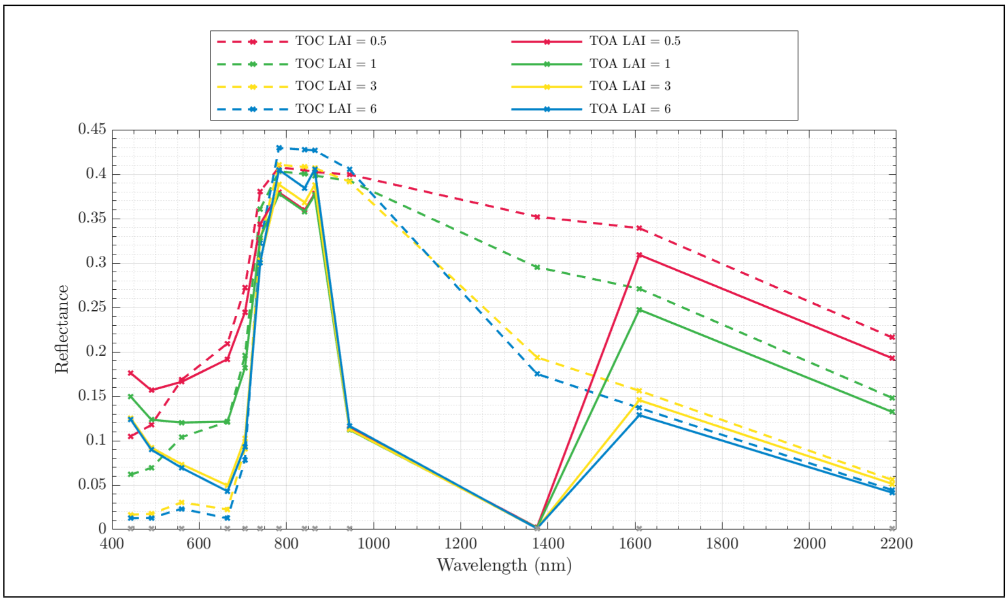

Figure 5.7: *Response of SPART model with varying LAI values*

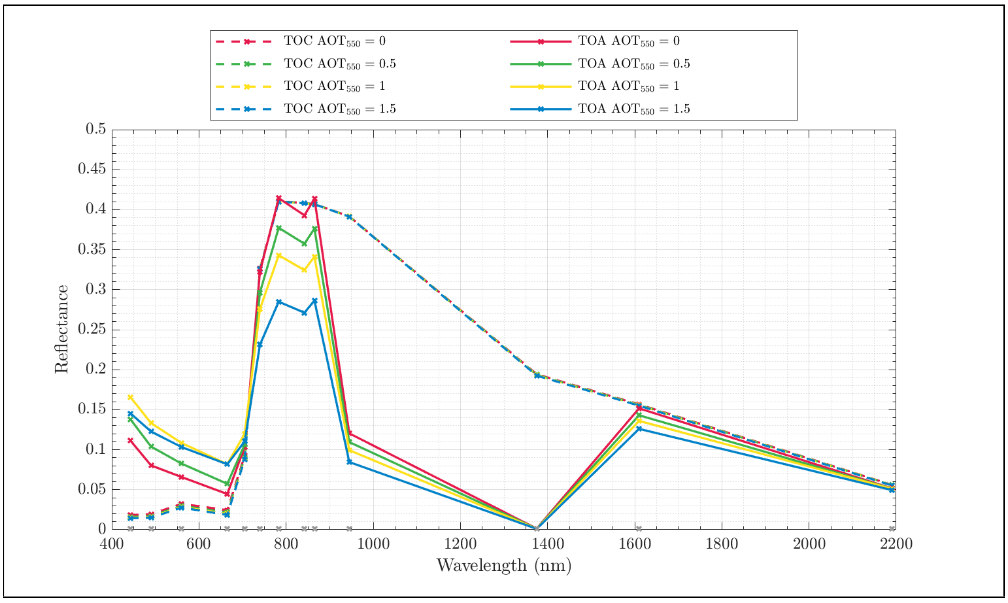

Figure 5.8: *Response of SPART model with varying AOT values*

5.3 RETRIEVAL OF CROP BIOPHYSICAL, SOIL AND ATMOSPHERIC PARAMETERS

5.3.1 Inversion of RTMo of SCOPE

A total of 4 different combinations (Table 4.4) were used to retrieve 10 crop biophysical parameters and 3 soil parameters (Table 4.3) with or without using prior information.

The time-series of retrieved parameters from Sentinel-3 data for the crop season 2018-19 is given in Figure 5.9 for the location 2018_a. Similarly, Figure 5.10 shows the retrieval results for 2019_a.

RTMo was also inverted to retrieve the same parameters using S2 data. The time-series of retrieved parameters from Sentinel-2 data are provided in Figures 5.11 and 5.12 for the locations 2018_a and respectively. The retrieval results for other point locations using both S3 and S2 data are provided in Appendix A. These retrieval results are presented after removing the retrieval where spectral fit was not very well.

Although in some cases the retrieval shows the expected pattern of crop growth, it can be observed that the retrievals are not very stable (considering the fact that plant parameters do not change rapidly) in most of the cases. Overall retrieval of some parameters using S2 data is bit better in comparison to S3 data. For example, the retrieval of LAI and senescent material (Cs) for 2019-20 season shows a typical seasonal cycle when using S2 observations as input.

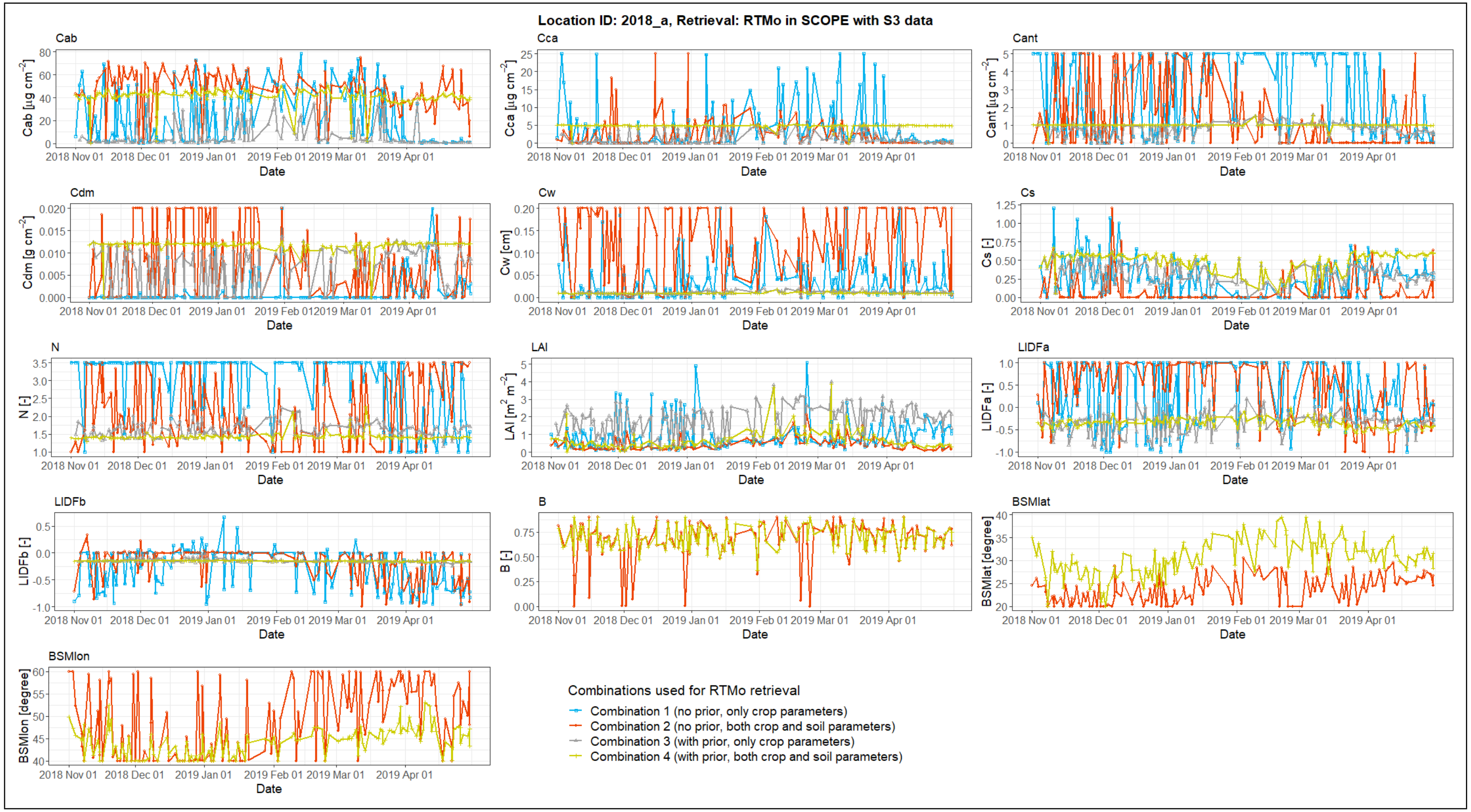

Figure 5.9: *Time-series of retrieved parameters from S3 data using different settings of RTMo for the point 2018_a*

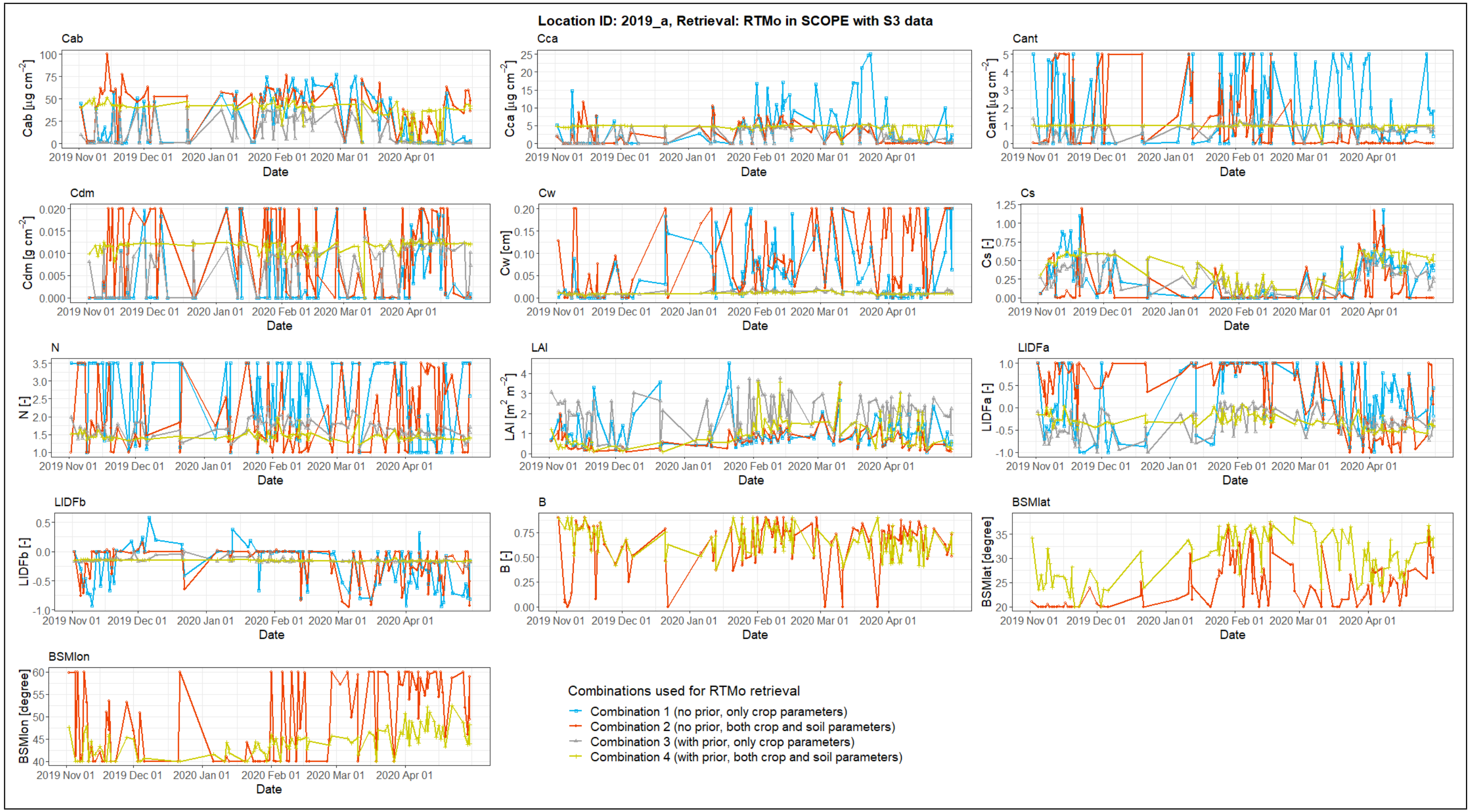

Figure 5.10: *Time-series of retrieved parameters from S3 data using different settings of RTMo for the point 2019_a*

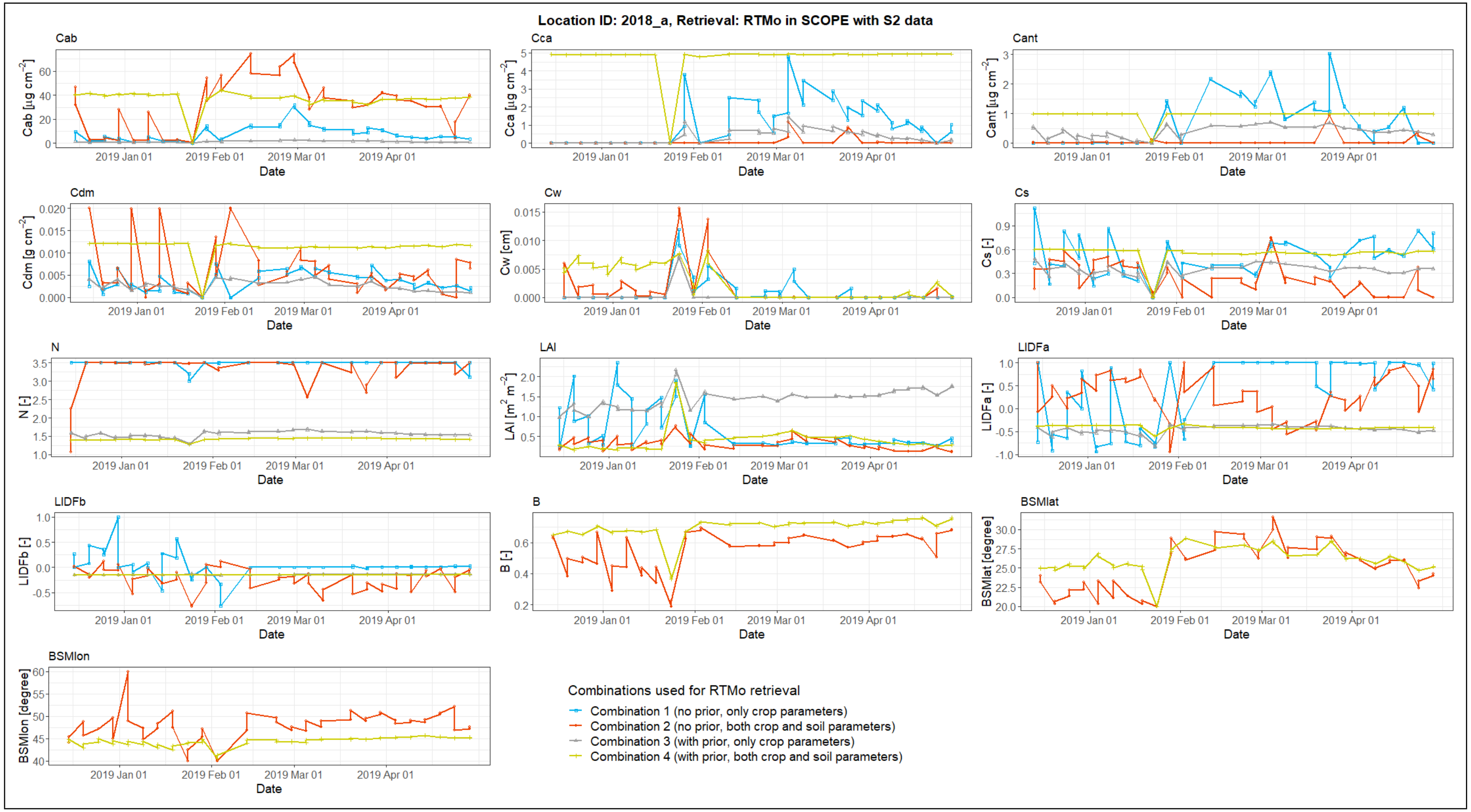

Figure 5.11: *Time-series of retrieved parameters from S2 data using different settings of RTMo for the point 2018_a*

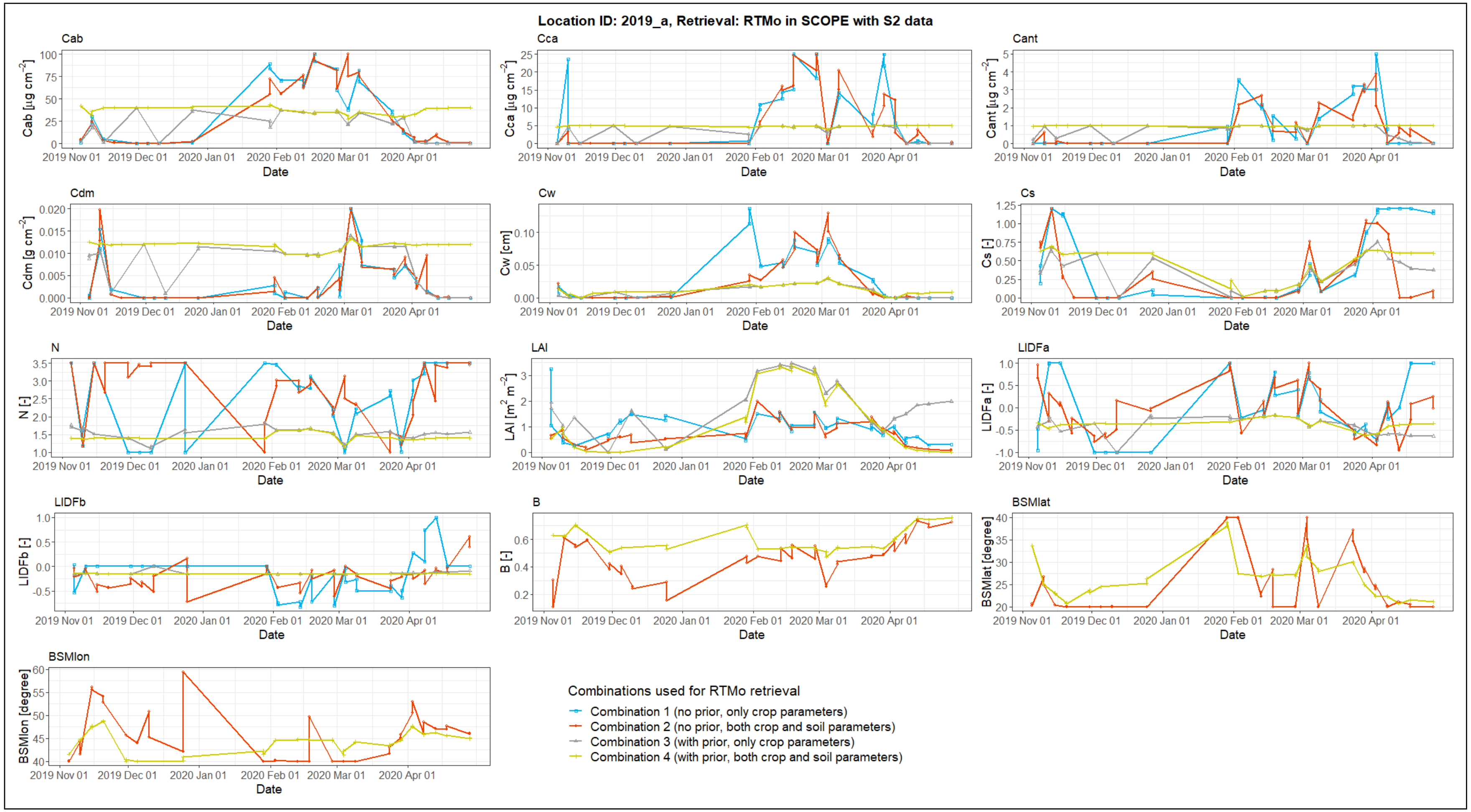

Figure 5.12: *Time-series of retrieved parameters from S2 data using different settings of RTMo for the point 2019_a*

5.3.2 Inversion of SPART

Effect on Retrievals using Different Weight Values to the Prior

The values of retrieved parameters with SPART model depend on the weight given to the prior information while using it in the cost function (Equation 4.15). If a higher weight is given to the prior, the values of retrieved parameters become closer to the initial guess, whereas a lower weight yields values of retrieved parameters closer to the retrieval without using any prior information in cost function. So, 7 different values ranging from 0.005 to 0.05 were assigned to the weight and investigated which value can give a more realistic retrieval results.

In case of S3 data, the effect of weight on the retrieval results were checked only for LAI and Cab, as shown in Figure 5.13. It can be observed that retrievals with weights between 0.05 and 0.03 converge to the prior values, whereas retrieval with weight 0.005 converge to the retrievals using no prior at all. For other values of weight ranging from 0.006 to 0.01, retrievals are somewhere in the middle.

In case of S2, the effect of weight on retrieval results were assessed for 13 different soil, vegetation and atmospheric parameters and shown in Figure 5.14. It can be observed that for some parameters (e.g. LAI, B), there is limited effect of using prior information (with different weight) on the retrieval, whereas for other parameters (e.g. Cs), retrieval using prior removes all variability from the retrieved values.

Finally, a very small value of 0.006 was assigned to the weight for performing SPART retrievals with prior information for both S3 and S2 data. This analysis was done only with the retrievals using satellite observations for location 2019_a.

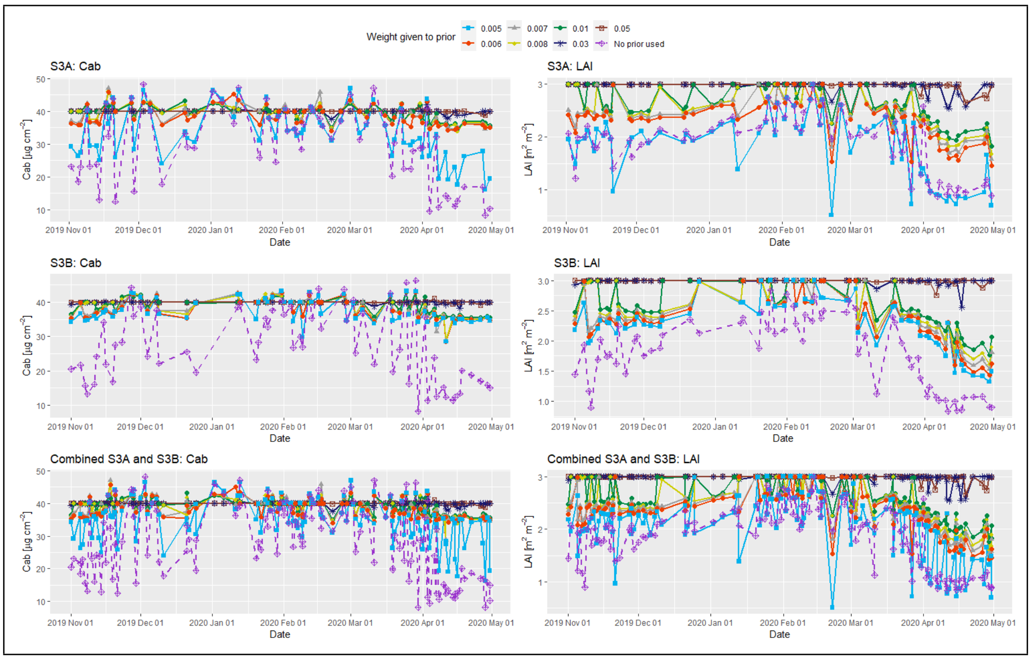

Figure 5.13: *Sensitivity analysis of retrieval of Cab and LAI using SPART and S3 data for different values of weight to the prior information in the cost function (for location 2019_a)*

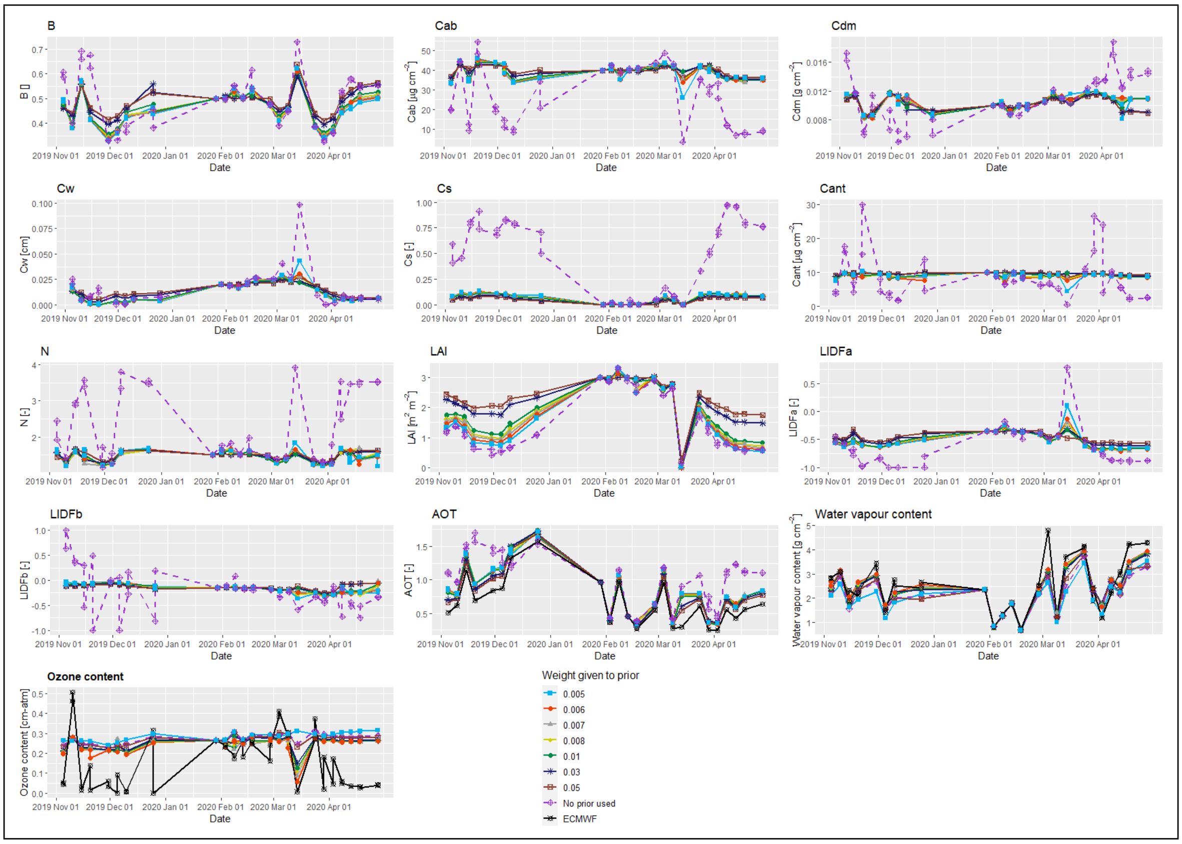

Figure 5.14: *Sensitivity analysis of SPART retrievals using S2 data for different values of weight to the prior information in the cost function (for location 2019_a)*

Retrieval of soil, vegetation and atmospheric parameters using SPART

Thereafter, soil, vegetation (leaf and canopy) and atmospheric parameters (AOT) were retrieved for all the 5 point locations both with or without using prior information in the cost function in the SPART model from the S3 and S2 observed TOA radiance.

The results of retrieved leaf, canopy and soil parameters from S3 data for the location 2018_a and 2019_a are shown in Figures 5.15 and 5.16 respectively. The results of retrieved leaf, canopy and soil parameters from S2 data for the location 2018_a, 2019_a are shown in Figures 5.17 and 5.18 respectively. The retrieval results for other point locations using both S3 and S2 data are provided in Appendix A. These retrieval results are presented after removing the retrieval where spectral fit was not very well.

It can be observed that even the retrievals from SPART using TOA observations of S3 exhibit spikes. The retrievals from S2 data show better result in some cases (for example, retrieval of LAI and Cs in Figure 5.18). The fixed value of 0.006 to the weight of the prior also resulted in retrievals close to the initial guess for many parameters in different locations.

Figure 5.15: *SPART retrieval results from S3 data for point 2018_a*

Figure 5.16: *SPART retrieval results from S3 data for point 2019_a*

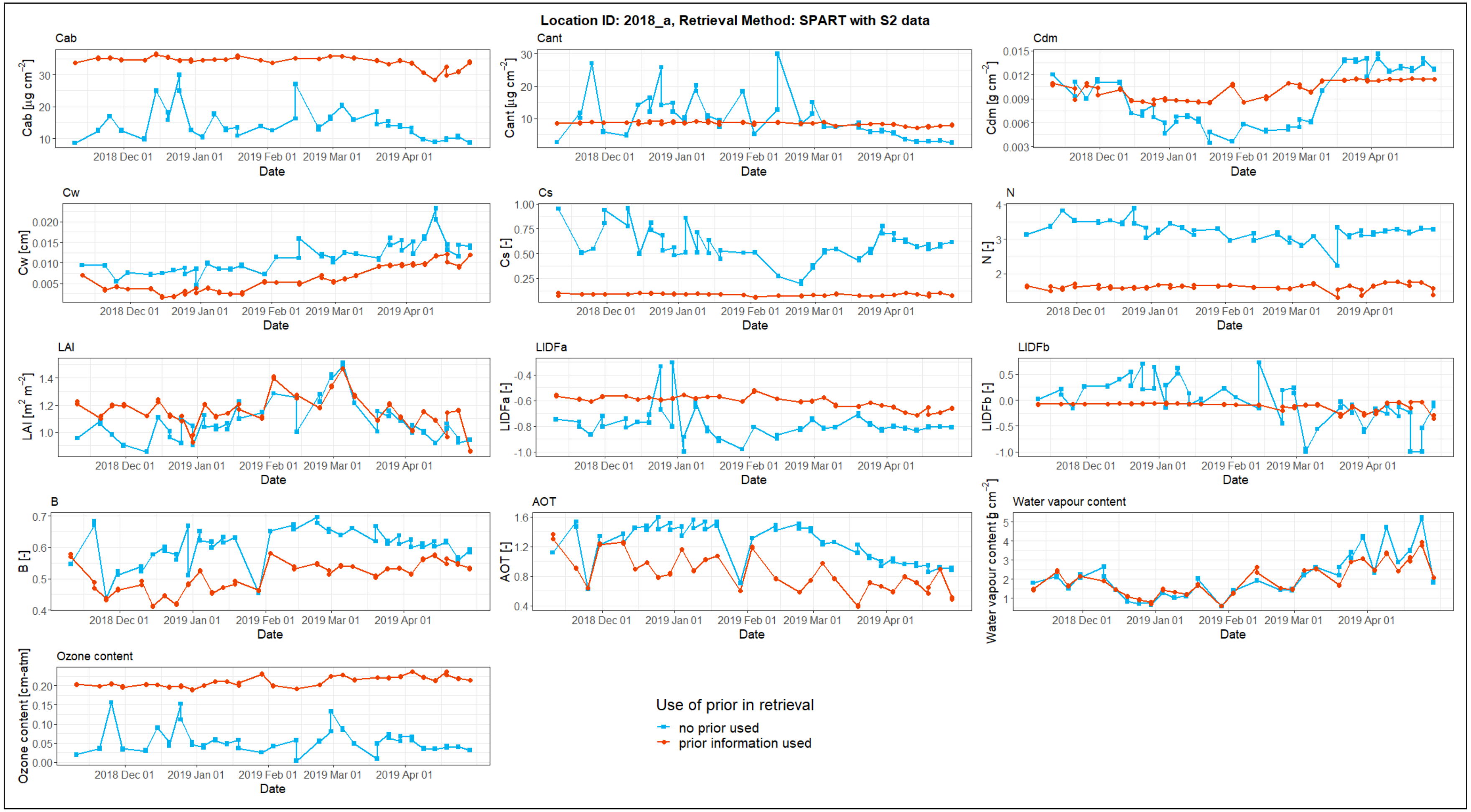

Figure 5.17: *SPART retrieval results from S2 data for point 2018_a*

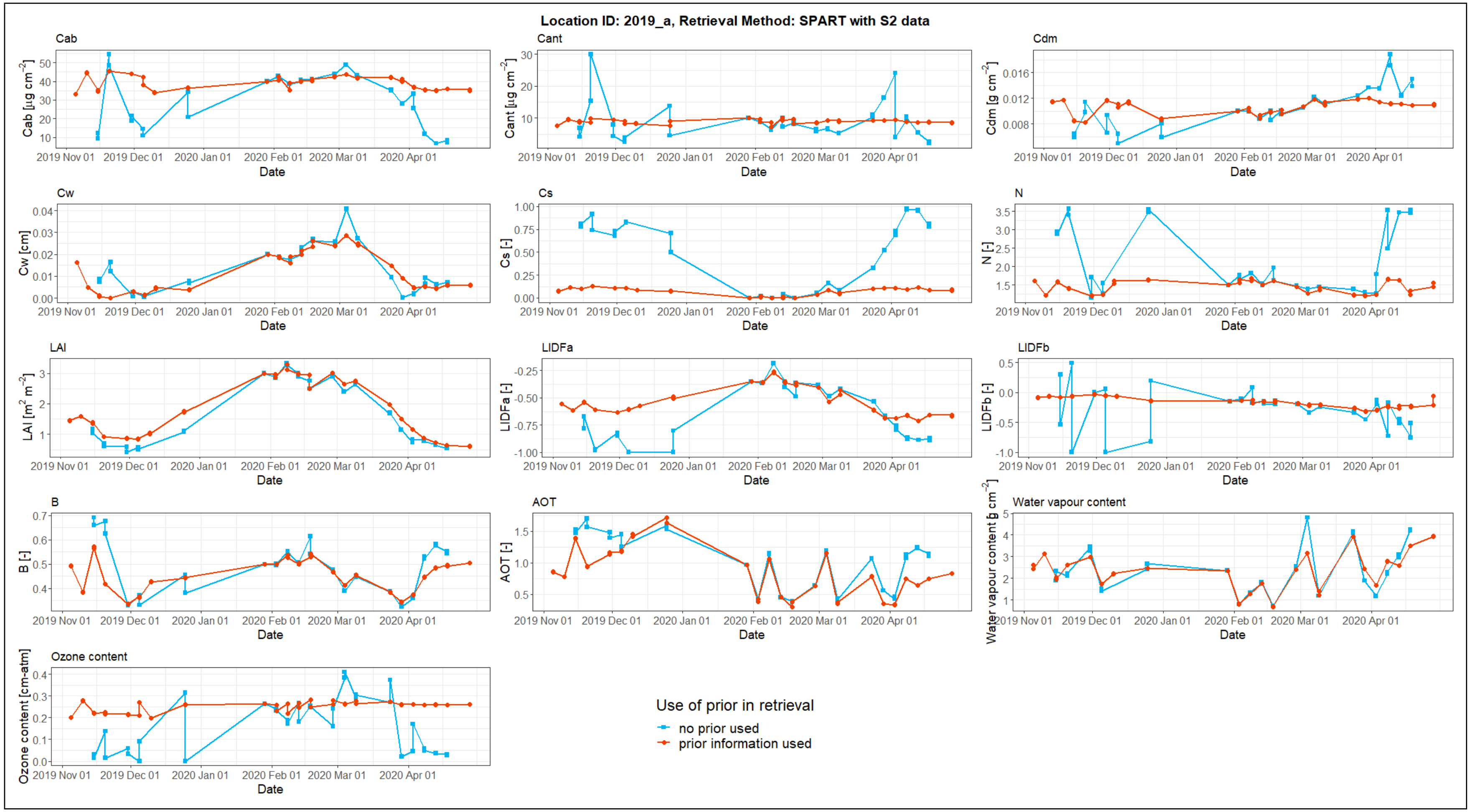

Figure 5.18: *SPART retrieval results from S2 data for point 2019_a*

5.4 RMSE FILTERING OF RETRIEVED TIME-SERIES

There were some unexpected fluctuations in all the retrieval results. Histograms of RMSE between modelled and measured spectra were plotted for each of the cases in order to chose a threshold RMSE value to filter out the retrievals where a spectral fit is of poor quality. These histogram plots for different sensor and model combination are shown in Figure 5.19 for point location 2019_a.

Constant threshold RMSE values were chosen for each sensor and model combination (for SPART with S3 data, two different thresholds were chosen for using prior or no prior in the cost function), and are given in Table 5.1.

The retrieval results in the above section (Section 5.3) are presented after doing this RMSE based filtering.

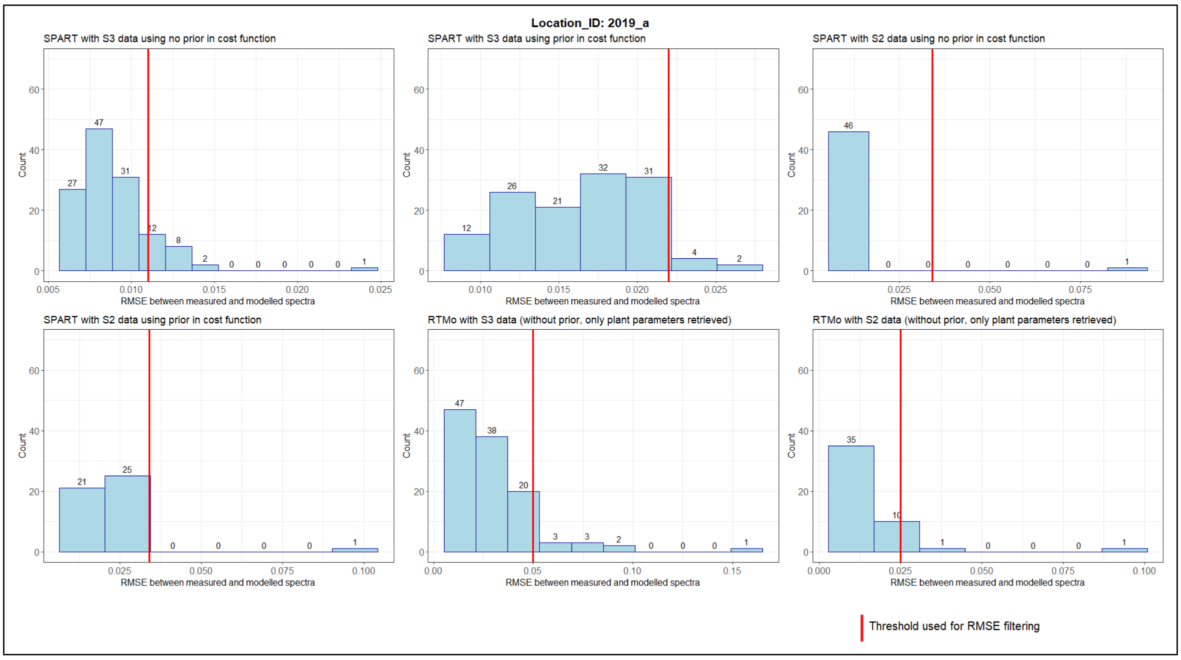

Figure 5.19: *Histogram of RMSE between measured and modelled spectra for different sensor and model combination (for location 2019_a)*

Table 5.1 Threshold used for RMSE based filtering for different sensor and model combination

Combinations	Threshold values of RMSE
SPART with S3	
no prior	0.011 $W/m^2/sr/nm$
with prior	0.022 $W/m^2/sr/nm$
SPART with S2	0.034 [-]
RTMo with S3	0.05 [-]
RTMo with S2	0.025 [-]

5.5 EVALUATION OF RETRIEVED PARAMETERS

5.5.1 Parameters Retrieved from Sentinel-3 OLCI Data

Figure 5.20 and 5.21 show the comparative plot between MODIS LAI and LAI retrieved using RTMo and SPART respectively. An underestimation of LAI values with respect to the MODIS can be noticed in both the Figures (Figure 5.20 and 5.21). The LAI retrievals using RTMo show a lot of unrealistic spikes. Although these fluctuations also exists in retrievals from SPART, the extent of fluctuations is less.

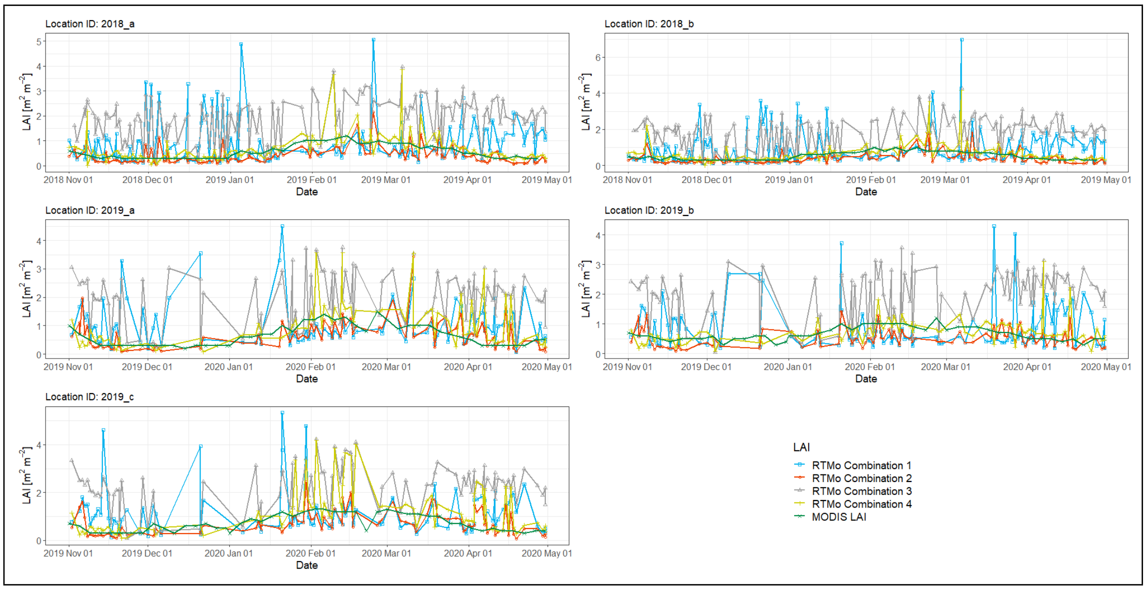

Figure 5.20: *An inter-comparison between MODIS LAI and LAI retrieved from S3 observations using RTMo*

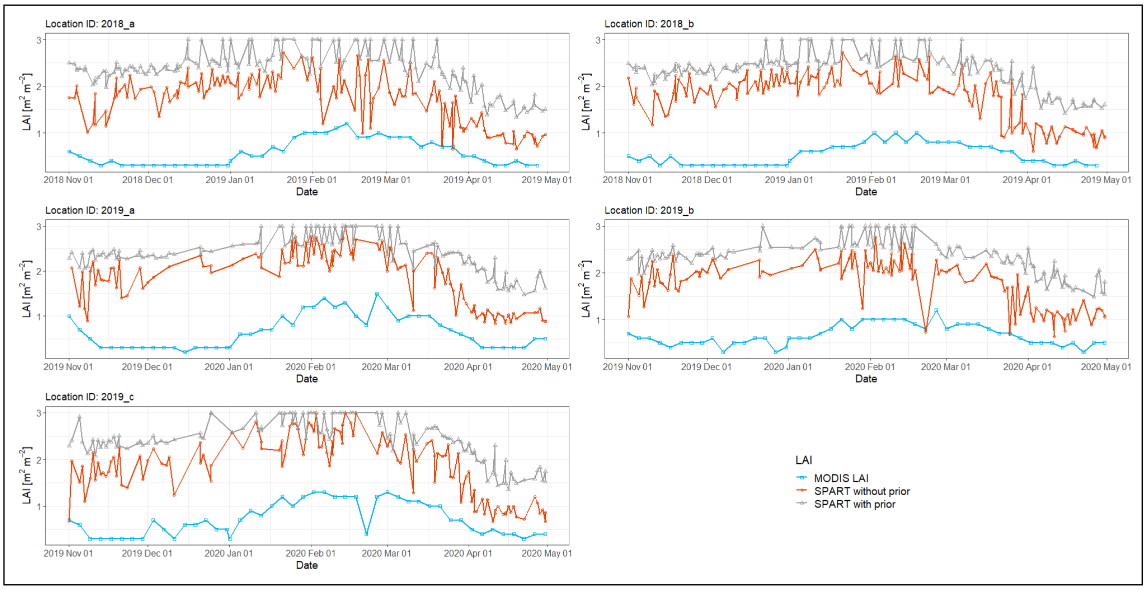

Figure 5.21: *An inter-comparison between MODIS LAI and LAI retrieved from S3 observations using SPART*

The SPART retrieved AOT were compared against interpolated ECMWF AOT values (as described in 4.2.2) at the time of S3 overpass and shown in Figure 5.22. The general trend of AOT from SPART matches with the one from ECMWF. But there quite some spikes observable in both ECMWF and AOT values that do not always co-locate in time.

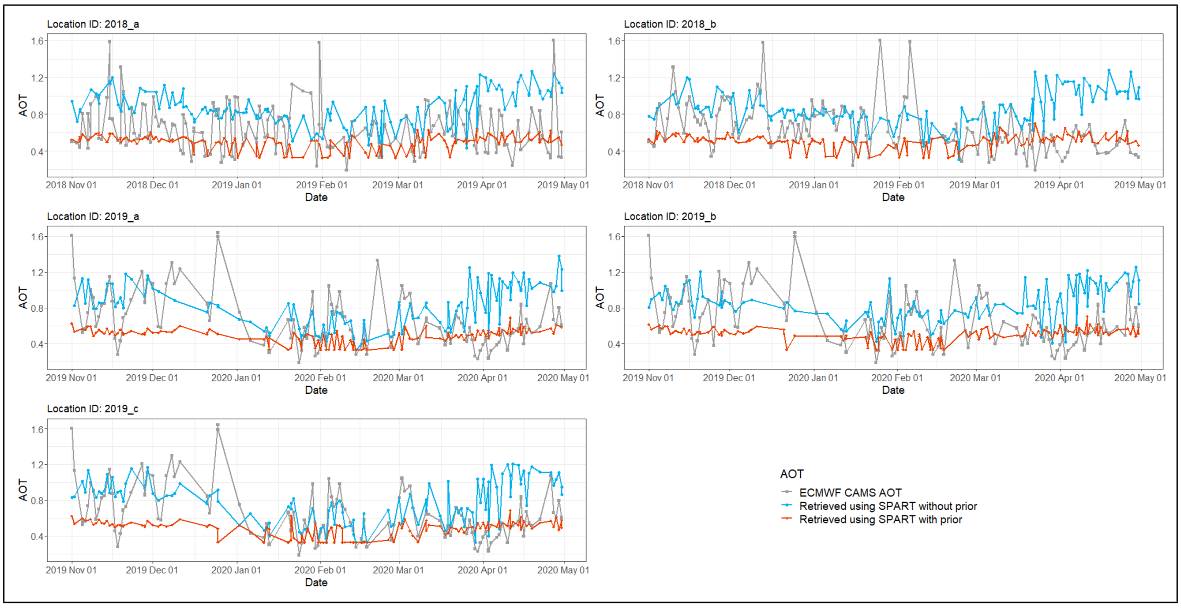

Figure 5.22: *Comparison of AOT values retrieved from S3 TOA observations using SPART, with interpolated ECMWF AOT values*

5.5.2 Parameters Retrieved from Sentinel-2 MSI Data

Figure 5.23 and 5.24 show an inter-comparison between MODIS LAI, in-situ LAI measurements and LAI retrieved from S2 observations using RTMo and SPART respectively. It can be observed that in-situ LAI measurements are comparatively low and match with the lower LAI estimations from MODIS data. The LAI retrieval using SPART (without using prior in cost function) matches well with the in-situ LAI for 2018_a and 2018_b. The LAI retrieved using SPART also shows the expected trend for all the points in the 2019-20 season. In case of retrievals using RTMo, ground LAI measurements matches with retrieval using combination 1 and 2 (Table 4.4) for point 2019_a and 2019_c.

Table 5.2 provides the r, R^2 and RMSE between the measured and modelled LAI values using different combinations for the coordinates of interest. In some cases (e.g. for combination 3 and 4 for the point 2019_c) the RMSE values is relatively high, but the correlation R^2 is relatively high too. For 2018_a and 2018_b (combination 4 and 3 respectively), a good agreement can be found between measured and retrieved LAI. In some case, the values of r is negative, showing a worse correlation of the retrievals with the observations than the prior values.

Figure 5.25 was plotted to show the agreement of RTMo retrieved LAI with in-situ LAI measurements either on same day or the closest day to the day of S2 overpass. It can be observed that in some cases, the LAI retrieved from RTMo is somewhat higher values than the measured value.

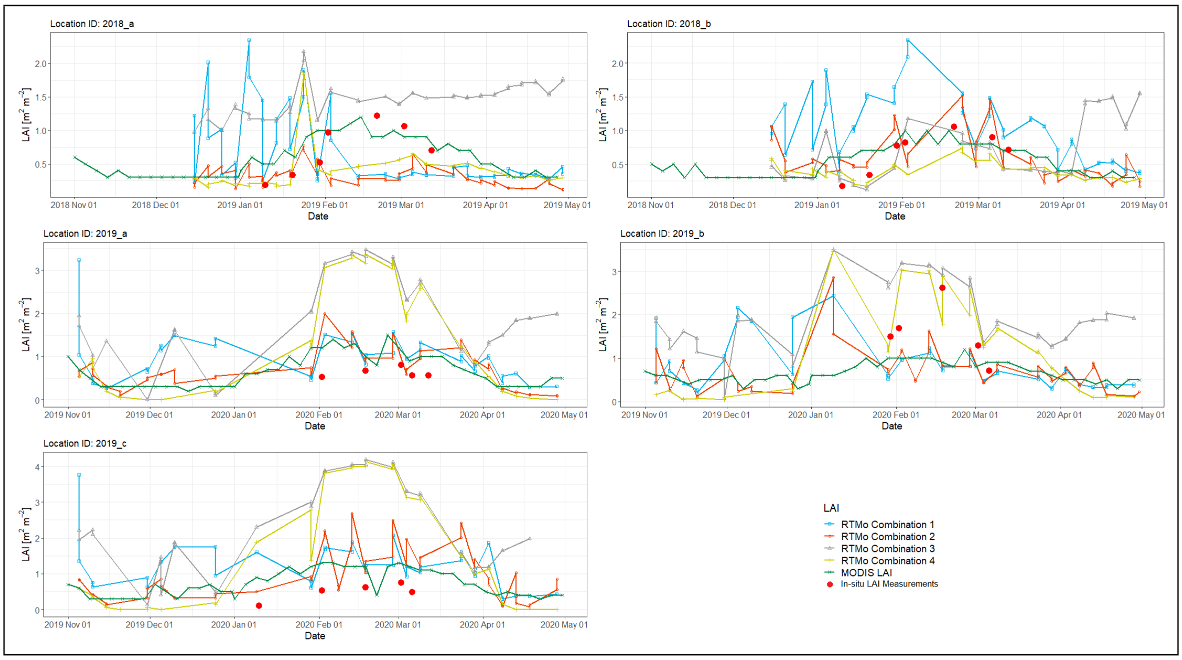

Figure 5.23: *An inter-comparison between MODIS LAI, in-situ LAI measurements and LAI retrieved from S2 observations using RTMo*

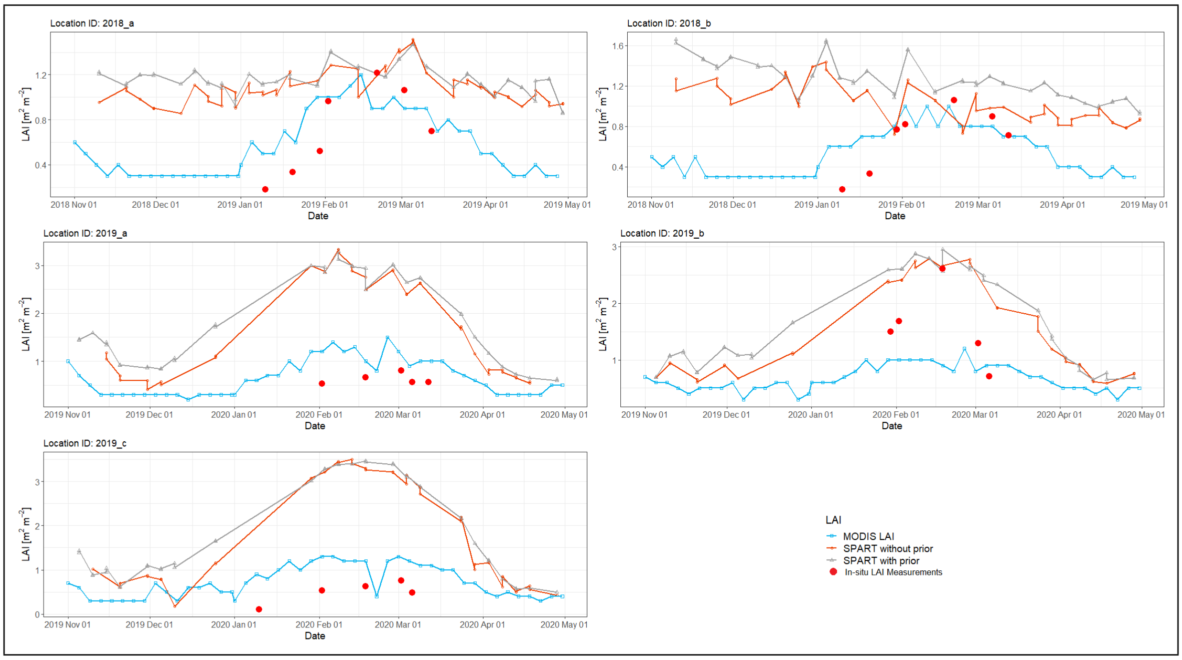

Figure 5.24: *An inter-comparison between MODIS LAI, in-situ LAI measurements and LAI retrieved from S2 observations using SPART*

Table 5.2 Correlation coefficient (r), R^2 and RMSE between LAI retrieved from S2 using different settings of RTMo and in-situ measurements

	Combination 1			Combination 2			Combination 3			Combination 4		
Location ID	r [-]	R^2 [-]	RMSE	r [-]	R^2 [-]	RMSE	r [-]	R^2 [-]	RMSE	r [-]	R^2 [-]	RMSE
2018_a	-0.26	0.07	0.67	0.10	0.01	0.51	0.84	0.70	0.73	0.80	0.64	0.40
2018_b	0.49	0.24	0.80	0.74	0.54	0.33	0.81	0.67	0.23	0.81	0.65	0.29
2019_a	-0.64	0.41	0.60	-0.78	0.60	0.78	-0.12	0.01	2.19	-0.30	0.09	2.05
2019_b	0.33	0.11	1.05	0.24	0.06	0.99	0.71	0.50	1.06	0.44	0.20	0.80
2019_c	-0.52	0.27	0.86	0.51	0.26	1.01	0.62	0.38	2.98	0.64	0.40	2.86

Here unit of RMSE is $m^2\ m^{-2}$

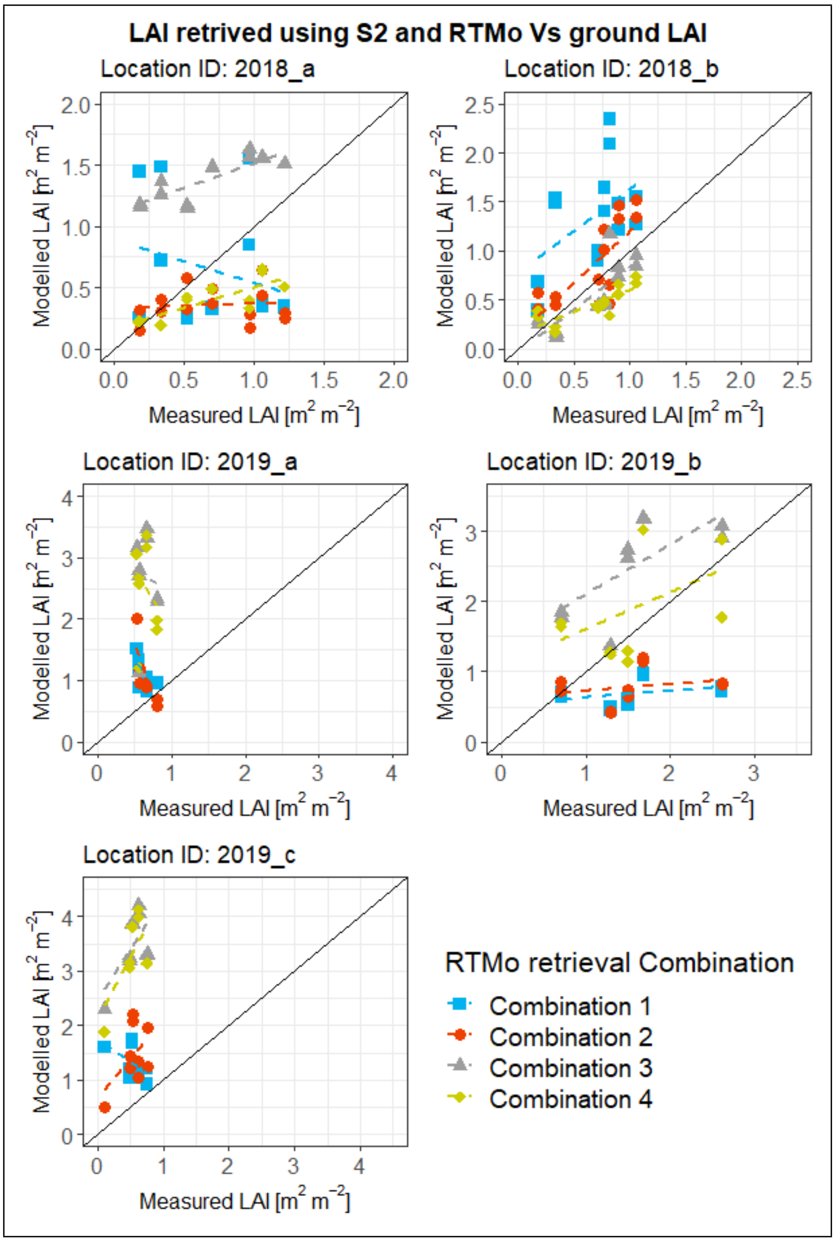

Figure 5.25: *Comparison of LAI retrieved from S2 data using RTMo with in-situ measurements (trend-lines are given as dashed lines)*

Comparative plots between in-situ measurements of LAI and SPART retrieved LAI were prepared for all the 5 point locations and shown in Figure 5.26. These plots show the overestimation of LAI with SPART in some cases (2019_a and 2019_c). Further Table 5.3 was prepared to present the r, R^2 and RMSE between the in-situ LAI measurements and SPART retrieval with S2 data. In some cases, comparatively better agreement between SPART retrieval and in-situ measurements can be found (e.g. 2018_a, 2019_b).

Table 5.3 Correlation coefficient, R^2 and RMSE between LAI retrieved from S2 using SPART and in-situ measurements

	Without using prior information			With prior information		
Location ID	r [-]	R^2 [-]	RMSE	r [-]	R^2 [-]	RMSE
2018_a	0.92	0.84	0.67	0.92	0.85	0.66
2018_b	-0.52	0.27	0.46	-0.03	0.0007	0.72
2019_a	-0.69	0.47	1.99	-0.45	0.20	2.11
2019_b	0.96	0.92	0.83	0.82	0.68	1.10
2019_c	0.27	0.07	2.49	0.28	0.08	2.59

Here unit of RMSE is $m^2\ m^{-2}$

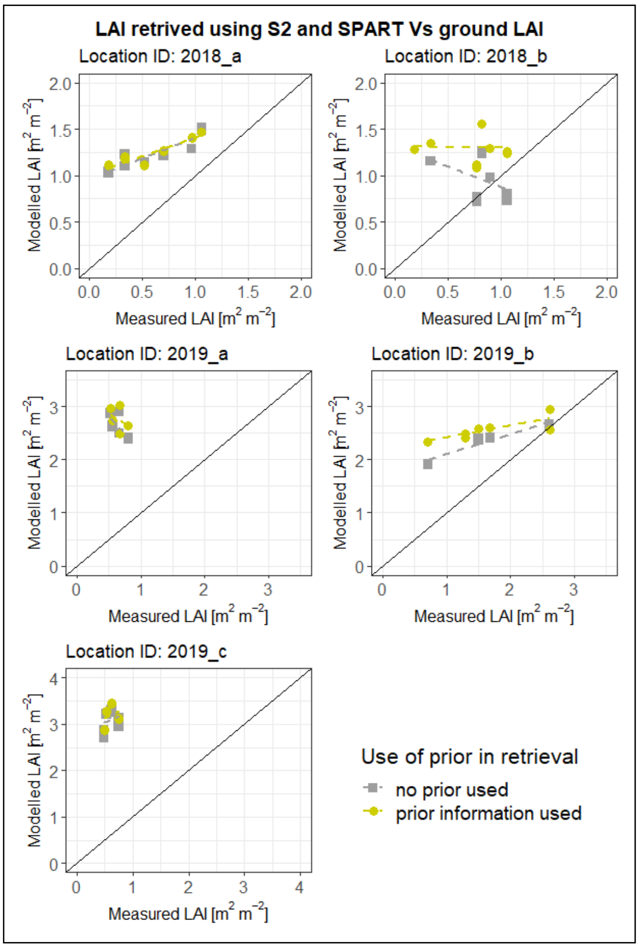

Figure 5.26: *Comparison of LAI retrieved from S2 data using SPART with in-situ measurements (trend-lines are given as dashed lines)*

The atmospheric parameters from ECMWF was supplied as initial guess of to the SPART model and then the model optimized the parameters for the spectral fit of TOA reflectance while performing the model inversion. The inter-comparison between the initial guess from ECMWF and the one retrieved from SPART are plotted in Figures 5.27, 5.28, 5.29, 5.30 and 5.31 for the location 2018_a, 2018_b, 2019_a, 2019_b and 2019_c respectively. It can be observed that the retrieved AOT and H_2O remained closer to the initial guess, whereas a large difference between initial guess and retrieval can be found for O_3 in case of not using any prior in cost function. This difference is not reasonable as concentration of O_3 remains almost constant over time. Thus, use of prior in cost function is necessary for retrieval of O_3 using SPART.

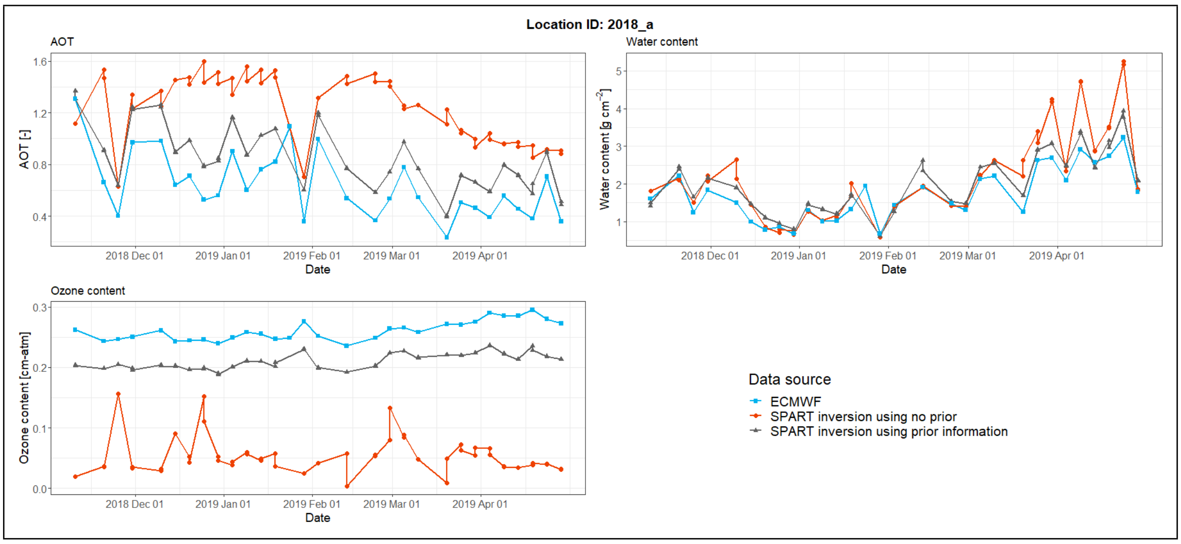

Figure 5.27: *Comparison between atmospheric parameters retrieved from S2 observations using SPART model with the ECMWF estimation (for 2018_a)*

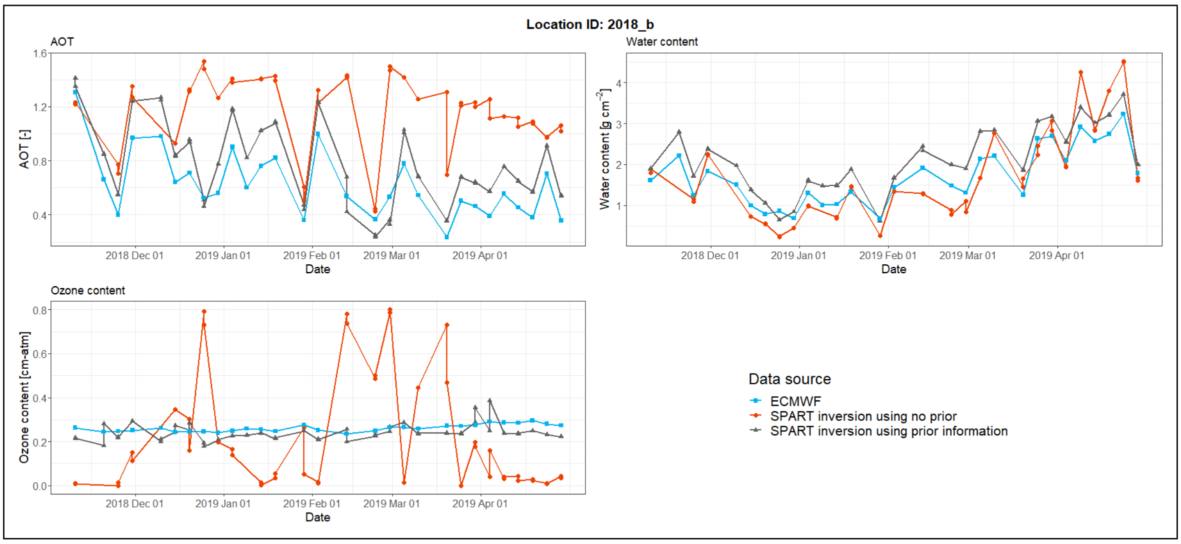

Figure 5.28: *Comparison between atmospheric parameters retrieved from S2 observations using SPART model with the ECMWF estimation (for 2018_b)*

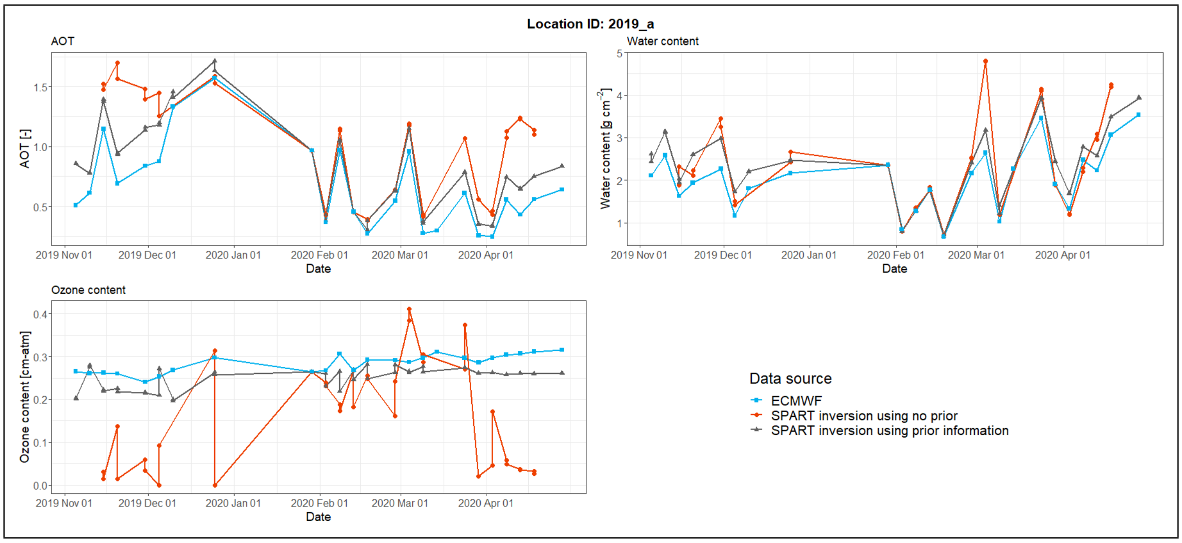

Figure 5.29: *Comparison between atmospheric parameters retrieved from S2 observations using SPART model with the ECMWF estimation (for 2019_a)*

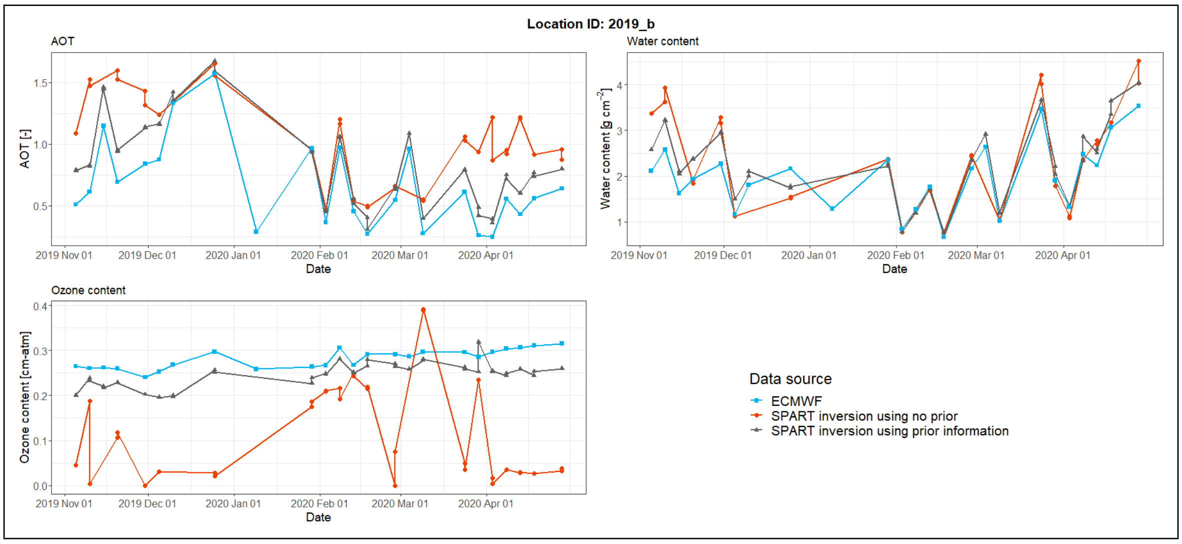

Figure 5.30: *Comparison between atmospheric parameters retrieved from S2 observations using SPART model with the ECMWF estimation (for 2019_b)*

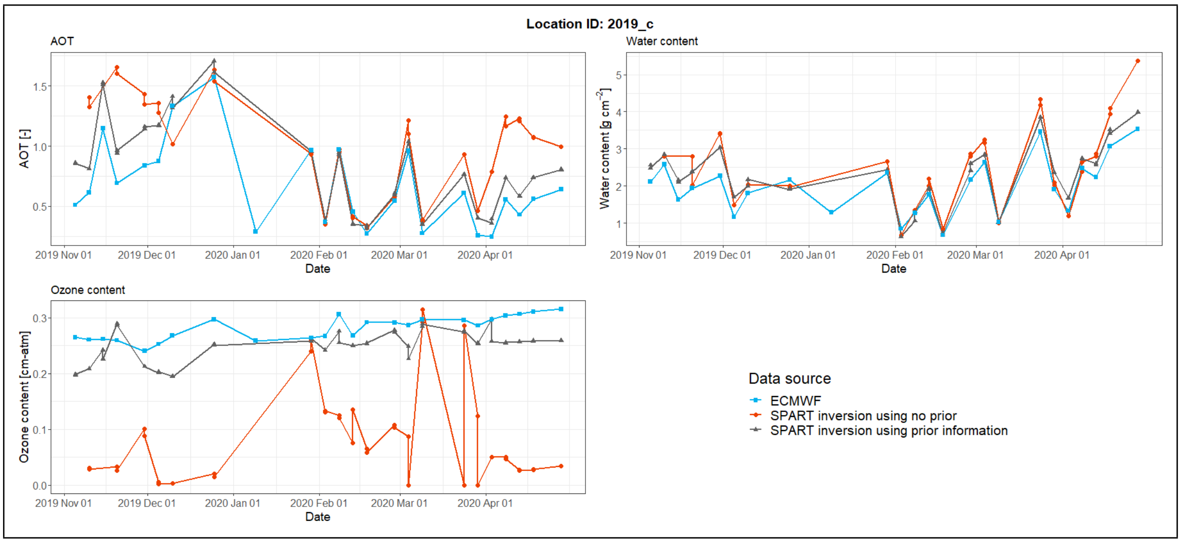

Figure 5.31: *Comparison between atmospheric parameters retrieved from S2 observations using SPART model with the ECMWF estimation (for 2019_c)*

5.6 PREPARING TIME-SERIES OF RETRIEVED PARAMETERS AS INPUT TO THE SCOPE

5.6.1 Choosing Best Performing Time-series

The best performing time-series of the retrieved parameters for further use in SCOPE was chosen based on the criteria described in Section 4.7.1. Table 5.2 and 5.3 have been used for this purpose. The chosen time-series are summarized in Table 5.4.

Table 5.4 The best performing time-series chosen for further use in SCOPE modelling

Location ID	SPART with S2 data	RTMo with S2 data	SPART with S3 data
2018_a	retrieval with prior	Combination 4	retrieval without prior
2018_b	retrieval without prior	Combination 3	retrieval without prior
2019_a	retrieval without prior	Combination 1	retrieval without prior
2019_b	retrieval without prior	Combination 4	retrieval without prior
2019_c	retrieval without prior	Combination 1	retrieval without prior

5.6.2 LOESS Curve Fitting

It was found that the chosen time-series contain some fluctuations. So, it was decided to smoothen the time-series by fitting a LOESS curve. Moreover, the fitted curve can be used to interpolate values of the retrieved parameters at a daily time scale. The LOESS curve fitting was performed for all the retrieved parameters for the 15 chosen time-series (Table 5.4). But here only LOESS fitting for the 2019_b point location from the chosen time-series of SPART with S2 data has been shown in Figure 5.32.

This step is useful for interpolating crop parameters at a daily time scale which is helpful for simulation of ecosystem flux at a daily time-scale using SCOPE. But now the values in the time-series are interpolated from the fitted curve (not retrieved from actual satellite observations). In some cases, there may be considerable time gap between consecutive observations. In that case, the interpolation result may not be very well.

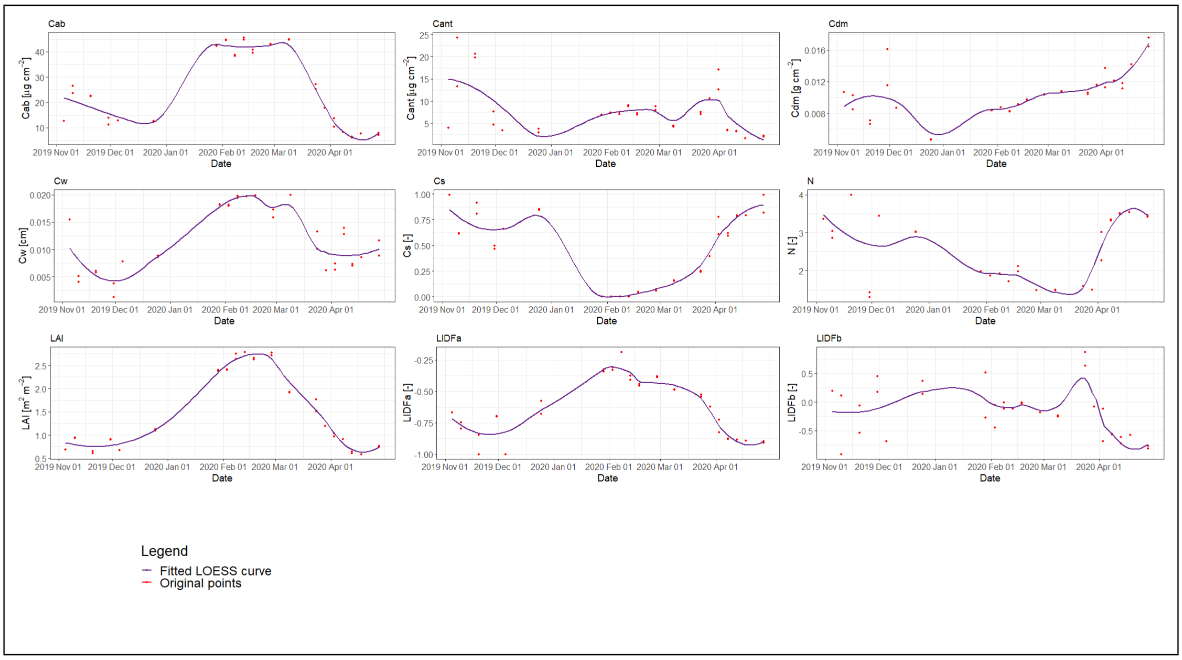

Figure 5.32: *LOESS curve fitting for the time-series chosen from SPART S2 retrievals (for 2019_b)*

5.7 RESULTS AND EVALUATION OF SCOPE SIMULATION

It was found during SCOPE simulation that for some days, the ecosystem fluxes can not be simulated using input data obtained by inversion of RTMo module of SCOPE from S2 observations. In some cases, there were also energy balance closure error for a few days. Those data were removed. These data gaps can be observed in the plots of simulated ecosystem flux.

5.7.1 GPP/ Photosynthesis

GPP or photosynthesis was simulated for all the 5 points of interest for the two crop growing seasons using parameters retrieved in combination of SPART or RTMo of SCOPE and S3 or S2 observations as described in earlier Sections (Section 4.7.1 and 5.6.1). The time-series of simulated GPP were plotted along with GPP from MODIS data and an unified vegetation index (kNDVI). This is shown in Figure 5.33.

It can be observed that GPP simulated from SPART retrieved data is quite flat and does not exhibit a seasonal variation very well, whereas GPP simulation using the RTMo retrieved parameters shows the variation expected in this ecosystem (especially for 2019-20 season). In some cases (2019_a and 2019_c), the values of GPP can not be simulated for a few days with input data obtained using RTMo from S2 observations. It can also be noticed that GPP simulation in the middle of the season (1st December to 31st March) is almost similar even with using different sets of input data.

The GPP estimation from Terra or Aqua MODIS data is somewhat lower than the simulations in this study. The kNDVI values are also mostly lower and remain close to the MODIS estimation. The range of simulated GPP varies within 0 to 12 $\mu mol\ m^2 s^{-1}$ for both the crop growing seasons.

5.7.2 Evapotranspiration (ET)

The water fluxes or ET were simulated as well with the SCOPE model with different time-series of retrieved parameters. The simulated ET along with MODIS based ET products and ET estimations from ECOSTRESS are shown in Figure 5.34. The pattern of ET is quite similar to the pattern of simulated GPP. The ET simulation using RTMo retrieved data captures the expected variation (higher ET during the growth period) a bit better. The MODIS ET estimation is also bit lower. But the ET estimation from ECOSTRESS is quite higher than the simulated ET flux. It is emphasized that there are very few observations from ECOSTRESS due to various reasons described in Section 3.2.5.

5.7.3 Sensible and Ground Heat Fluxes

The SCOPE simulated H and ground heat flux (G) are shown in Figures 5.35 and 5.36 respectively. There are sudden rise in the heat fluxes at the beginning or end of the season in case of simulation with parameters retrieved using RTMo from S2 data. In other parts of the season the heat flux matches quite well with each other from different simulations.

5.8 ECOSYSTEM EFFICIENCY PARAMETERS AND CROP YIELD ESTIMATION

5.8.1 Ecosystem Efficiency Parameters

Three of the ecosystem efficiency parameters, i.e. WUE, LUE and EF have been plotted in Figure 5.37, 5.38, and 5.39 respectively. In Figure 5.38, for point 2019_a, a few negative values of LUE have been found with simulation using input data using RTMo from S2 observations.

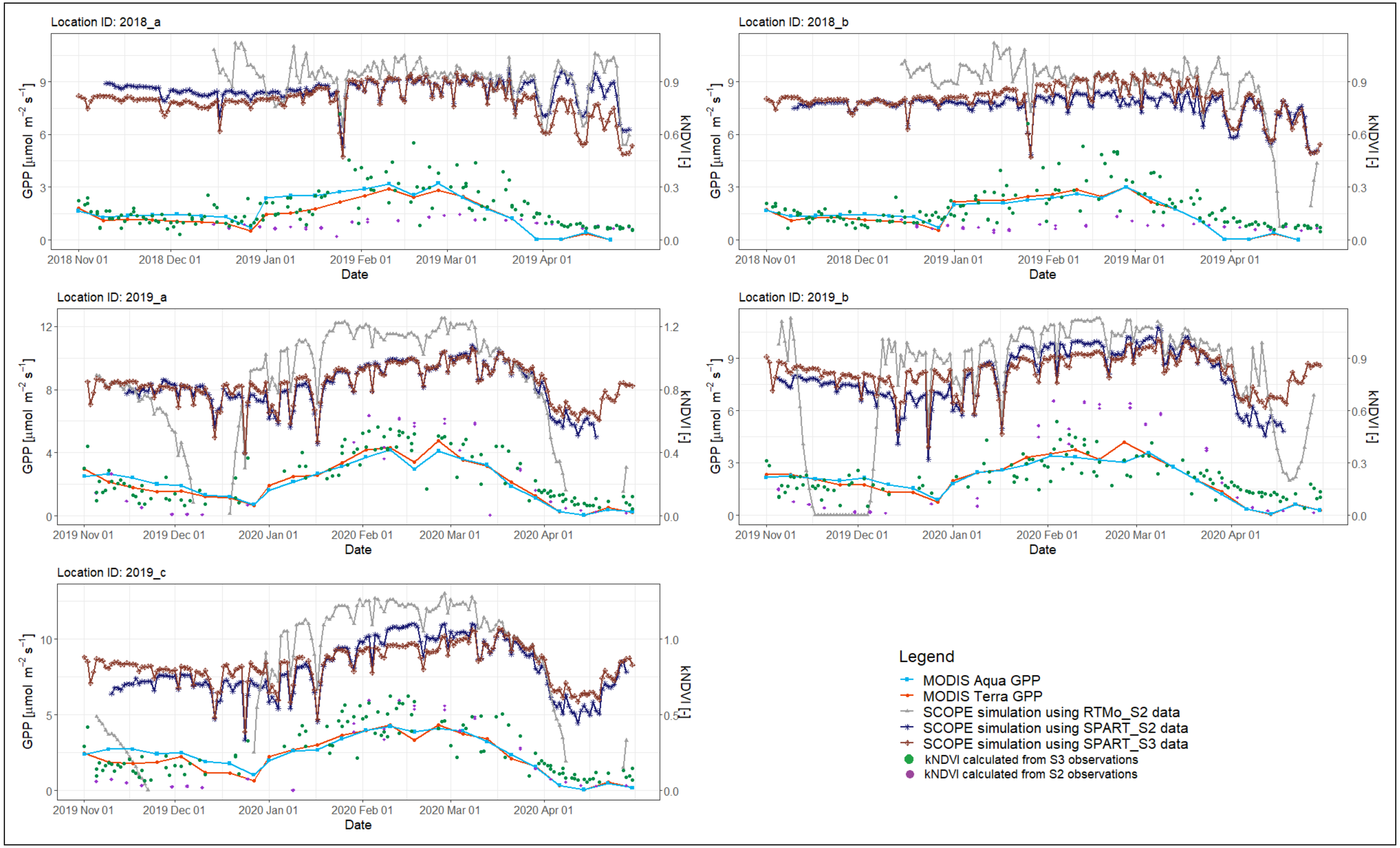

Figure 5.33: *Variation of simulated GPP flux in the study area and its evaluation against other GPP products and kNDVI*

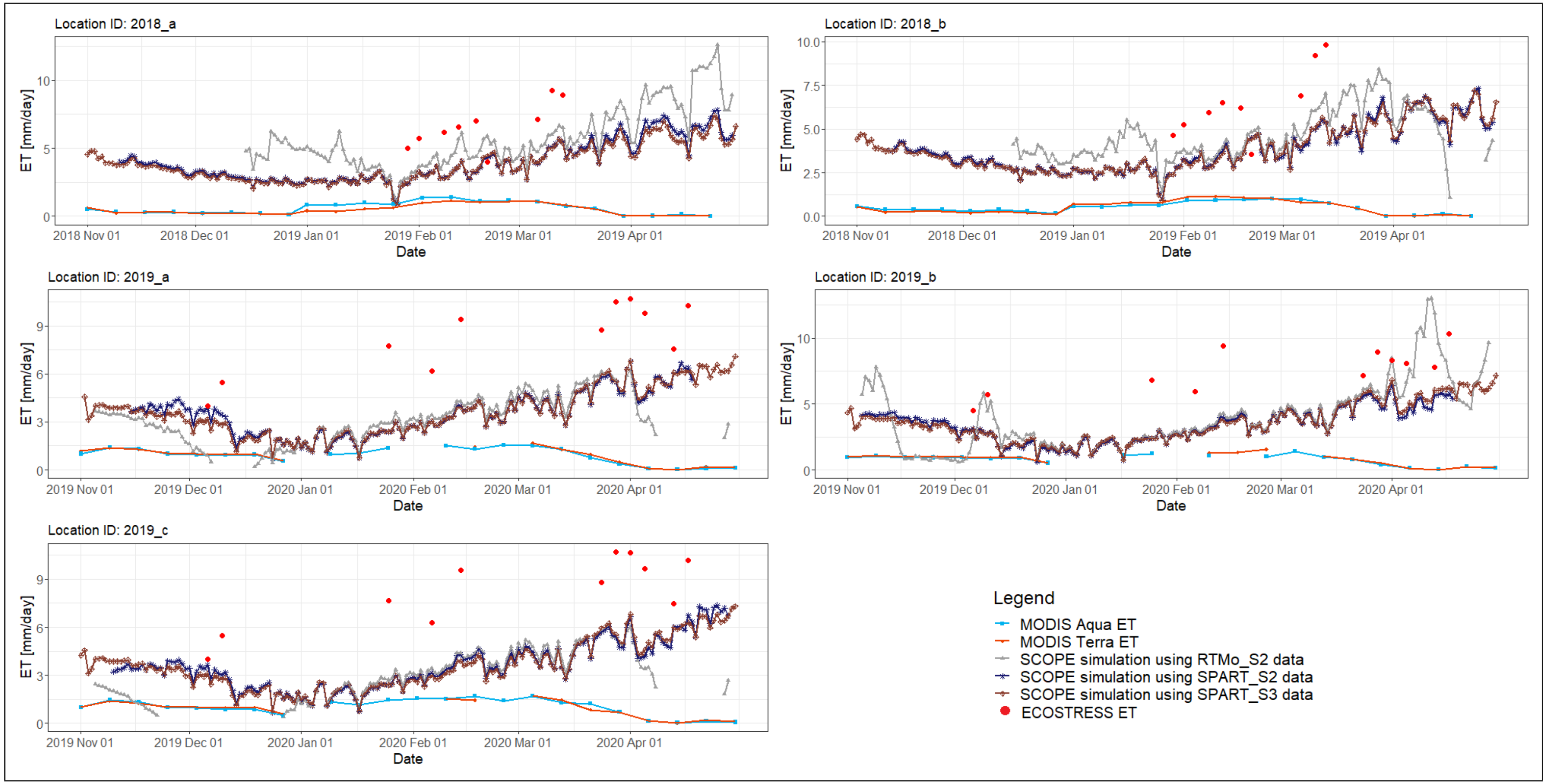

Figure 5.34: *Variation of simulated ET flux in the study area and its evaluation against other remote sensing based ET products*

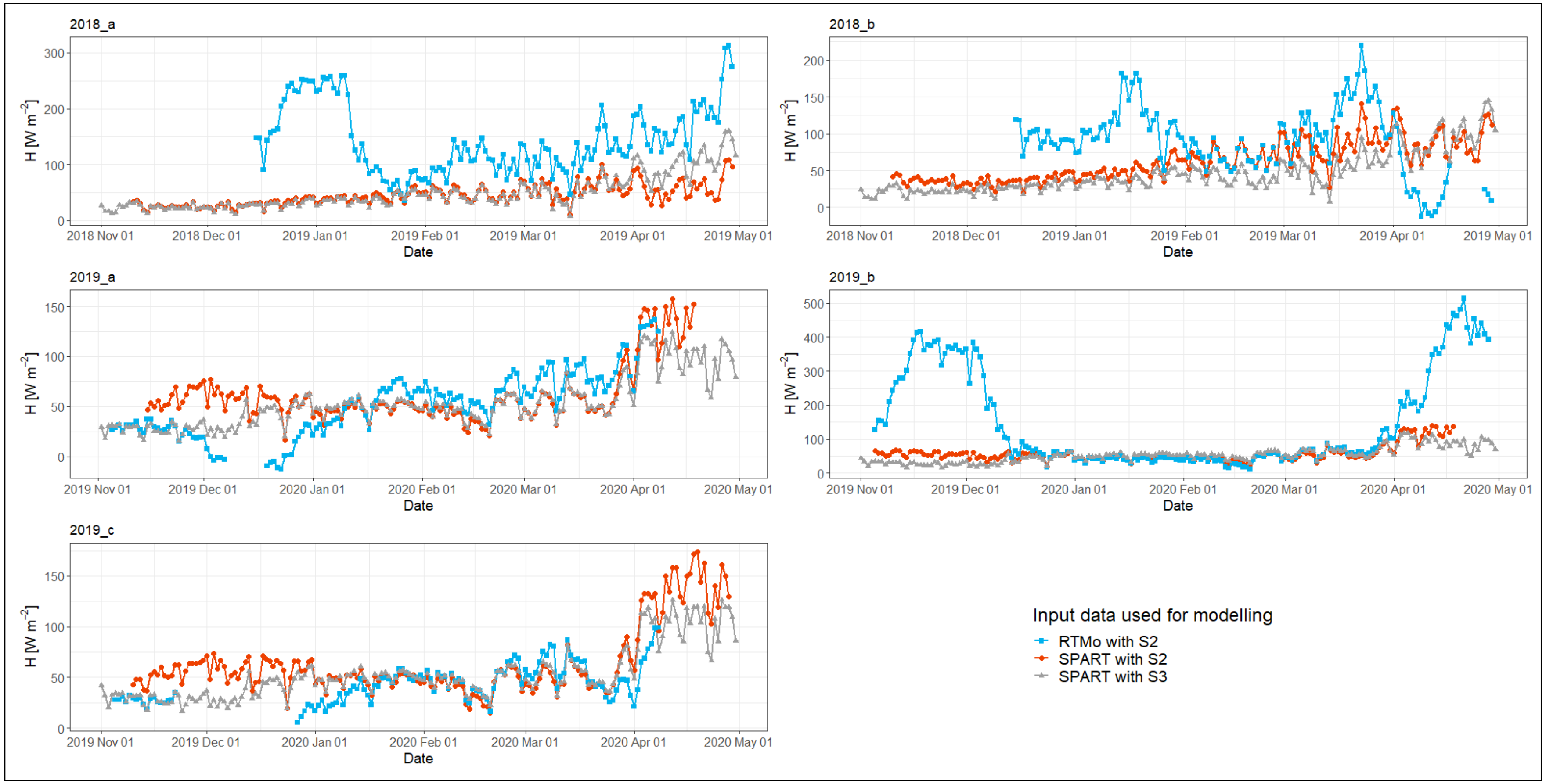

Figure 5.35: *Variation of simulated sensible heat flux in the study area*

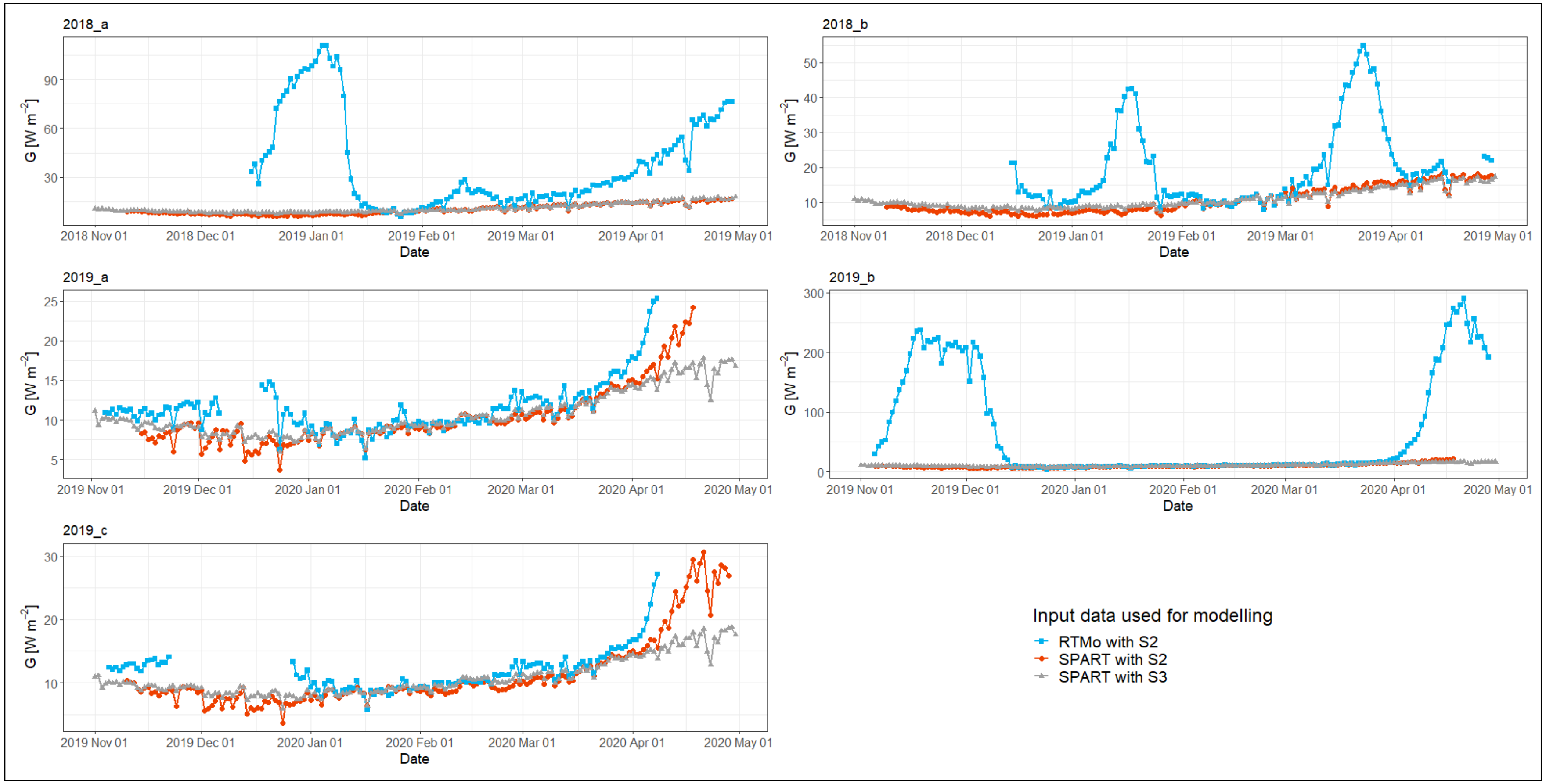

Figure 5.36: *Variation of simulated ground heat flux in the study area*

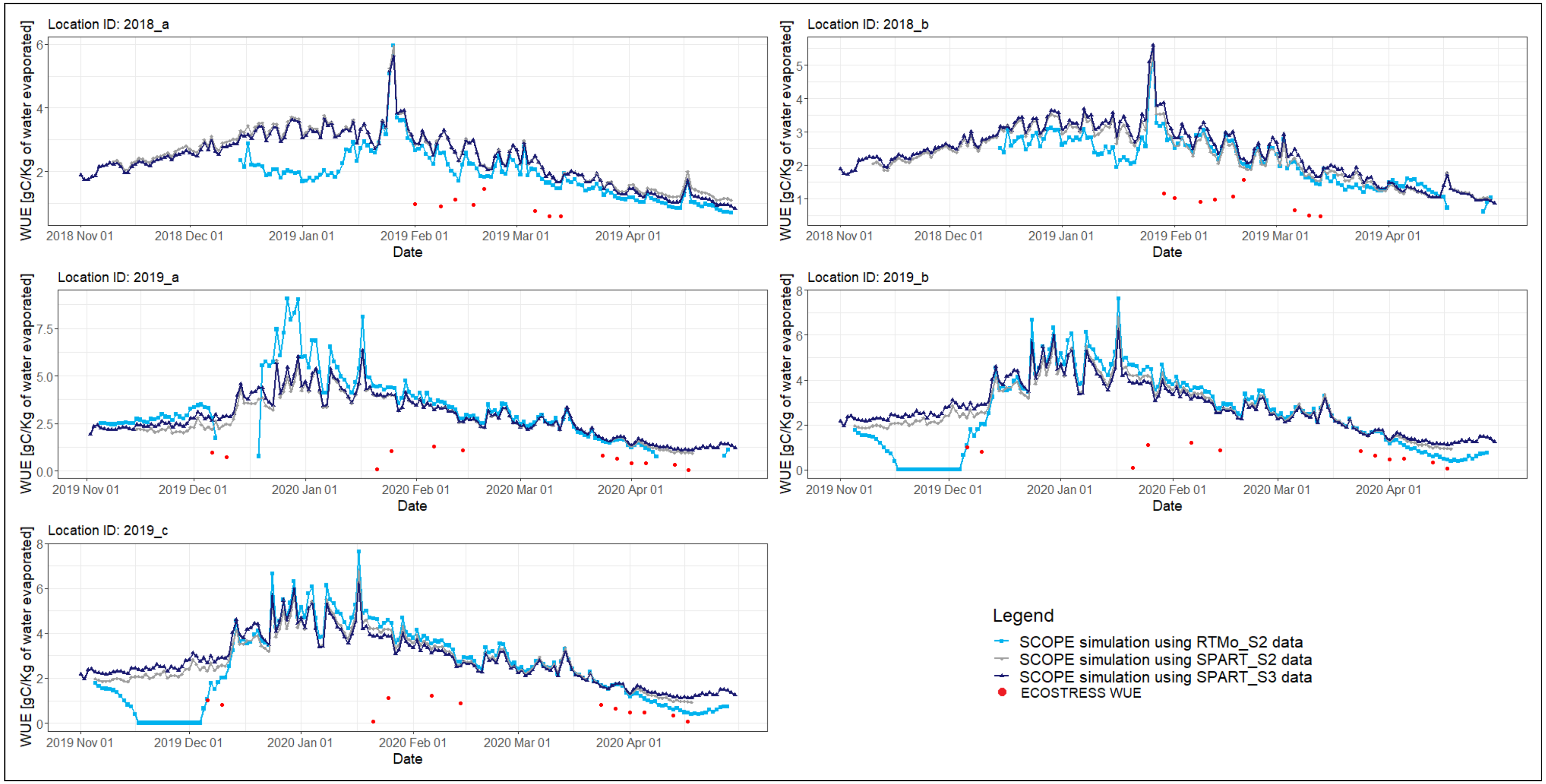

Figure 5.37: *Variation of water use efficiency in the study area*

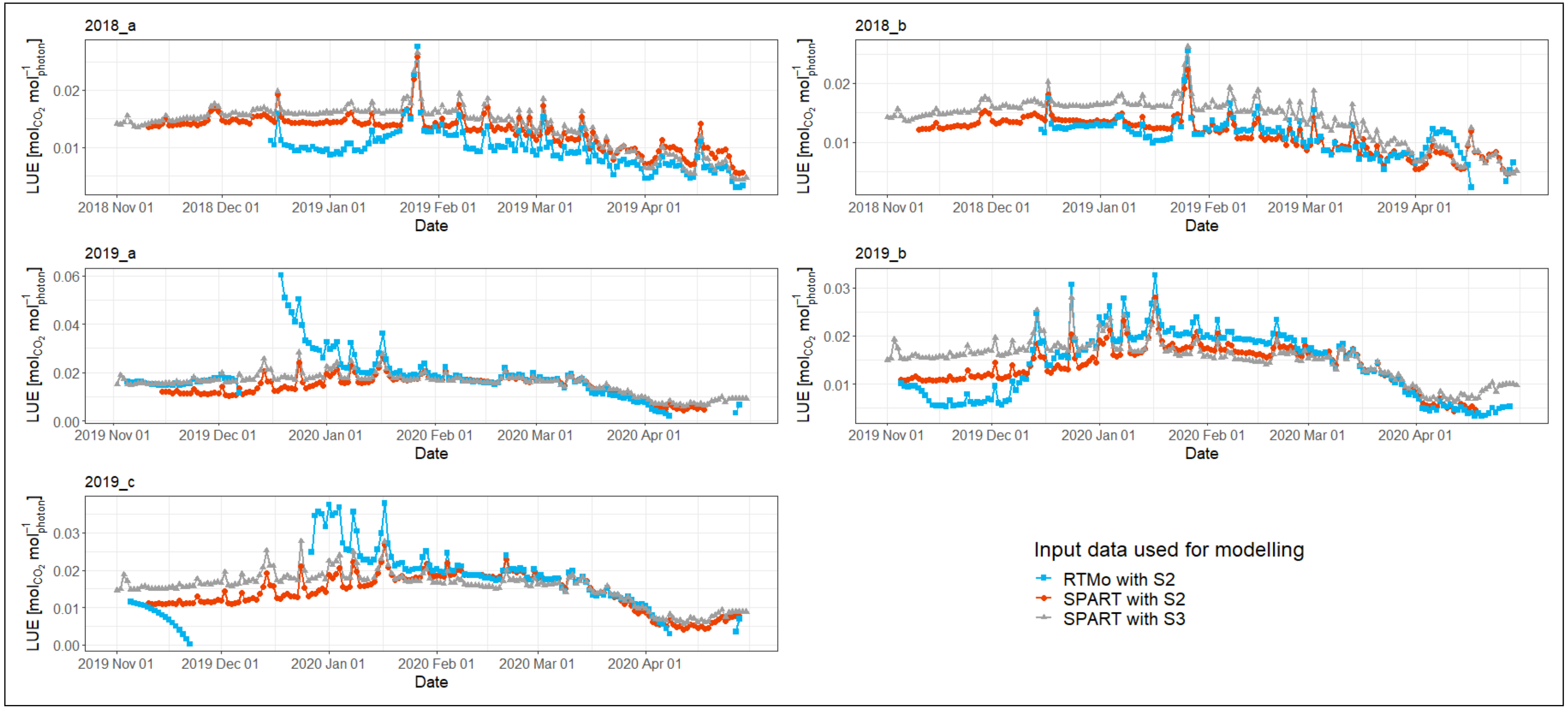

Figure 5.38: *Variation of light use efficiency in the study area*

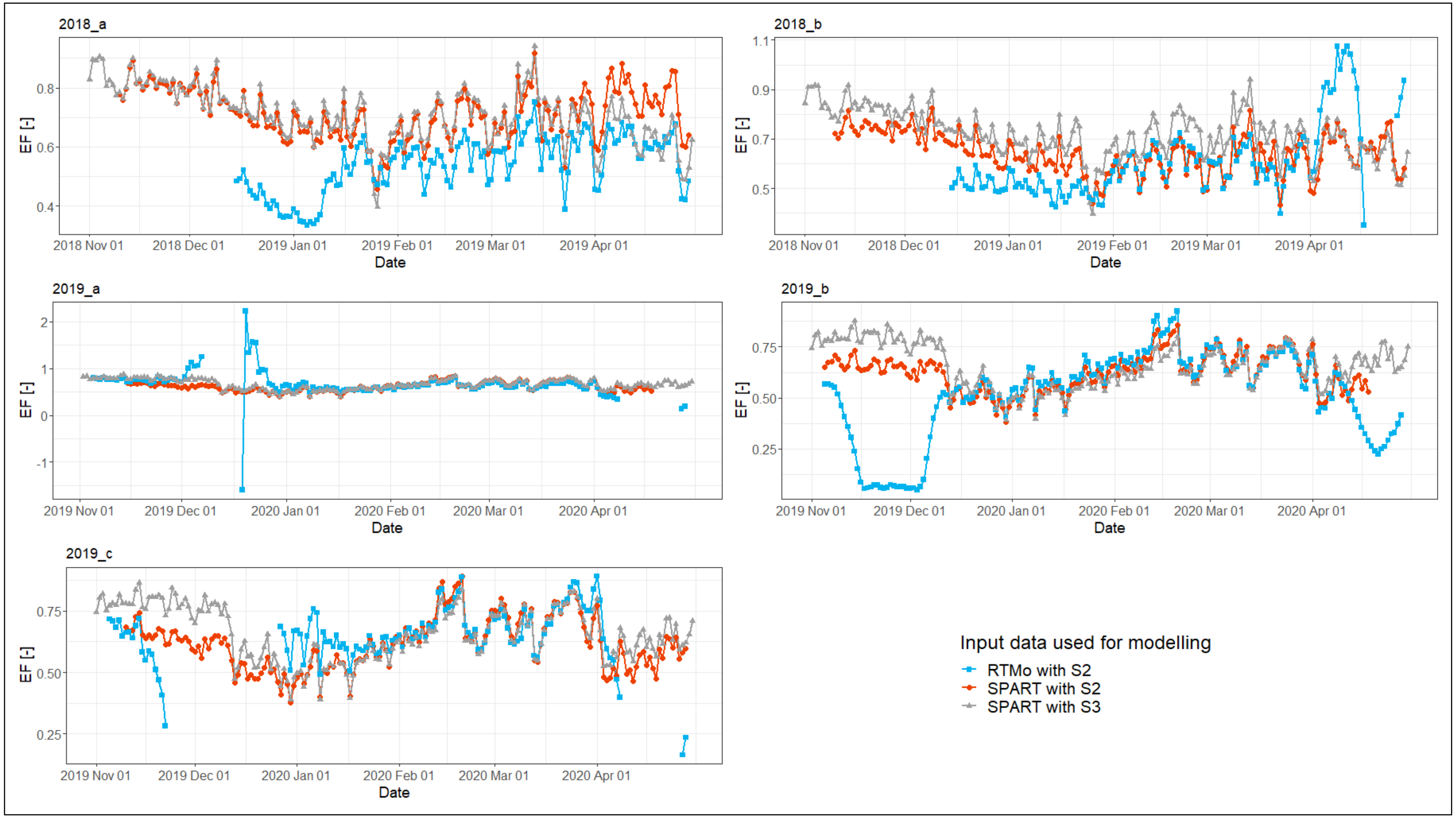

Figure 5.39: *Variation of evaporative fraction in the study area*

5.8.2 Crop Yield Estimation

Table 5.5 has been prepared to show the estimated crop yield from different SCOPE simulations as well as the absolute difference between estimated and actual crop yield. The crop yield estimation is little bit higher than the actual yield in most of the cases.

Table 5.5 Crop yield (in t/ha) estimation for the study area

		Estimated crop yield			Absolute difference between actual and estimated crop yield		
Location ID	**Actual crop yield**	**RTMo_S2**	**SPART_S2**	**SPART_S3**	**RTMo_S2**	**SPART_S2**	**SPART_S3**
2018_a	4.66	4.83	4.96	4.70	0.17	0.30	0.04
2018_b	4.42	4.66	4.28	4.55	0.24	0.14	0.13
2019_a	4.30	5.02	5.07	5.16	0.72	0.77	0.86
2019_b	4.20	5.03	4.62	4.69	0.83	0.42	0.49
2019_c	3.60	4.48	4.76	4.82	0.88	1.16	1.22

Here unit of crop yield is t/ha

This page is intentionally left blank.

Chapter 6

Discussions

This chapter intends to answer the research questions (formulated in Section 1.7) from the results obtained in Chapter 5. Some of the limitations or challenges of this study will also be discussed in the last section of this chapter.

6.1 COMPARISON OF RETRIEVAL FROM TOC AND TOA OBSERVATIONS USING RTMo IN SCOPE AND SPART MODEL

The SPART model used in this study, simulates radiative transfer in the soil, vegetation and atmosphere continuum, whereas RTMo, a sub-model of SCOPE accounts only for soil and vegetation. Either model has its own set of advantages or disadvantages.

The main advantage of using SPART is its ability to account for the atmosphere by implementing a modified SMAC. This SMAC model was modified by Yang, van der Tol, Yin et al., 2020 to account for the anisotorpic surface reflection. It enables user to retrieve various atmospheric parameters, such as H_2O, AOT and O_3 which is demonstrated in this study. Moreover, it is not necessary to perform atmospheric correction of satellite observations by the user. Both TOA radiance or reflectance can be directly used to retrieve a wide range of soil, vegetation and atmosphere related parameters with the SPART. In this study, TOA radiance from S3 and TOA reflectance from S2 have been used. A wide range of satellites, such as Landsat 4,5,7 and 8, Sentinel-3A and 3B, Terra/Aqua MODIS were already present in the existing SPART model. The capability of SPART to simulate S2 observations has also been extended in this study. In some cases, it has been observed that the retrieval using SPART is a bit more stable and there are less unexpected fluctuations depending on the sensor used.

There are certain limitations of the SPART. The SMAC model in SPART is a simplified version of 6S model. Though the SMAC model can simulate atmospheric radiative transfer well, it is not very accurate. Besides, SMAC model needs 49 different coefficients. Although these coefficients for a variety of satellites or sensors have already been calculated, the code for calculating these coefficients is not publicly available. It makes the inclusion of new sensors little difficult. It can be observed quite often when a prior information is used in the cost function during inversion of SPART, the retrieved values tend to go near the initial guess. So, a more robust implementation of this prior information may be necessary as suggested by Yang et al., 2021.

In case of RTMo thus in SCOPE, a very user friendly model inversion approach has already been developed and publicly made available. It enables user to retrieve vegetation or soil parameters very easily if surface or TOC reflectance is available as RTMo does not have an atmospheric component. So, it may be easy to use for sensors like S2 for which globally atmospherically corrected data is available for most of the recent times. For S3, it is possible to use an atmospherically corrected synergy product of OLCI and SLSTR, but atmospheric corrections for all the bands are not available there. If any user wants to use a single sensor or use some other bands, they have to perform atmospheric correction themselves as demonstrated in this study. This step may make the usage of RTMo a bit difficult, as performing atmospheric correction is not very easy and time consuming due to different reasons, including the (un)availability of atmospheric parameters and the computational demand.

6.2 COMPARISON BETWEEN USING SENTINEL-3 AND SENTINEL-2 DATA

The most important parameters for comparison between two satellites for remote sensing applications are their spectral characteristics, spatial resolution and revisit time.

S3 OLCI sensor has 21 bands ranging from 400 nm to 2190 nm. This large number of bands are very useful for retrieving a wide variety of parameters by radiative transfer model inversions. Moreover, S3 has a high revisit time of 1.1 days which helps to obtain a more complete time-series. These high temporal resolution is achieved through multiple orbits, which produces jumping pixel centres (as described in Section 4.6.1). This makes comparison between in-situ measurements at a certain point with values retrieved from a S3 OLCI pixel data very unsuitable. Besides, S3 OLCI has a coarse spatial resolution of 300 m (as this sensor was mainly designed for ocean monitoring), which is unsuitable for monitoring small agricultural fields in most parts of the world.

S2 MSI has 13 bands with a wider range from of 440 nm to 2190 nm. Thus, fewer parameters may be retrieved at once with MSI data. S2 achieves a revisit time of 5 days with its twin satellites. But due to cloud and other atmospheric conditions, it is always not possible to get a very complete time-series from S2 observations. On the other hands, the biggest advantage of MSI is, many of its band has a very high spatial resolution of 10 m which is very useful for many applications.

There is also another aspect regarding downloading or extraction of observation data from these two satellites. Both TOA and TOC S2 MSI data along with all the required metadata are readily available at GEE platform. So, extracting S2 data for a point of interest is relatively easy with GEE and it also requires less computational power and storage space. In contrast S3 data in GEE have been found to deviate from the official release, and as quite some metadata are missing there (Prikaziuk et al., 2021). As an alternative all the official S3 images can be downloaded and point data can be extracted (as done in this study). But this procedure is time consuming.

6.3 ONE-TO-ONE COMPARISON BETWEEN RETRIEVED PARAMETERS AND IN-SITU MEASUREMENTS

There were very limited in-situ measurements available for this study area. Only the comparison of ground measurements and retrieved values for LAI was approached. Moreover, the values retrieved from S3 has a very coarse spatial resolution and affected by other problems. It was decided to carry out a one-to-one comparison between data retrieved from S2 observations and measurements only, while for S3 this was not performed. A one-to-one comparison between LAI retrieved from S2 data and ground measurements was performed. It was found that their agreement is poor and higher resolution remote sensing products are needed in order to get detailed information about these fields. The other option is to use the similar methodology for a professional study site (where experimental field size matches with satellite pixel and intensive ground measurements are available) in order to perform a detailed evaluation between different combinations of radiative transfer models and satellite observations.

6.4 ECOSYSTEM FLUX SIMULATION AND THEIR EVALUATION

One of the main challenges in ecosystem flux simulation with SCOPE is choosing suitable time-series of input parameters. Time-series of various SCOPE input parameters were retrieved in this study using various combinations of integrated radiative transfer models and satellite observations. The final time-series used as SCOPE input were chosen solely based on the comparison of LAI retrieval as ground measurements of no other variable were available. This method may not be very optimal. Moreover, the values of few other important input parameters, such as V_{cmo}, m were kept constant. Actual crop specific measurements of these values may help to obtain a better simulation result.

The SCOPE model able to simulate various ecosystem carbon, water and heat fluxes mostly within expected ranges. But there are some cases, where the SCOPE can not simulate ecosystem fluxes (especially where input data is retrieved using RTMo of SCOPE from S2 observations). The SCOPE can capture the expected variation of the fluxes in some cases based on the input data used. It was found, the MODIS based remote sensing products have comparatively lower values than the simulated ones, whereas, ECOSTRESS data provide an overestimation in comparison to the simulated result. Although in some cases, the values of kNDVI were agreeing with the simulated GPP, mostly its values are less than the modelled results.

6.5 CROP YIELD ESTIMATION

The crop yield estimation from carbon flux simulated by SCOPE has a higher value than the actual yield measurements at the study site. This is expected as SCOPE can not account for crop respiration and provide simulated NPP. Most probably using NPP, for crop yield estimation could have provided a more closer results to the actual yield.

6.6 LIMITATIONS OF THIS STUDY

One of the major limitation in this study is lack of validation data. An intensive measurements of various crop parameters could be helpful for choosing a good input data for SCOPE simulation. It could be also useful to get a more complete idea about performance of the retrieval algorithms or to come to solid conclusion if a certain retrieval algorithm is superior to the other. In-situ eddy covariance flux measurements also could have used to further validate the simulated ecosystem fluxes or to calibrate the SCOPE model.

Numerical optimization methods were implemented for model inversion during retrieval. This optimization methods find a local minima based on the initial guess and various such local minima or various solutions are possible. This leads to the problem of equifinality or ill-posed retrievals.

Optical remote sensing data were mainly used in this study. But optical remote sensing observations gets affected by the weather conditions or cloud. It can lead to significant gaps or incomplete time-series.

Chapter 7

Conclusions and Recommendations

7.1 CONCLUSIONS

The main objective of this research was simulating ecosystem fluxes with SCOPE in the study area for wheat growing seasons. Crop biophysical parameters and weather data are the main input parameters for the SCOPE. Two retrieval algorithms, i.e. RTMo of SCOPE and SPART, were used to retrieve soil, crop and atmospheric parameters from S2 and S3 data using both TOA and TOC observations, whereas ERA5 data was used to get the time-series of required weather variables. Finally, crop yields were estimated from simulated carbon fluxes.

A wide variety of crop and soil parameters can be retrieved using both RTMo of SCOPE and SPART. But SPART has the advantage of retrieving additional atmospheric parameters. In both cases, the retrieval results contain many unrealistic deviation or spikes. Some of them can be removed using various filtering criteria (for example, a threshold based on RMSE between measured and modelled spectra was used in this study). Another option is to use a prior information in the cost function of these retrieval algorithms, which can stabilize the retrievals. But it was also found that the use of prior removes the seasonal variability in some cases and retrieval results tends to remain near the initial guess. Overall, it can be concluded that this radiative transfer models can be used to get an idea of seasonal variation of crop parameters from satellite data, as in many cases, the expected variation of Cab, LAI and Cs was observed. Besides, users need to be careful in using good quality satellite observations and remove any retrieval where the spectral fitting is not very well.

One of the main challenges in this study remains the evaluation between retrieved parameters from satellite observations and ground measurements. It is mainly due to the coarse spatial resolution of satellite data, small field size and a limited number of ground measurements (in some cases, the in-situ measurements were also not done on the same overpass date). This task became more challenging, as the pixel centres of S3 does not co-locate well with ground measurements and ultimately, evaluation between S3 based retrievals and in-situ measurements were aborted. It was found that ground LAI measurements were somewhat lower than the expected LAI values of wheat crop as well as, MODIS based LAI estimate was also lower than the retrieved LAI values. For some cases, a good agreement was found between LAI retrieved from S2 data and that of in-situ measurements.

The input time-series of retrieved parameters for further modelling using SCOPE were also chosen mostly based on the RMSE between retrieved LAI and ground LAI measurements. This method was not probably very accurate and it should have been chosen, taking multiple retrieved parameters into account. But this kind of approach could not be implemented in this study due to limited in-situ measurements. It is of utmost importance to use good input data for further modelling tasks in order to get expected output results. It can be concluded that a more robust, multi-criteria based approach should be used to choose input time-series, whenever possible.

SCOPE was able to simulate different ecosystem fluxes, such as photosynthesis or carbon flux, sensible, ground and latent heat flux within expected range in most cases. There are a few days where SCOPE could not simulate the fluxes and also there are cases where some unexpected rise or decline in heat fluxes can be found (specially either at the beginning or end of the simulation). It is also noticeable that the values of SCOPE simulated fluxes were higher than MODIS based estimates, whereas ECOSTRESS based ET has higher values than that of SCOPE simulation. The crop yield estimates from GPP simulation of SCOPE also seems to be promising. It can be concluded that SCOPE can be used with remote sensing data to realistically simulate ecosystem fluxes. A more professional experimental scheme could also be developed where the input parameters of SCOPE can be tuned based on the in-situ flux measurements and later use it as an operational scheme for monitoring of ecosystem fluxes.

7.2 RECOMMENDATIONS

The following recommendations can be considered for future studies.

- Instrumentation for in-situ measurements, such as eddy covariance flux tower data can be installed which can be used for validation of simulation results. Intensive in-situ measurements of crop parameters, such as Cab, LAI can be used to better assess the retrieval algorithms. This can help to better select certain data and tune the models and later an operational scheme could be developed solely based on modelling approaches.
- Weather station capable of recording measurements with high temporal resolution can be established in the study location. Use of these data may improve SCOPE simulation results.
- In case of remote sensing based monitoring, aerial or Unmanned Aerial Vehicle (UAV) based data can also be used to monitor small agricultural fields with more details.
- Observations from other types of sensor such as, Synthetic-aperture Radar (SAR), Light Detection and Ranging (LiDAR) or microwave instruments can be integrated with optical remote sensing for all weather monitoring of vegetation.
- The radiative transfer models can be used in a spatially distributed manner for the whole scene to get a more complete information. This can be computationally intensive. So, data driven or hybrid modelling approaches can be used to replace intensive numerical parts or increasing model efficiency.
- SCOPE can not currently simulate plant respiration components. The capability of this model can be extended to get a more intensive information on carbon cycle.
- In this study, the focus was only on agricultural ecosystem. This kind of study can also be extended to several other biome classes.

Appendix A

Additional Results

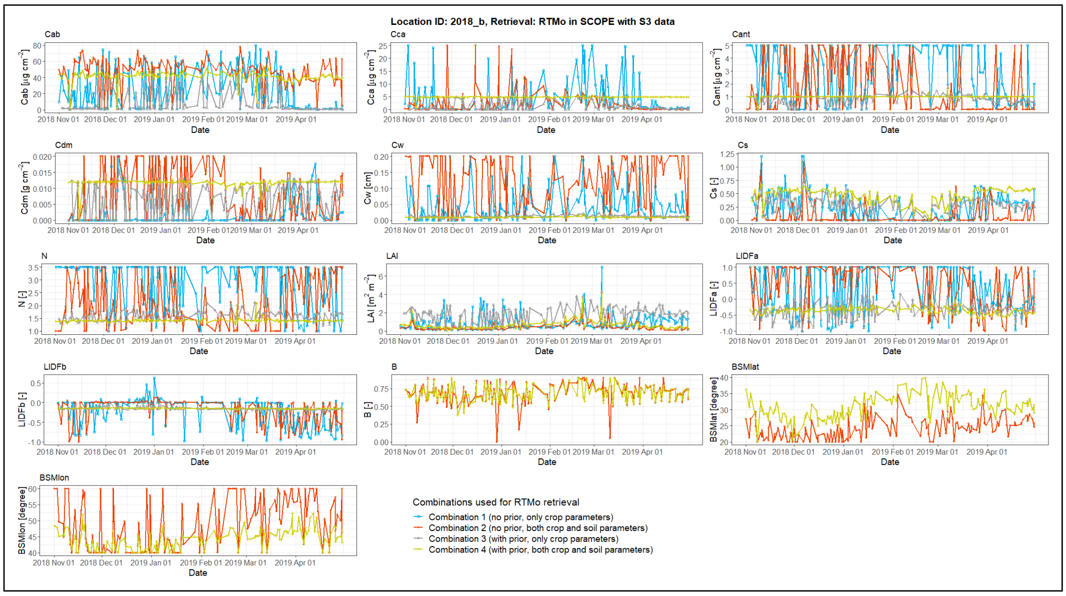

Figure A.1: *Time-series of retrieved parameters from S3 data using different settings of RTMo for the point 2018_b*

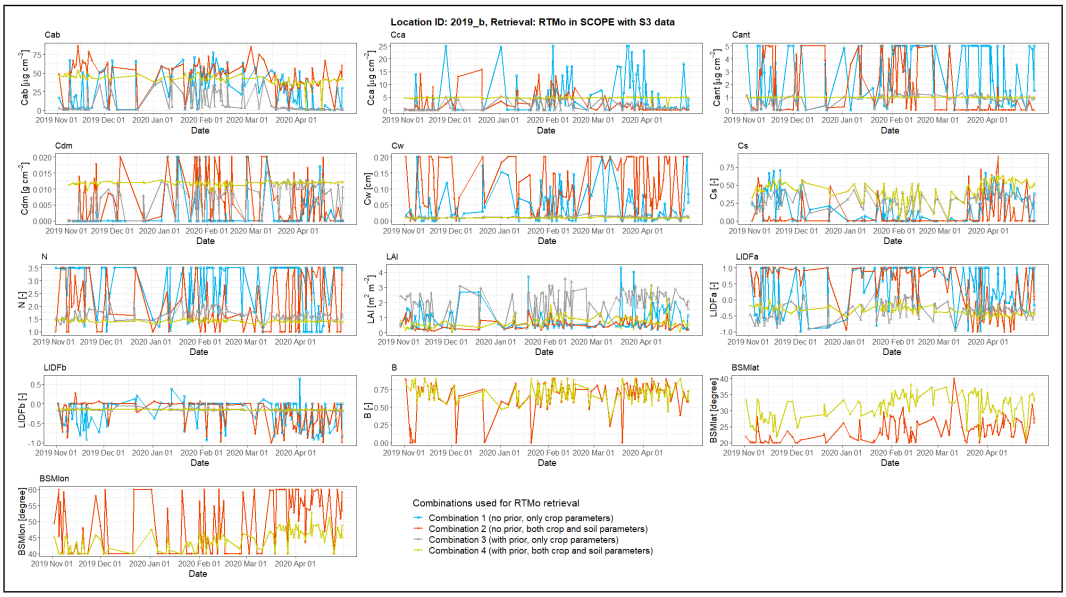

Figure A.2: *Time-series of retrieved parameters from S3 data using different settings of RTMo for the point 2019_b*

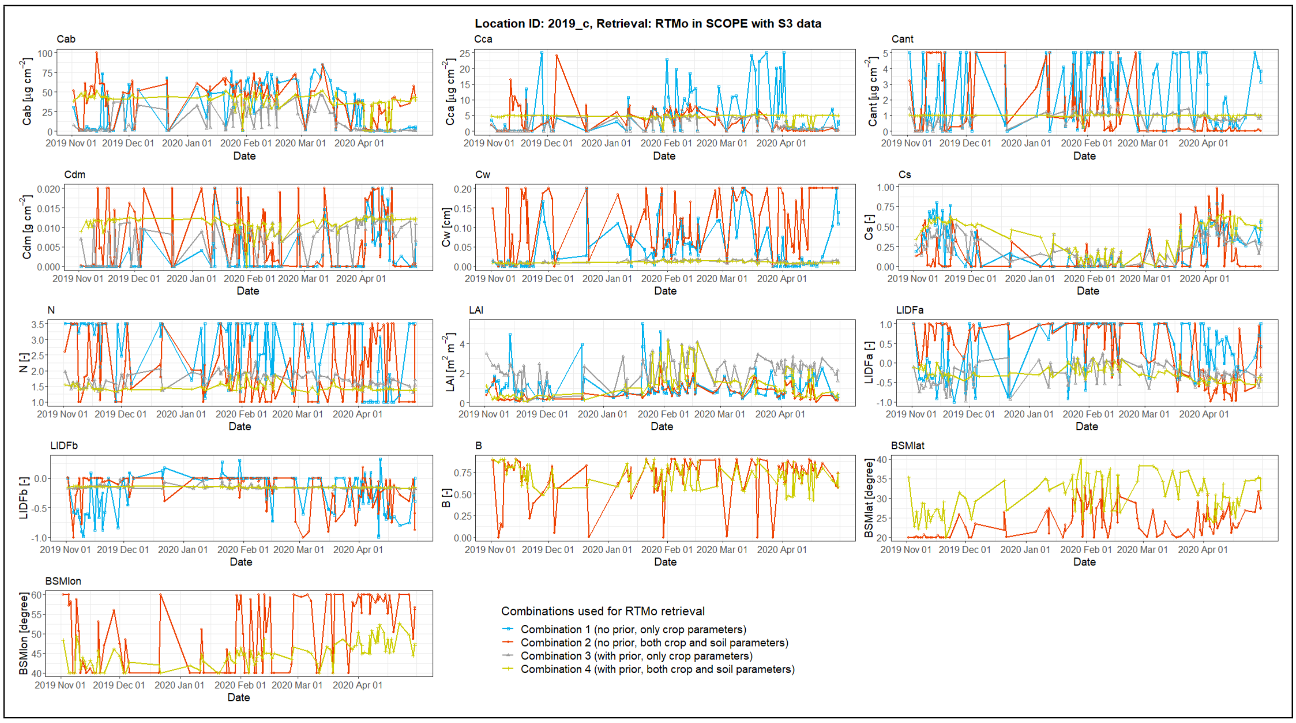

Figure A.3: *Time-series of retrieved parameters from S3 data using different settings of RTMo for the point 2019_c*

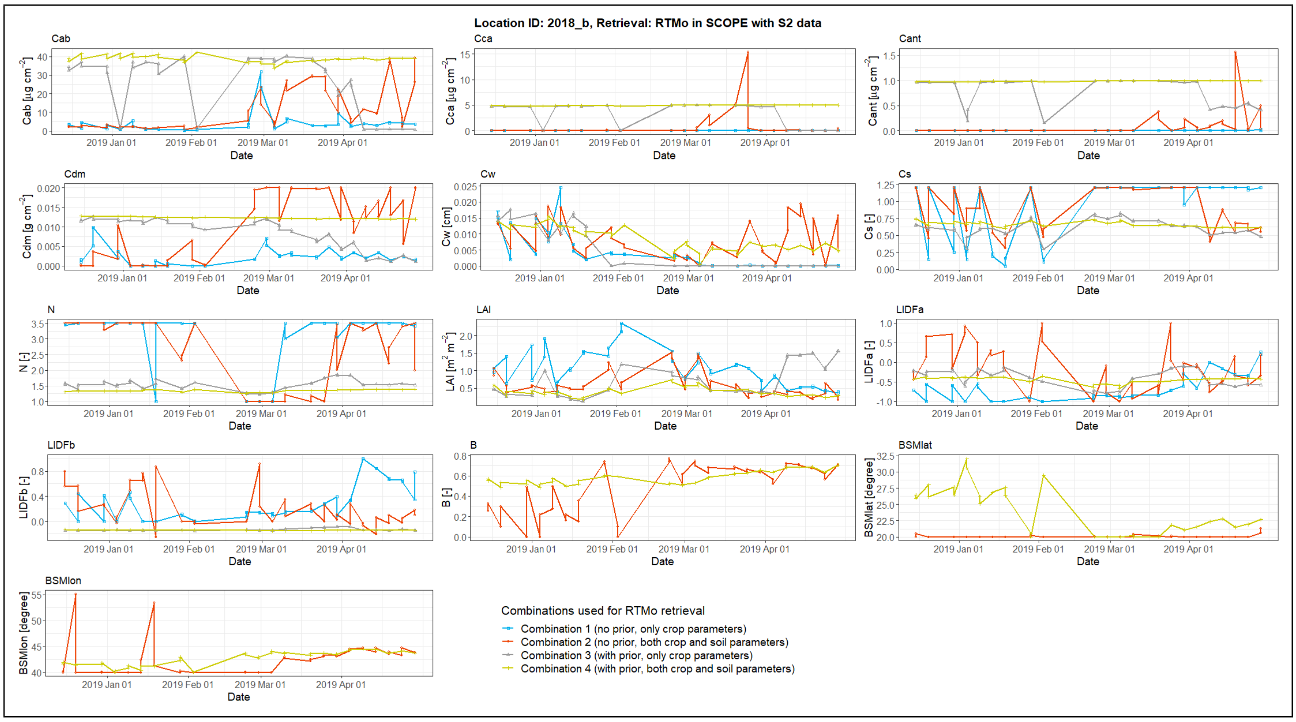

Figure A.4: *Time-series of retrieved parameters from S2 data using different settings of RTMo for the point 2018_b*

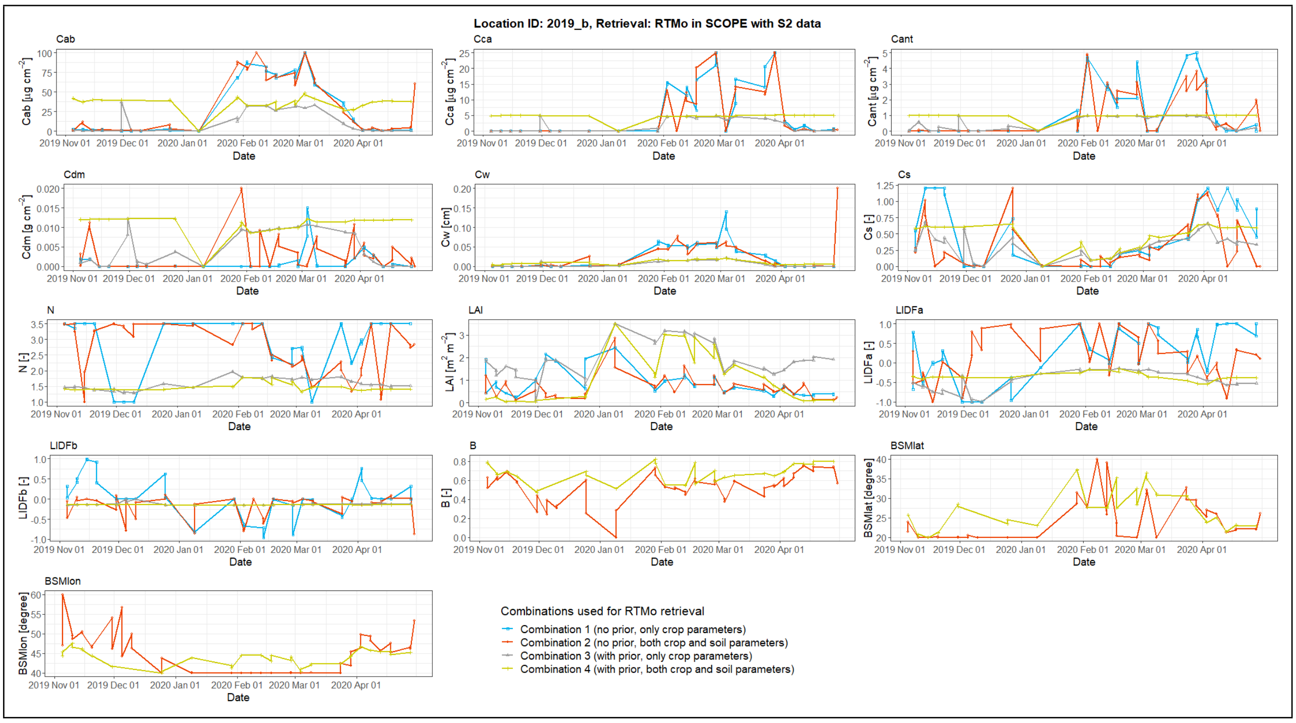

Figure A.5: *Time-series of retrieved parameters from S2 data using different settings of RTMo for the point 2019_b*

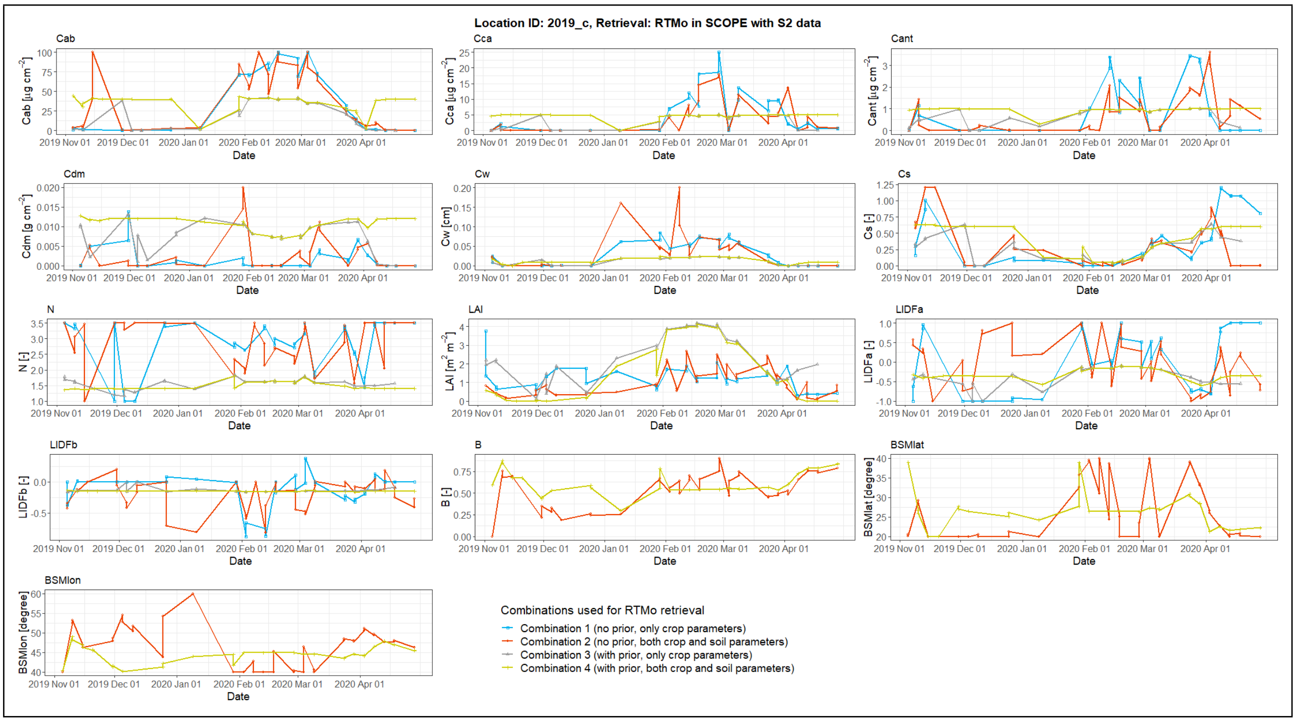

Figure A.6: *Time-series of retrieved parameters from S2 data using different settings of RTMo for the point 2019_c*

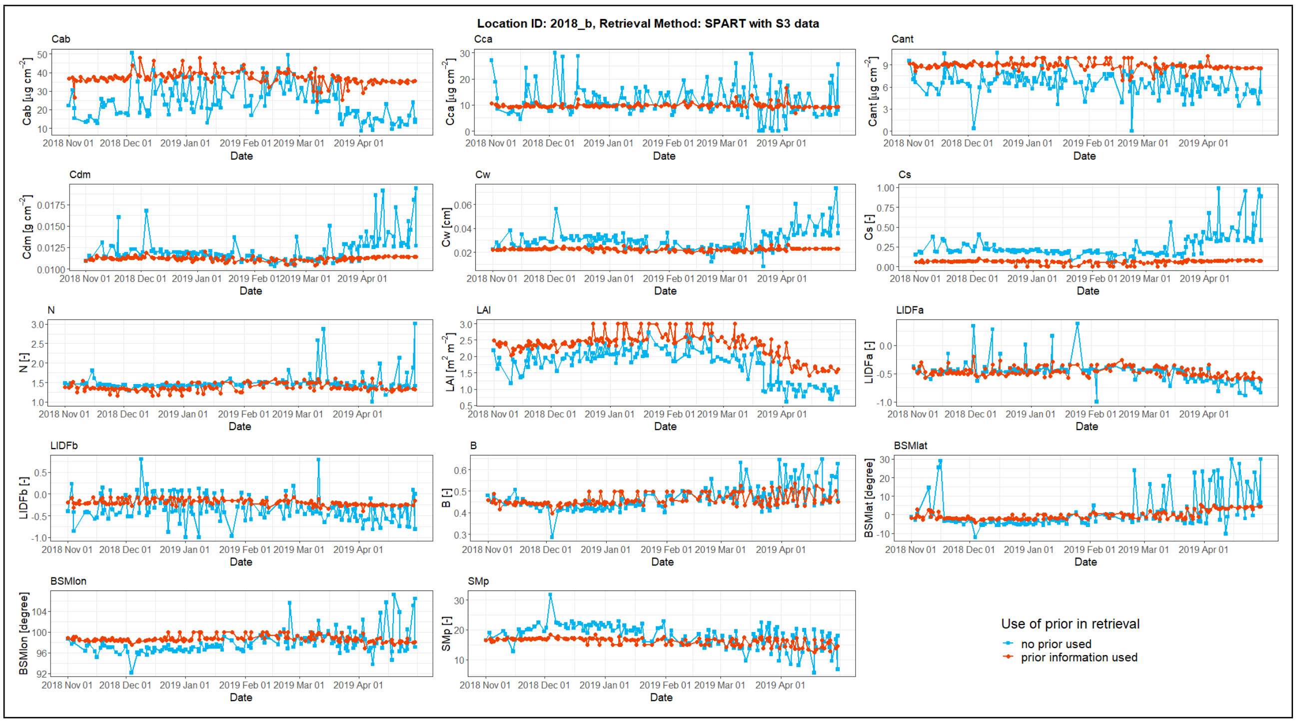

Figure A.7: *SPART retrieval results from S3 data for point 2018_b*

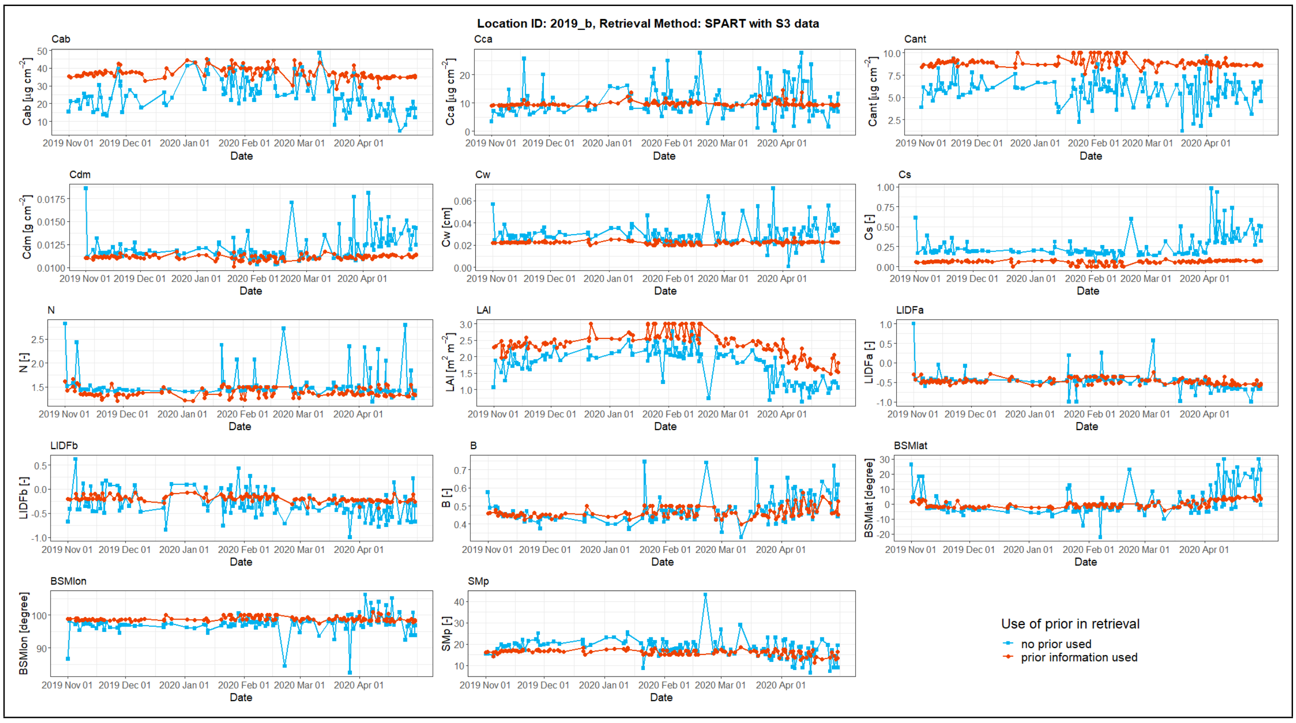

Figure A.8: *SPART retrieval results from S3 data for point 2019_b*

Figure A.9: *SPART retrieval results from S3 data for point 2019_c*

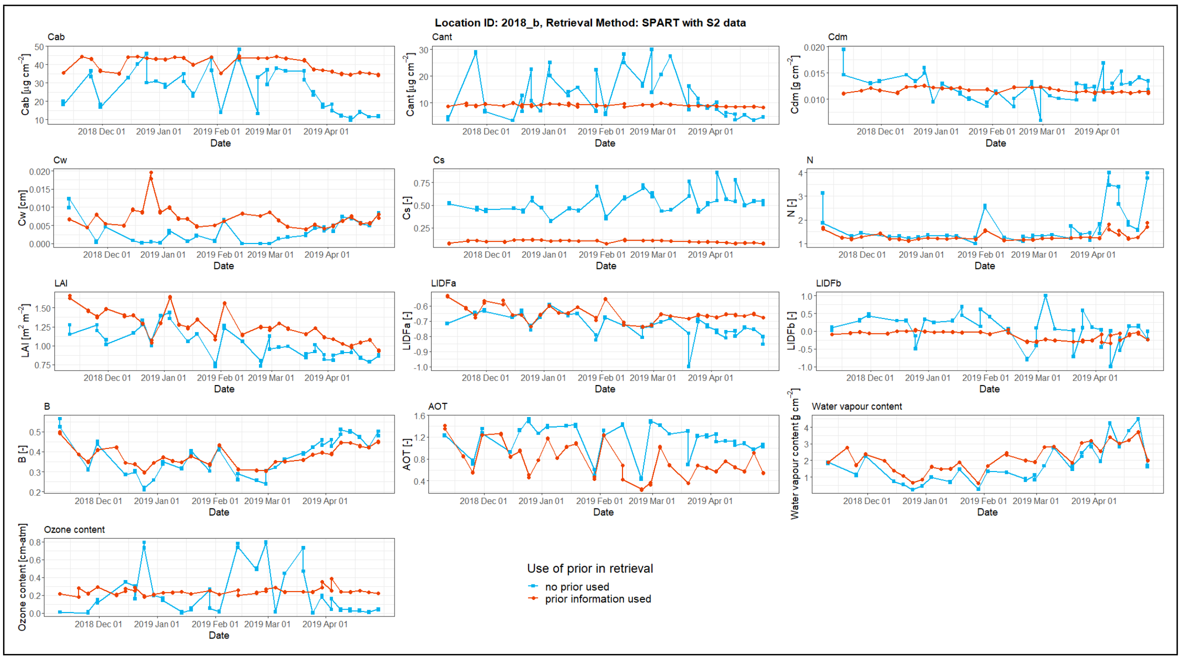

Figure A.10: *SPART retrieval results from S2 data for point 2018_b*

Figure A.11: *SPART retrieval results from S2 data for point 2019_b*

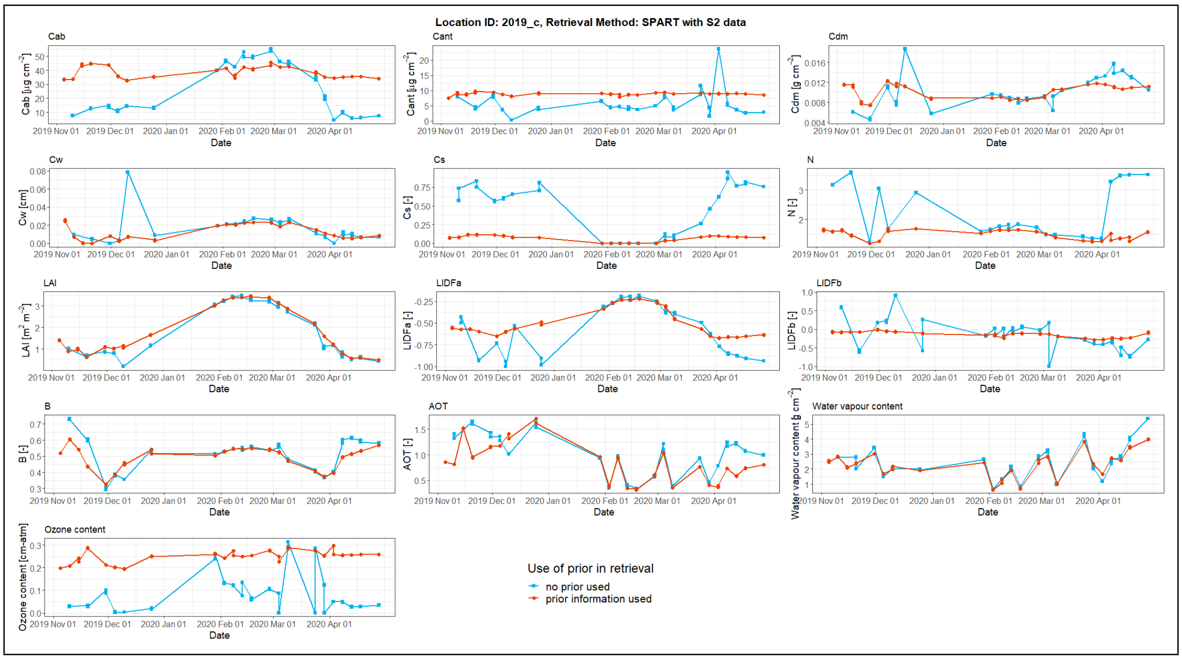

Figure A.12: *SPART retrieval results from S2 data for point 2019_c*

Appendix B

Sources of Data and Code

Sl. No.	Data/ code	Source/ URL
Code/ Application		
1	SCOPE v.2.0	https://doi.org/10.5281/zenodo.4309327 docs:https://scope-model.rtfd.io
2	RTMo/ SCOPE retrieval algorithm	https://github.com/Prikaziuk/retrieval_rtmo docs:https://scope-model.readthedocs.io/en/latest/retrieval.html
4	SPART Forward Model	https://github.com/peiqiyang/SPART
5	Py6S (6S model with a Python wrapper)	https://github.com/robintw/Py6S docs:https://py6s.readthedocs.io/en/latest/
6	LPDAAC A$\rho\rho$EEARS	https://lpdaacsvc.cr.usgs.gov/appeears/
7	aria2	https://aria2.github.io/ docs:https://aria2.github.io/manual/en/html/index.html Bulk downloading Sentinel images with aria2: https://un-spider.org/links-and-resources/data-sources/batch-download-sentinel
8	GEE code for S2 data extraction	https://code.earthengine.google.com/2f4be36dff6109058b6309d9aa9e983c?noload=true (Prikaziuk et al., 2021)
Data		
1	Sentinel - 2 MSI	TOA reflectance: https://developers.google.com/earth-engine/datasets/catalog/COPERNICUS_S2 Surface reflectance: https://developers.google.com/earth-engine/datasets/catalog/COPERNICUS_S2_SR

Continued on next page

Continued from previous page

Sl. No.	Data/ code	Source/ URL
2	Sentinel - 3 OLCI Level-1 full resolution (OL_1_EFR)	Offline data [for 2018-19]:https://www.onda-dias.eu/cms/data/catalogue/sentinel-3/ https://www.onda-dias.eu/cms/knowledge-base/odata-odata-open-data-protocol/ Online data [for 2019-20]: https://scihub.copernicus.eu/dhus
3	Sentinel - 2 MSI SRF	https://sentinel.esa.int/web/sentinel/user-guides/sentinel-2-msi/document-library/-/asset_publisher/Wk0TKajiISaR/content/sentinel-2a-spectral-responses
4	SMAC coefficients	http://tully.ups-tlse.fr/olivier/smac-python/tree/master/COEFS
5	Total Aerosol Optical Depth at 550 nm	https://apps.ecmwf.int/datasets/data/cams-nrealtime
6	MCD15A3H v006 MODIS/Terra+Aqua 4 day LAI/FPAR	https://doi.org/10.5067/MODIS/MCD15A3H.006
7	MCD15A3H v061 MODIS/Terra+Aqua 4 day LAI/FPAR (latest version)	https://doi.org/10.5067/MODIS/MCD15A3H.061
8	ERA5-Land hourly data from 1981 to present	https://doi.org/10.24381/cds.e2161bac
9	MOD16A2 v006 MODIS/Terra 8 day Net Evapotranspiration	https://doi.org/10.5067/MODIS/MOD16A2.006
10	MOD16A2GF v006 MODIS/Terra 8 day Net Evapotranspiration Gap-Filled	https://doi.org/10.5067/MODIS/MOD16A2GF.006
11	MYD16A2 v006 MODIS/Aqua 8 day Net Evapotranspiration	https://doi.org/10.5067/MODIS/MYD16A2.006
12	MYD16A2GF v006 MODIS/Aqua 8 day Net Evapotranspiration Gap-Filled	https://doi.org/10.5067/MODIS/MYD16A2GF.006
13	MOD17A2H v006 MODIS/Terra 8 day Gross Primary Productivity	https://doi.org/10.5067/MODIS/MOD17A2H.006
14	MOD17A2HGF v006 MODIS/Terra 8 day Gross Primary Productivity Gap-Filled	https://doi.org/10.5067/MODIS/MOD17A2HGF.006

Continued on next page

Continued from previous page

Sl. No.	Data/ code	Source/ URL
15	MYD17A2H v006 MODIS/Aqua 8 day Gross Primary Productivity	https://doi.org/10.5067/MODIS/MYD17A2H.006
16	MYD17A2HGF v006 MODIS/Aqua 8 day Gross Primary Productivity Gap-Filled	https://doi.org/10.5067/MODIS/MYD17A2HGF.006
17	ECO3ETPTJPL v001 ECOSTRESS Evapotranspiration PT-JPL	https://doi.org/10.5067/ECOSTRESS/ECO3ETPTJPL.001
18	ECO4WUE v001 ECOSTRESS Water Use Efficiency	https://doi.org/10.5067/ECOSTRESS/ECO4WUE.001
19	In-situ LAI measurements	Acquired directly from SHUATS, Prayagraj, India

List of Acronyms and Symbols

Symbols

ϕ soil spectral latitude. 10, 34
λ soil spectral longitude. 10, 34
λE latent heat flux. 12
ρTOC TOC reflectance. 7
6S Second Simulation of the Satellite Signal in the Solar Spectrum. 11, 22, 29, 81

A

A$\rho\rho$EEARS Application for Extracting and Exploring Analysis Ready Samples. 22, 23, 24
AOT Aerosol Optical Thickness. 3, 22, 29, 31, 34, 35, 49, 56, 63, 67, 81
aPAR Absorbed Photosynthetically Active Radiation. 23, 42
API Application programming interface. 20
API Hub Application programming interface Hub. 20

B

B soil brightness. 9, 10, 55
BSM Brightness-Shape-Moisture. 3, 4, 7, 8, 9, 12, 14, 31, 34

C

Cab chlorophyll concentration. 3, 31, 48, 55, 85, 86
car Companion to Applied Regression. 38
Cca leaf carotenoid content. 34
CESBIO Centre d'Etudes Spatiales de la Biosphère. 30
CNES Centre national d'études spatiales. 30
CONUS continental United States. 24
Cs senescent material. 50, 55, 56, 85
Cw equivalent leaf water thickness. 3
Cwa humid subtropical climate. 17

D

d2m 2m dewpoint temperature. 24, 30
DHUS Copernicus Open Access Data Hub Service. 36
DIAS Data and Information Access Services. 20, 36
DisALEXI Disaggreagtion of Atmosphere–Land Exchange Inverse. 24
DOY Day of Year. 34

E

E_{dif} diffuse TOC irradiance. 7
E_{dir} direct TOC irradiance. 7
e_{ebal} energy balance closure error. 12, 14
ea atmospheric vapour pressure. 30
ECMWF European Centre for Medium-Range Weather Forecasts. 22, 24, 29, 35, 36, 37, 63, 67
ECO3ETPTJPL ECOSTRESS Evapotranspiration PT-JPL Daily L3 Global 70 m. 24
ECO4WUE ECOSTRESS Water Use Efficiency Daily L4 Global 70 m. 24
ECOSTRESS ECOsystem Spaceborne Thermal Radiometer Experiment on Space Station. 23, 24, 41, 71, 83, 86
EF Evaporative fraction. 42, 71
ERA5 ECMWF Reanalysis 5th Generation. 24, 30, 39, 45, 85
ESA European Space Agency. 20, 31
ET Evapotranspiration. 2, 5, 6, 22, 24, 41, 42, 71, 86

F

FASAL Forecasting Agricultural output using Space, Agro-meteorological and Land based observation. 2
FLEX Fluorescence Explorer. 20

G

NIR Near-infrared. 42, 49
NPP Net Primary Production. 23, 83

O

O_3 GEMS total columnar ozone. 22, 27, 29, 34, 35, 67, 81
OAA Observation Azimuth Angle. 29, 34
OData Open Data Protocol. 20
OLCI Ocean and Land Color Imager. 20, 27, 29, 31, 32, 33, 34, 36, 41, 42, 82
OZA Observation Zenith Angle. 29, 34

P

p air pressure. 30
PHyTIR Prototype HyspIRI Thermal Infrared Radiometer. 23
PM Penman-Monteith. 22
PROSAIL PROSPECT + SAIL. 3, 8, 10
PT-JPL Priestley-Taylor Jet Propulsion Laboratory. 24
Py6S A Python interface to 6S. 29

Q

q hot-spot parameter. 34

R

r correlation coefficient. 37, 63, 66
R^2 coefficient of determination. 37, 63, 66
r_{dd} bihemispherical. 7
r_{do} hemispherical-directional. 7
R_n net radiation. 12
r_{sd} directional-hemispherical. 7
r_{so} bidirectional. 7
R_{TOC} TOC reflectance. 29, 32
Rdparam respiration rate as proportion of V_{cmo}. 39
Rin integrated incoming shortwave radiation. 30
Rli integrated incoming longwave radiation. 30
RMSE Root Mean Square Error. 32, 35, 37, 38, 61, 63, 66, 85
RTM Radiative Transfer Module. 12
RTMo Optical Radiative Transfer Routine. 3, 4, 5, 6, 7, 8, 10, 14, 31, 32, 33, 35, 38, 50, 62, 63, 70, 71, 81, 82, 83, 85

S

S2 Sentinel-2. 2, 3, 4, 5, 6, 12, 21, 29, 30, 31, 32, 33, 34, 36, 38, 42, 50, 55, 56, 63, 66, 69, 70, 71, 81, 82, 83, 85, 93
S3 Sentinel-3. 2, 3, 4, 5, 6, 20, 27, 29, 30, 31, 32, 33, 34, 35, 36, 38, 42, 45, 50, 55, 56, 61, 63, 70, 81, 82, 85
SAA Solar Azimuth Angle. 29, 34
SAR Synthetic-aperture Radar. 86
SCOPE Soil Canopy Observation of Photosynthesis and Energy fluxes. 3, 4, 5, 6, 7, 9, 10, 12, 13, 14, 15, 24, 30, 31, 32, 35, 38, 39, 41, 42, 43, 45, 69, 70, 71, 79, 81, 83, 85, 86
SEBS Surface Energy Balance System. 6
SIF Sun-Induced Fluorescence. 4, 20, 42
SLSTR Sea and Land Surface Temperature Radiometer. 20, 82
SMAC Simplified Method for Atmospheric Correction. 3, 9, 11, 30, 81, 94
SMp soil moisture volume percentage. 34
SNAP SeNtinel Application Platform. 27, 36
sp surface pressure. 24, 30
SPART Soil-Plant-Atmosphere Radiative Transfer. 3, 4, 5, 6, 7, 8, 9, 10, 11, 12, 22, 29, 30, 31, 33, 34, 35, 36, 37, 38, 48, 49, 55, 56, 61, 62, 63, 66, 67, 69, 70, 81, 85
SRAL Synthetic Aperture Radar Altimeter. 20
SRF Spectral Response Function. 20, 21, 31, 94
ssrd surface solar radiation downwards. 24, 30
strd surface thermal radiation downwards. 24, 30
SZA Solar Zenith Angle. 29, 32, 34

T

T 2m dewpoint temperature in degree centigrade. 30
t2m 2m temperature. 24, 30
Ta air temperature. 30
TOA Top of Atmosphere. 3, 5, 9, 11, 12, 21, 29, 31, 32, 33, 34, 36, 45, 48, 49, 56, 67, 81, 82, 85, 93, 97
TOC Top of Canopy. 3, 5, 7, 8, 9, 10, 12, 21, 29, 31, 32, 42, 45, 48, 49, 81, 82, 85, 98
tts solar zenith angle in SCOPE. 39

U

u Wind speed. 30

V

W

List of References

Abd El Baki, A. (2013). Estimation of evapotranspiration from ariborne hyperspectral scanner data using the SCOPE model [Master's thesis, University of Twente]. http://essay.utwente.nl/84735/

Anderson, M., Norman, J., Diak, G., Kustas, W. & Mecikalski, J. (1997). A two-source time-integrated model for estimating surface fluxes using thermal infrared remote sensing. *Remote Sensing of Environment*, *60*(2), 195–216. https://doi.org/10.1016/S0034-4257(96)00215-5

Ångström, A. (1925). The albedo of various surfaces of ground. *Geografiska Annaler*, *7*(4), 323–342.

Basso, B., Cammarano, D. & Carfagna, E. (n.d.). *Review of Crop Yield Forecasting Methods and Early Warning Systems* (tech. rep.). http://www.fao.org/fileadmin/templates/ess/documents/meetings_and_workshops/GS_SAC_2013/Improving_methods_for_crops_estimates/Crop_Yield_Forecasting_Methods_and_Early_Warning_Systems_Lit_review.pdf

Bayat, B., van der Tol, C. & Verhoef, W. (2018). Integrating satellite optical and thermal infrared observations for improving daily ecosystem functioning estimations during a drought episode. *Remote Sensing of Environment*, *209*, 375–394. https://doi.org/10.1016/j.rse.2018.02.027

Bayat, B., van der Tol, C., Yang, P. & Verhoef, W. (2019). Extending the SCOPE model to combine optical reflectance and soil moisture observations for remote sensing of ecosystem functioning under water stress conditions. *Remote Sensing of Environment*, *221*, 286–301. https://doi.org/10.1016/j.rse.2018.11.021

Beck, H. E., Zimmermann, N. E., McVicar, T. R., Vergopolan, N., Berg, A. & Wood, E. F. (2018). Present and future köppen-geiger climate classification maps at 1-km resolution. *Scientific Data*, *5*(1), 1–12. https://doi.org/10.1038/sdata.2018.214

Berger, K., Verrelst, J., Féret, J.-B., Hank, T., Wocher, M., Mauser, W. & Camps-Valls, G. (2020). Retrieval of aboveground crop nitrogen content with a hybrid machine learning method. *International Journal of Applied Earth Observation and Geoinformation*, *92*, 102174. https://doi.org/10.1016/j.jag.2020.102174

Camps-Valls, G., Campos-Taberner, M., Moreno-Martínez, Á., Walther, S., Duveiller, G., Cescatti, A., Mahecha, M. D., Muñoz-Marí, J., García-Haro, F. J., Guanter, L., Jung, M., Gamon, J. A., Reichstein, M. & Running, S. W. (2021). A unified vegetation index for quantifying the terrestrial biosphere. *Science Advances*, *7*(9). https://doi.org/10.1126/sciadv.abc7447

Celesti, M., van der Tol, C., Cogliati, S., Panigada, C., Yang, P., Pinto, F., Rascher, U., Miglietta, F., Colombo, R. & Rossini, M. (2018). Exploring the physiological information of sun-induced chlorophyll fluorescence through radiative transfer model inversion. *Remote Sensing of Environment*, *215*, 97–108. https://doi.org/10.1016/j.rse.2018.05.013

Chipanshi, A., Zhang, Y., Newlands, N., Hill, H. & Zamar, D. (2012). Canadian crop yield forecaster (CCYF): a GIS and statistical integration of agro-climates and remote sensing information. In H. Yingbin, C. Youqi & Y. Yanmin (Eds.), *The application of remote sensing and GIS technology on crops productivity* (p. 3). APEC Agricultural Technical Cooperation Working Group. https://www.apec.org/-/media/APEC/Publications/2012/11/The-Application-of-Remote-Sensing-and-GIS-Technology-on-Crops-Productivity/2012_atc_GISproceeding.pdf#page=9

Cleveland, W., Grosse, E. & Shyu, W. (1992). Chapter 8: Local regression models. In J. Chambers, T. Hastie, Wadsworth & Brooks/Cole (Eds.), *Statistical models in S*.

Coleman, T. F. & Yuying, L. (1994). An interior trust region approach for nonlinear minimization subject to bounds. *Mathematical Programming*, *67*, 189–224. https://doi.org/10.1007/BF01582221

Coleman, T. F. & Yuying, L. (1996). An interior trust region approach for nonlinear minimization subject to bounds. *SIAM Journal on Optimization*, *6*(2), 418–445. https://doi.org/10.1137/0806023

Collatz, G., Ribas-Carbo, M. & Berry, J. (1992). Coupled Photosynthesis-Stomatal Conductance Model for Leaves of C4 Plants. *Journal of Functional Plant Biology*, *19*(5), 519–538. https://doi.org/10.1071/PP9920519

Collatz, G., Ball, J., Grivet, C. & Berry, J. A. (1991). Physiological and environmental regulation of stomatal conductance, photosynthesis and transpiration: a model that includes a laminar boundary layer. *Agricultural and Forest Meteorology*, *54*(2), 107–136. https://doi.org/10.1016/0168-1923(91)90002-8

Combal, B., Baret, F., Weiss, M., Trubuil, A., Macé, D., Pragnère, A., Myneni, R., Knyazikhin, Y. & Wang, L. (2003). Retrieval of canopy biophysical variables from bidirectional reflectance: Using prior information to solve the ill-posed inverse problem. *Remote Sensing of Environment*, *84*(1), 1–15. https://doi.org/10.1016/S0034-4257(02)00035-4

Copernicus Open Access Hub. (2021). *Long Term Archive (LTA) Access*. Retrieved March 3, 2021, from https://scihub.copernicus.eu/userguide/LongTermArchive

Darvishzadeh, R., Skidmore, A., Schlerf, M. & Atzberger, C. (2008). Inversion of a radiative transfer model for estimating vegetation LAI and chlorophyll in a heterogeneous grassland Earth Observations for Terrestrial Biodiversity and Ecosystems Special Issue. *Remote Sensing of Environment*, *112*(5), 2592–2604. https://doi.org/10.1016/j.rse.2007.12.003

De Grave, C., Verrelst, J., Morcillo-Pallarés, P., Pipia, L., Rivera-Caicedo, J. P., Amin, E., Belda, S. & Moreno, J. (2020). Quantifying vegetation biophysical variables from the Sentinel-3/FLEX tandem mission: Evaluation of the synergy of OLCI and FLORIS data sources. *Remote Sensing of Environment*, *251*, 112101. https://doi.org/10.1016/j.rse.2020.112101

Denis, D. (2013). Irrigation performance assessment using SEBS and SCOPE : A case study of tons pump canal command in india [Master's thesis, University of Twente]. http://essay.utwente.nl/84739/

Department of Agriculture, Cooperation and Farmers Welfare, Government of India. (2019). *Annual Report 2018 - 19* (tech. rep.). New Delhi. http://agricoop.nic.in/sites/default/files/AR_2018-19_Final_for_Print.pdf

Department of Agriculture, Cooperation and Farmers Welfare, Government of India. (2020). *All India Report on Agricultural Census 2015-16* (tech. rep.). New Delhi. http://agcensus.nic.in/document/agcen1516/ac_1516_report_final-220221.pdf

Directorate of Census Operations, Uttar Pradesh. (2011). *Distric Census Handbook, Allahabad* (tech. rep.). New Delhi. https://censusindia.gov.in/2011census/dchb/0944_PART_B_DCHB_ALLAHABAD.pdf

Féret, J.-B., Gitelson, A., Noble, S. & Jacquemoud, S. (2017). Prospect-d: Towards modeling leaf optical properties through a complete lifecycle. *Remote Sensing of Environment*, *193*, 204–215.

Fisher, J. B. & ECOSTRESS Algorithm Development Team. (2015). *ECOsystem Spaceborne Thermal Radiometer Experiment on Space Station (ECOSTRESS): Level-3 Evapotranspiration Algorithm Theoretical Basis Document* (tech. rep.). Jet Propulsion Laboratory, Pasadena. https://lpdaac.usgs.gov/documents/335/ECO3ETPTJPL_ATBD_V1.pdf

Fisher, J. B. & ECOSTRESS Algorithm Development Team. (2018). *ECOsystem Spaceborne Thermal Radiometer Experiment on Space Station (ECOSTRESS): Level-4 Water Use Efficiency Algorithm Theoretical Basis Document* (tech. rep.). Jet Propulsion Laboratory, Pasadena. https://lpdaac.usgs.gov/documents/346/ECO4WUE_ATBD_V1.pdf

Fisher, J. B., Tu, K. P. & Baldocchi, D. D. (2008). Global estimates of the land–atmosphere water flux based on monthly avhrr and islscp-ii data, validated at 16 fluxnet sites. *Remote Sensing of Environment*, *112*(3), 901–919. https://doi.org/10.1016/j.rse.2007.06.025

Flach, M., Brenning, A., Gans, F., Reichstein, M., Sippel, S. & Mahecha, M. D. (2021). Vegetation modulates the impact of climate extremes on gross primary production. *Biogeosciences*, *18*(1), 39–53. https://doi.org/10.5194/bg-18-39-2021

Fox, J. & Weisberg, S. (2019). *An R companion to applied regression* (Third). Sage. https://socialsciences.mcmaster.ca/jfox/Books/Companion/

Genovese, G., Bettio, M., Orlandi, S., Boogaard, H., Petrakos, M., Stavropoulos, P., Tassoula, I. & Glossioti, M. (2004). *Methodology of the MARS crop yield forecasting system. Vol. 4 statistical data collection, processing and analysis*. EC. https://research.wur.nl/en/publications/methodology-of-the-mars-crop-yield-forecasting-system-vol-4-stati

Godfray, H. C. J., Beddington, J. R., Crute, I. R., Haddad, L., Lawrence, D., Muir, J. F., Pretty, J., Robinson, S., Thomas, S. M. & Toulmin, C. (2010). Food security: The challenge of feeding 9 billion people. https://doi.org/10.1126/science.1185383

Harris, C. R., Millman, K. J., van der Walt, S. J., Gommers, R., Virtanen, P., Cournapeau, D., Wieser, E., Taylor, J., Berg, S., Smith, N. J., Kern, R., Picus, M., Hoyer, S., van Kerkwijk, M. H., Brett, M., Haldane, A., del R'10, J. F., Wiebe, M., Peterson, P., … Oliphant, T. E. (2020). Array programming with NumPy. *Nature*, *585*(7825), 357–362. https://doi.org/10.1038/s41586-020-2649-2

Hook, S. & Fisher, J. (2019a). *ECOSTRESS Evapotranspiration PT-JPL Daily L3 Global 70 m V001 [Data set]* Accessed: 2021-03-07. NASA EOSDIS Land Processes DAAC. https://doi.org/10.5067/ECOSTRESS/ECO3ETPTJPL.001

Hook, S. & Fisher, J. (2019b). *ECOSTRESS Water Use Efficiency Daily L4 Global 70 m V001 [Data set]* Accessed: 2021-03-07. NASA EOSDIS Land Processes DAAC. https://doi.org/10.5067/ECOSTRESS/ECO4WUE.001

Jacquemoud, S. & Baret, F. (1990). PROSPECT: A model of leaf optical properties spectra. *Remote sensing of environment*, *34*(2), 75–91.

Jiang, C. & Fang, H. (2019). GSV: a general model for hyperspectral soil reflectance simulation. *International Journal of Applied Earth Observation and Geoinformation*, *83*, 101932.

Knyazikhin, Y., Martonchik, J. V., Myneni, R. B., Diner, D. J. & Running, S. W. (1998). Synergistic algorithm for estimating vegetation canopy leaf area index and fraction of absorbed photosynthetically active radiation from MODIS and MISR data. *Journal of Geophysical Research: Atmospheres*, *103*(D24), 32257–32275. https://doi.org/10.1029/98JD02462

Lumen learning. (n.d.). *Introduction to statistics: The uniform distribution*. Retrieved March 6, 2021, from https://courses.lumenlearning.com/odessa-introstats1-1/chapter/the-uniform-distribution/

Maheswarappa, H., Srinivasan, V. & Lal, R. (2011). Carbon Footprint and Sustainability of Agricultural Production Systems in India. *Journal of Crop Improvement*, *25*(4), 303–322. https://doi.org/10.1080/15427528.2011.567382

Mandal, D. & Rao, Y. S. (2020). SASYA: An integrated framework for crop biophysical parameter retrieval and within-season crop yield prediction with SAR remote sensing data. *Remote Sensing Applications: Society and Environment*, *20*, 100366. https://doi.org/10.1016/j.rsase.2020.100366

Maxwell, K. & Johnson, G. N. (2000). Chlorophyll fluorescence—a practical guide. *Journal of Experimental Botany*, *51*(345), 659–668. https://doi.org/10.1093/jexbot/51.345.659

Merriott, D. (2016). Factors associated with the farmer suicide crisis in india. *Journal of Epidemiology and Global Health*, *6*, 217–227. https://doi.org/10.1016/j.jegh.2016.03.003

Migliavacca, M., Perez-Priego, O., Rossini, M., El-Madany, T. S., Moreno, G., van der Tol, C., Rascher, U., Berninger, A., Bessenbacher, V., Burkart, A., Carrara, A., Fava, F., Guan, J.-H., Hammer, T. W., Henkel, K., Juarez-Alcalde, E., Julitta, T., Kolle, O., Martín, M. P., … Reichstein, M. (2017). Plant functional traits and canopy structure control the relationship between photosynthetic CO_2 uptake and far-red sun-induced fluorescence in a Mediterranean grassland under different nutrient availability. *New Phytologist*, *214*(3), 1078–1091. https://doi.org/10.1111/nph.14437

Mu, Q., Zhao, M. & Running, S. (2013). *MODIS Global Terrestrial Evapotranspiration (ET) Product (NASA MOD16A2/A3) Algorithm Theoretical Basis Document* (tech. rep.). NASA Headquarters, Washington DC. https://lpdaac.usgs.gov/documents/93/MOD16_ATBD.pdf

Muñoz Sabater, J. (2019). *ERA5-Land hourly data from 1981 to present [Data set]* Accessed: 2021-03-05. Copernicus Climate Change Service (C3S) Climate Data Store (CDS). https://doi.org/10.24381/cds.e2161bac

Myneni, R., Knyazikhin, Y. & Park, T. (2015). *MCD15A3H MODIS/Terra+Aqua Leaf Area Index/FPAR 4-day L4 Global 500m SIN Grid V006 [Data set]* Accessed: 2021-03-05. NASA EOSDIS Land Processes DAAC. https://doi.org/10.5067/MODIS/MCD15A3H.006

Pardo, N., Sánchez, M. L., Su, Z., Pérez, I. A. & García, M. A. (2018). SCOPE model applied for rapeseed in Spain. *Science of the Total Environment*, *627*, 417–426. https://doi.org/10.1016/j.scitotenv.2018.01.247

Parihar, J. S. & Oza, M. P. (2006). FASAL: an integrated approach for crop assessment and production forecasting. In R. J. Kuligowski, J. S. Parihar & G. Saito (Eds.), *Agriculture and hydrology applications of remote sensing* (p. 641101). SPIE. https://doi.org/10.1117/12.713157

Prikaziuk, E., van der Tol, C. & Migliavacca, M. (2020). Global maps of ecosystem functional properties with the SCOPE model on Google earth engine Sentinel-2 composites EGU General Assembly 2020, Online, 4–8 May 2020, EGU2020-10347. https://doi.org/10.5194/egusphere-egu2020-10347

Prikaziuk, E. & van der Tol, C. (2019). Global Sensitivity Analysis of the SCOPE Model in Sentinel-3 Bands: Thermal Domain Focus. *Remote Sensing*, *11*(20). https://doi.org/10.3390/rs11202424

Prikaziuk, E., Yang, P. & van der Tol, C. (2021). Google Earth Engine Sentinel-3 OLCI Level-1 Dataset Deviates from the Original Data: Causes and Consequences. *Remote Sensing*, *13*(6). https://doi.org/10.3390/rs13061098

R Core Team. (2020). *R: A language and environment for statistical computing*. R Foundation for Statistical Computing. Vienna, Austria. https://www.R-project.org/

Rahman, H. & Dedieu, G. (1994). Smac: A simplified method for the atmospheric correction of satellite measurements in the solar spectrum. *Remote Sensing*, *15*(1), 123–143.

Running, S., Mu, Q. & Zhao, M. (2015a). *MOD17A2H MODIS/Terra Gross Primary Productivity 8-Day L4 Global 500m SIN Grid V006 [Data set]* Accessed: 2021-03-07. NASA EOSDIS Land Processes DAAC. https://doi.org/10.5067/MODIS/MOD17A2H.006

Running, S., Mu, Q. & Zhao, M. (2015b). *MYD17A2H MODIS/Aqua Gross Primary Productivity 8-Day L4 Global 500m SIN Grid V006 [Data set]* Accessed: 2021-03-07. NASA EOSDIS Land Processes DAAC. https://doi.org/10.5067/MODIS/MYD17A2H.006

Running, S., Mu, Q. & Zhao, M. (2017a). *MOD16A2 MODIS/Terra Net Evapotranspiration 8-Day L4 Global 500m SIN Grid V006 [Data set]* Accessed: 2021-03-07. NASA EOSDIS Land Processes DAAC. https://doi.org/10.5067/MODIS/MOD16A2.006

Running, S., Mu, Q. & Zhao, M. (2017b). *MYD16A2 MODIS/Aqua Net Evapotranspiration 8-Day L4 Global 500m SIN Grid V006 [Data set]* Accessed: 2021-03-07. NASA EOSDIS Land Processes DAAC. https://doi.org/10.5067/MODIS/MYD16A2.006

Running, S., Mu, Q. & Zhao, M. (2019a). *MOD16A2GF MODIS/Terra Net Evapotranspiration Gap-Filled 8-Day L4 Global 500m SIN Grid V006 [Data set]* Accessed: 2021-03-07. NASA EOSDIS Land Processes DAAC. https://doi.org/10.5067/MODIS/MOD16A2GF.006

Running, S., Mu, Q. & Zhao, M. (2019b). *MYD16A2GF MODIS/Aqua Net Evapotranspiration Gap-Filled 8-Day L4 Global 500 m SIN Grid V006 [Data set]* Accessed: 2021-03-07. NASA EOSDIS Land Processes DAAC. https://doi.org/10.5067/MODIS/MYD16A2GF.006

Running, S., Nemani, R., Glassy, J. & Thornton, P. (1999). *Modis Daily Photosynthesis (PSN) And Annual Net Primary Production (NPP) Product (MOD17) Algorithm Theoretical Basis Document* (tech. rep.). NASA. https://lpdaac.usgs.gov/documents/95/MOD17_ATBD.pdf

Running, S. & Zhao, M. (2019). *MOD17A2HGF MODIS/Terra Gross Primary Productivity Gap-Filled 8-Day L4 Global 500 m SIN Grid V006 [Data set]* Accessed: 2021-03-07. NASA EOSDIS Land Processes DAAC. https://doi.org/10.5067/MODIS/MOD17A2HGF.006

Sentinel, C. (2018). Copernicus open access hub. *Sentinel Data Hub*.

Sinha, S. K., Padalia, H., Patel, N. & Chauhan, P. (2020). Estimation of Seasonal Sun-Induced Fluorescence Dynamics of Indian Tropical Deciduous Forests using SCOPE and Sentinel-2 MSI. *International Journal of Applied Earth Observation and Geoinformation*, *91*, 102155. https://doi.org/10.1016/j.jag.2020.102155

The pandas development team. (2020). *pandas-dev/pandas: Pandas* (Version 1.0.5). Zenodo. https://doi.org/10.5281/zenodo.3509134

United Nations, Department of Economic and Social Affairs, Population Division. (2019). *World Population Prospects 2019: Ten Key Findings* (tech. rep.). https://population.un.org/wpp/Publications/Files/WPP2019_10KeyFindings.pdf

van der Tol, C., Verhoef, W., Timmermans, J., Verhoef, A. & Su, Z. (2009). An integrated model of soil-canopy spectral radiances, photosynthesis, fluorescence, temperature and energy balance. *Biogeosciences*, *6*(12), 3109–129. https://doi.org/10.5194/bg-6-3109-2009

van der Tol, C., Rossini, M., Cogliati, S., Verhoef, W., Colombo, R., Rascher, U. & Mohammed, G. (2016). A model and measurement comparison of diurnal cycles of sun-induced chlorophyll fluorescence of crops. *Remote Sensing of Environment*, *186*, 663–677. https://doi.org/10.1016/j.rse.2016.09.021

van der Tol, C., Berry, J. A., Campbell, P. K. E. & Rascher, U. (2014). Models of fluorescence and photosynthesis for interpreting measurements of solar-induced chlorophyll fluorescence. *Journal of Geophysical Research: Biogeosciences*, *119*(12), 2312–2327. https://doi.org/10.1002/2014JG002713

Verhoef, W. (1998). *Theory of radiative transfer models applied in optical remote sensing of vegetation canopies [Doctoral dissertation, Wageningen University]*. https://edepot.wur.nl/210943

Verhoef, W. (1984). Light scattering by leaf layers with application to canopy reflectance modeling: The SAIL model. *Remote sensing of environment*, *16*(2), 125–141.

Verhoef, W., van der Tol, C. & Middleton, E. M. (2018). Hyperspectral radiative transfer modeling to explore the combined retrieval of biophysical parameters and canopy fluorescence from FLEX – Sentinel-3 tandem mission multi-sensor data. *Remote Sensing of Environment*, *204*, 942–963. https://doi.org/10.1016/j.rse.2017.08.006

Vermote, E. F., Tanré, D., Deuzé, J. L., Herman, M. & Morcrette, J. J. (1997). Second simulation of the satellite signal in the solar spectrum, 6s: an overview. *IEEE Transactions on Geoscience and Remote Sensing*, *35*(3), 675–686. https://doi.org/10.1109/36.581987

Vilfan, N., Van der Tol, C., Muller, O., Rascher, U. & Verhoef, W. (2016). Fluspect-B: A model for leaf fluorescence, reflectance and transmittance spectra. *Remote Sensing of Environment*, *186*, 596–615.

White, J., Berg, A. A., Champagne, C., Zhang, Y., Chipanshi, A. & Daneshfar, B. (2020). Improving crop yield forecasts with satellite-based soil moisture estimates: An example for township level canola yield forecasts over the Canadian Prairies. *International Journal of Applied Earth Observation and Geoinformation*, *89*, 102092. https://doi.org/10.1016/j.jag.2020.102092

Wilson, R. T. (2013). Py6S: A Python interface to the 6S radiative transfer model. *Computers and Geosciences*, *51*, 166–171. https://doi.org/10.1016/j.cageo.2012.08.002

Wolanin, A., Camps-Valls, G., Gómez-Chova, L., Mateo-García, G., van der Tol, C., Zhang, Y. & Guanter, L. (2019). Estimating crop primary productivity with Sentinel-2 and Landsat 8 using machine learning methods trained with radiative transfer simulations. *Remote Sensing of Environment*, *225*, 441–457. https://doi.org/10.1016/j.rse.2019.03.002

Wu, B., Meng, J., Li, Q., Yan, N., Du, X. & Zhang, M. (2014). Remote sensing-based global crop monitoring: experiences with China's CropWatch system. *International Journal of Digital Earth*, *7*(2), 113–137. https://doi.org/10.1080/17538947.2013.821185

Yang, P., Prikaziuk, E., Verhoef, W. & van der Tol, C. (2020). SCOPE 2.0: A model to simulate vegetated land surface fluxes and satellite signals. *Geoscientific Model Development Discussions [preprint]*, *2020*, 1–26. https://doi.org/10.5194/gmd-2020-251. in review

Yang, P., van der Tol, C., Verhoef, W., Damm, A., Schickling, A., Kraska, T., Muller, O. & Rascher, U. (2019). Using reflectance to explain vegetation biochemical and structural effects on sun-induced chlorophyll fluorescence. *Remote Sensing of Environment*, *231*, 110996. https://doi.org/10.1016/j.rse.2018.11.039

Yang, P., van der Tol, C., Yin, T. & Verhoef, W. (2020). The SPART model: A soil-plant-atmosphere radiative transfer model for satellite measurements in the solar spectrum. *Remote Sensing of Environment*, *247*, 111870. https://doi.org/10.1016/j.rse.2020.111870

Yang, P., Verhoef, W., Prikaziuk, E. & van der Tol, C. (2021). Improved retrieval of land surface biophysical variables from time series of Sentinel-3 OLCI TOA spectral observations by considering the temporal autocorrelation of surface and atmospheric properties. *Remote Sensing of Environment*, *256*, 112328. https://doi.org/10.1016/j.rse.2021.112328